APPROXIMATE ANALYSIS CONCERNING WAVE-POWER ABSORPTION BY HYDRODYNAMICALLY INTERACTING BUOYS

BY
ÅGE KYLLINGSTAD

INSTITUTT FOR EKSPERIMENTALFYSIKK
NORGES TEKNISKE HØGSKOLE
TRONDHEIM

APPROXIMATE ANALYSIS CONCERNING WAVE-POWER ABSORPTION BY HYDRODYNAMICALLY INTERACTING BUOYS

BY

AGE KYLLINGSTAD

This thesis is submitted to the University of Trondheim, The Norwegian Institute of Technology, Department of Physics, in partial fulfilment of the requirements for the degree of Dr.Ing.

September, 1982

N.T.H.-Trykk
Trondheim 1982

PREFACE.

This thesis work was carried out during the years 1980-1982 at Division of Experimental Physics, The Norwegian Institute of Technology (NTH). The computations were executed on a Univac 1100/62 computer at RUNIT, Trondheim.

I wish to thank my advisor Dr. Techn. Johannes Falnes for invaluable help and stimulating guidance during the work. I also want to thank Kjell Budal for useful discussions, Brian Count for his computer printouts and, finally, Randi Sortland and Tuyen Hagemann for excellent typing of the original manuscript.

ABSTRACT

The interaction effects for heaving axisymmetrical wave-power buoys in regular waves are studied. Analytic approximations for the hydrodynamical interaction forces are used for this purpose. A new mathematical model - called the low-scattering approximation - is derived. Since first order scattering effects are taken into account, it represents an improvement or sophistication of a previosly used approximation which totally neglects the diffracted waves. The low-scattering approximation is based upon the assumptions of small buoys and large buoy separations. Hence it neglects multiple scattering as well as local wave fields. However, comparison with accurate numerical results for a two-buoy system indicates that the low-scattering approximation is fairly good even when the buoy diameter is as large as 1/5 of the wavelength and the buoy spacing is as small as 5 buoy radii.

In contrast to most of the previous works in this field, the effects of power losses have been included in the phenomenological formulation. These losses - in practical systems they are inevitable - are represented by a so-called loss resistance matrix which is assumed to be constant and symmetrical. It enters the expressions for the useful power absorption and for the optimal buoy motion.

In order to make our mathematical model even more applicable to practical wave power buoys and to realistic sea conditions, a method for power maximising under motion constraints is described and implemented on a computer. The constraints examined are two quite different types: 1) restriction on the individual buoy amplitudes and 2) fixed values for some of the dynamical parameters such as the buoy phases and the load resistances governing the useful power take-off.

The computer program - mainly written with the intention of examining the power absorption characteristics - is used to produce a lot of quantitative results concerning different buoy configurations. Two different classes of buoy systems are analysed: 1) the focusing system consisting of many non-absorbing buoys acting as a dynamical reflector behind a power absorbing

buoy, and 2) systems of merely absorbing buoys. As for the former class it is demonstrated that dynamical focusing can be achieved even by relatively small systems or few reflecting buoys. The power available for the absorbing buoy, however, very much depends on the phase of the focused wave and on the angle of incidence. The results concerning the latter class of buoy systems comprise a variety of configurations, ranging from the simple two-buoy system to a linear row of twenty equally-spaced buoys. Although the interaction effects for such absorbing buoy systems are quite important,the total useful power is, in general, less dependent on the wave frequency and the angle of incidence than what is the case for dynamically focusing systems. Another important difference between the two classes is that the absorbed power per unit of volume displacement is substantially less for focusing systems than for the ones of merely absorbing buoys.

The effects of power losses and constraints are also quantitatively studied. Not unexpectedly, the results show that the hydrodynamical interacion forces become less influent on the useful absorbed power when the loss resistance increases and when the waves are high so that the buoy amplitudes have to be restricted.

CONTENTS.

1 INTRODUCTION.

After the so-called energy crisis in 1973 much interest has arosen on the development of alternative energy resources, in particular the renewable ones. One of these energy resources is the ocean wave power. For countries, like Norway, which has a long coast line, the ocean waves represent an enormous amount of energy[1,2].

A lot of different concepts for converting the wave energy economically have been proposed. One of these concepts is the Norwegian heaving buoy. Because of its small dimension, compared to the typical wavelength,it is often called a point absorber. A characteristical feature of the Norwegian buoy is the phase control. By means of a special mechanism the buoy is latched in certain time intervals of each cycle in order to obtain approximate optimal heave motion. This latching mechanism provides "artificial" resonance conditions over a wide range of frequencies.

A proposed wave power plant consists of many point absorbers. The interaction effects of such a multi-buoy system may be quite important, but in general it is extremely difficult to compute the interaction forces very accurately. It involves solving a partial differential equation with non-trivial boundary conditions. Except for rare and special cases the boundary value problem does not have any simple analytic solution. Different numerical methods have been used with success to calculate the hydrodynamical forces for two-body and three-body systems[3-6]. However, for multi-body systems of, say, ten buoys or more the numerical methods probably are too time consuming or expensive to use. For that reason it is desirable to have an approximate, but simple analytic model which can be applied for large systems. Analytic methods also have the advantage in preference to more accurate numerical methods that they more directly provide valuable insight into the physics of the problem.

A main topic of this thesis is, in fact, to derive an approximative analytic model reliable for axisymmetrical heaving bodies of the same order of size as the Norwegian buoy.

The approximation is based upon

1) the small-body assumption which means that the buoys are small compared to the wavelength, and

2) the far-field assumption, which implies that the buoys are separated widely enough to make the local or evanescent waves negligible.

The derivation proceeds in two steps. The first step leads to what we have called the non-scattering (NS) approximation. This approximation neglects cross-coupling forces due to scattering, and it represents a slight extension of an analytic method previously indicated by Falnes [7]. The second step leads to what we have called the low-scattering (LS) approximation. It is an improvement of the NS approximation and takes into account the first order scattering effects.

The superior purpose of developing those analytic approximations is to have a good tool for investigating the absorption characteristics for practical systems of heaving wave power buoys. A considerable part of this thesis therefore concerns applications of the analytic models. One of these applications is the dynamical focusing system. This is a sort of synthesis of the mentioned buoy concept and a focusing concept proposed by Mehlum [8]. In contrast to the latter concept, which uses static hydrodynamical "lenses" to accomplish the wave focusing, the dynamical focusing idea seeks to concentrate the wave energy by means of a dynamical, reflecting "mirror" consisting of heaving buoys. Curiosity on the absorption characteristics for such a system was, in fact, the starting point of the work on this thesis. However, having developed a quite general computer program for this task, it also became of interest to investigate other buoy systems and compare those with the focusing one.

The outline of the thesis is described briefly in the following.

Chapter 2 presents a phenomenological and linear theory for a general system of interacting bodies oscillating in monochromatic waves. From the complex equations of motion an expression

for the maximum useful power is derived. Finally, the chapter includes a justification that the complex representation of the dynamics applies even for phase-controlled buoys making non-sinusoidal heave motion.

In chapter 3 we specialise to small axisymmetrical and heaving buoys. Before deriving the analytical multi-body approximation already mentioned, some small-body results for isolated buoys are presented. This single-buoy case is relevant, because the NS approximation, as well as the LS approximation, is based upon the hydrodynamical coefficients for an isolated buoy.

The validity of the respective approximations is discussed in chapter 4. The discussion is based upon a comparative analysis of the hydrodynamical parameters and is restricted to a few two-buoy systems for which numerical results are available.

Chapter 5 concerns the computational methods used for investigating the characteristics for the various buoy systems. The computer program written also possesses the possibility of maximising the power under motion constraints. This is of great practical interest owing to the fact that the applied buoys are so small that a lot of realistic sea conditions require amplitude-restricted motion.

The main concern of chapter 6 is to present some quantitative results for dynamically focusing systems and for various configurations of merely absorbing buoys. On the basis of these results it is tried to reveal the main differences between two kinds of systems. In chapter 6 we also make some comments on the power absorption according to different mathematical models.

In the final chapter 7 we give a short summary of those parts of the thesis which are new and original contributions to the field. Moreover, a few recommendations for further progress are given.

2. MULTI-BODY WAVE INTERACTIONS

In this chapter we firstly present a phenomenological theory for a system of rigid bodies. The theory is quite general in the sence that no assumptions have been made on the body geometries. However, we adopt the usual assumptions of

i) ideal incompressible fluid
ii) irrotational flow
iii) small disturbances or oscillation amplitudes.

Then linear potential theory applies. See appendix A.

In the first two sections we also assume that the forces acting upon the bodies are sinusoidal. In the last section, however, is shown how the theory is modified when the forces are non-sinusoidal.

2.1 Equations of motion.

We consider a system of N oscillating bodies, partially or completely submerged in water. The system is schematically shown in fig. 1. The total number of oscillation modes - or degrees of freedom - is M. For rigid bodies $M \leq 6N$. The equality refers to the case when all bodies are free to move in any of its six modes. In marine terminology these modes are termed surge, sway, heave, roll, pitch and yaw-denoted by the indices 1,2,3,4,5 and 6, respectively.

Because the system is linear and the motion is harmonical we may write the equations of motion as a set of M complex, algebraic and linear equations:

$$(\underset{\sim}{Z} + \underset{\sim}{Z}_m)\underset{\sim}{u} = \underset{\sim}{F} \qquad (2.1)$$

or - in component form

$$\sum_{j,q} (Z_{ij}^{pq} + Z_{m,ij}^{pq})u_j^q = F_i^p \qquad (2.2)$$

where the subscripts i and j denote the body numbers and the superscripts p and q denote the oscillation modes of

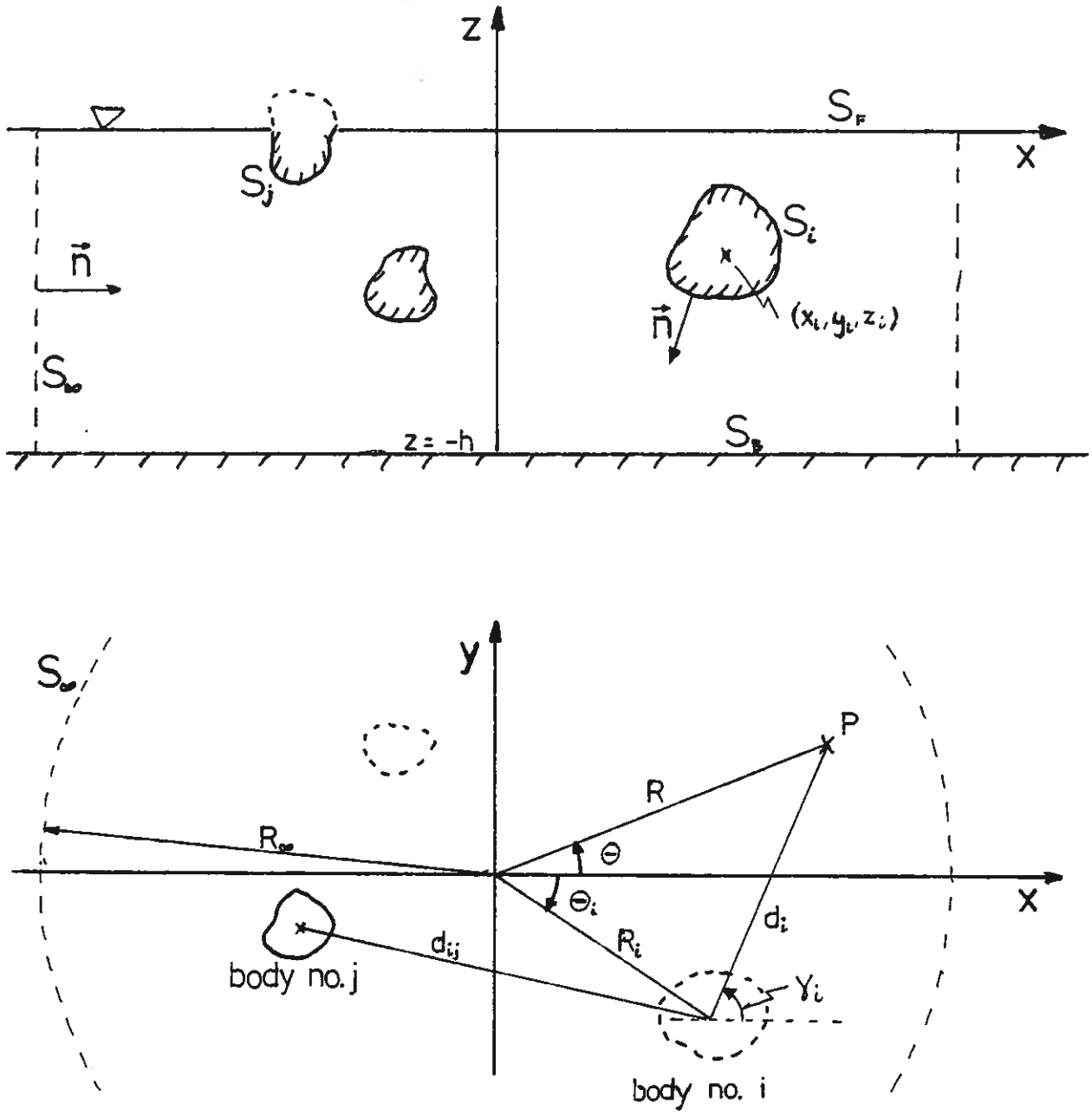

Fig. 1. Side view (above) and top view (below) of a general N-body system. The fluid domain is enclosed by the bottom surface S_B, the free surface S_F, the wetted body surfaces $\bigcup_{i=1}^{N} S_i$ and an imaginary cylindrical surface S_∞ of infinitely large radius R_∞. (x_i, y_i, z_i) and (R_i, θ_i, z_i) are Cartesian and cylinder coordinates for the center of gravity of buoy no. i, respectively. Local cylinder coordinates (relative to buoy no. i) of an arbitrary point P is (d_i, γ_i, z)

the bodies no. i and j, respectively. (For convenience we use the term "oscillator p(i)" for the oscillation mode no. p of body no. i.) The quantities which enter into the equations above are the following.

F_i^p is the generalised force acting on oscillator p(i) when all bodies are fixed. It is proportional to the undisturbed incident wave amplitude at (x_i, y_i) which are the horizontal components of the mean center of gravity of the body no. i. Using the plane wave potential ϕ_o of (A.19) this elevation is

$$\eta_o(i) = \eta_o e^{-ik(x_i \cos\beta + y_i \sin\beta)} \tag{2.3}$$

where $\eta_o(i)$ is an abbreviated notation for $\eta_o(x_i, y_i)$. The exciting force, then, may be expressed by

$$F_i^p = \kappa_i^p \eta_o(i) \tag{2.4}$$

where the complex constant of proportionality κ_i^p is termed the exciting force coefficient.

$\underset{\sim}{Z}$ is called the radiation impedance matrix. It represents the hydrodynamical forces arising when the bodies are oscillating. The product $-Z_{ij}^{pq} u_j^q$ is, per definition, the complex force amplitude acting on oscillator p(i) due to the motion of oscillator q(j) with velocity amplitude u_j^q. The radiation impedance matrix $\underset{\sim}{Z}$ may be decomposed into real and imaginary parts:

$$\underset{\sim}{Z} = \underset{\sim}{R} + i\underset{\sim}{X} = \underset{\sim}{R} + i\omega\underset{\sim}{m} \tag{2.5}$$

where $\underset{\sim}{R}$ and $\underset{\sim}{X}$ are here termed the radiation resistance matrix and radiation reactance matrix, respectively. The former is commonly termed the added damping matrix while the latter is often written as the product of the angular frequency ω and a so-called added mass matrix $\underset{\sim}{m}$.

$\underset{\sim}{Z}_m$ is called the mechanical impedance matrix. It takes care of the inertia forces, the loss and load damping forces and the spring forces. Its elements $Z_{m,ij}^{pq}$ may be defined in

the same way as for the radiation impedance matrix elements Z_{ij}^{pq}. For convenience, we shall throughout make the assumption that

$$Z_{m,ij}^{pq} = Z_{m,ji}^{qp} \tag{2.6}$$

Hence $\underset{\sim}{Z}_m$ is symmetrical as well as $\underset{\sim}{Z}$. See (A.42).

2.2 Maximising the useful power.

In many practical wave power systems some part of the total converted power will represent lost power, it be viscous friction losses or conversion losses. Although it may not always be true, we shall, for mathematical convenience, assume that these undesirable damping forces are linear functions of the variables (e.g. oscillation amplitudes). They may then be represented by a constant loss resistance matrix $\underset{\sim}{R}_l$ which is included in the mechanical impedance matrix

$$\underset{\sim}{Z}_m = \underset{\sim}{R}_c + \underset{\sim}{R}_l + i\underset{\sim}{X}_m \tag{2.7}$$

The "conversion resistance matrix" $\underset{\sim}{R}_c$ then represents the useful part P_c of the absorbed power. An expression for this useful power may be found as outlined in the following.

The real force balance equation is, according to (A.10) and the complex matrix equation (2.1)

$$(\underset{\sim}{R} + \underset{\sim}{R}_c + \underset{\sim}{R}_l)\mathrm{Re}\{\underset{\sim}{u}e^{i\omega t}\} - (\underset{\sim}{X} + \underset{\sim}{X}_m)\mathrm{Im}\{\underset{\sim}{u}e^{i\omega t}\} = \mathrm{Re}\{\underset{\sim}{F}e^{i\omega t}\} \tag{2.8}$$

By premultiplying this equation by the transposed real velocity vector $\mathrm{Re}\{\tilde{\underset{\sim}{u}}e^{i\omega t}\}$ and taking the time average of the product we obtain the following power balance equation:

$$P_c = P_e - (P_r + P_l) \tag{2.9}$$

Here P_e is the so-called[9] exciting power, given by

$$P_e = \frac{1}{4}(\tilde{u}\underset{\sim}{F}^* + \tilde{u}^*\underset{\sim}{F}) \equiv \frac{1}{2}\,\mathrm{Re}\{\tilde{u}^*\underset{\sim}{F}\} \tag{2.10}$$

P_r and P_l are the radiated and the lost power, respectively, related to the corresponding radiation and loss resistance matrices by

$$P_r = \frac{1}{2}\,\tilde{u}\underset{\approx}{R}\underset{\sim}{u} \tag{2.11}$$

and

$$P_l = \frac{1}{2}\,\tilde{u}\underset{\approx}{R}_l\underset{\sim}{u} \tag{2.12}$$

Rewriting (2.9) in a more explicit form we have for the converted useful power

$$P_c = \frac{1}{4}\sum_{i,p}(F_i^p u_i^{p*} + F_i^{p*}u_i^p) - \frac{1}{2}\sum_{\substack{i,p\\ j,q}} u_i^{p*}(R_{ij}^{pq} + R_{l,ij}^{pq})u_j^q \tag{2.13}$$

In the case of no motion constraints the maximum of P_c has to satisfy $2M$ derivative conditions:

$$\frac{\partial P_c}{\partial u_k^r} = \frac{\partial P_c}{\partial u_k^{r*}} = 0 \tag{2.14}$$

This leads to the following matrix equation for the optimum velocity vector $\underset{\sim}{u}_{opt}$

$$(\underset{\approx}{R} + \underset{\approx}{R}_l)\underset{\sim}{u}_{opt} = \frac{1}{2}\,\underset{\sim}{F} \tag{2.15}$$

The corresponding power maximum is

$$P_{c,max} = \frac{1}{2}\,\tilde{u}_{opt}^*(\underset{\approx}{R} + \underset{\approx}{R}_l)\underset{\sim}{u}_{opt} \tag{2.16}$$

Provided that $(\underset{\approx}{R} + \underset{\approx}{R}_l)$ is not singular (2.16) may alternatively be written

$$P_{c,max} = \frac{1}{8}\,\tilde{F}^*(\underset{\approx}{R} + \underset{\approx}{R}_l)^{-1}\underset{\sim}{F} \tag{2.17}$$

Note that eqs. (2.15) to (2.17) represent an extension of corresponding equations obtained by Evans[10] and Falnes[11]; they

did not take any losses into account. Results similar to (2.16) and (2.17) are derived previously[12] for the special case when $M = 1$.

The velocity amplitude vector $\underset{\sim}{u}$ has to satisfy the equation of motion (2.1). The requirement (2.15) on $\underset{\sim}{u}_{opt}$, therefore, is a requirement on the matrices $\underset{\sim}{R}_c$ and $\underset{\sim}{X}_m$. Stated in an other way: optimising P_c with respect to the $2M$ real varables of $\underset{\sim}{u}$ is mathematically equivalent to optimising P_c with respect to $2M$ unbounded parameters of the conversion resistance matrix $\underset{\sim}{R}_c$ and the mechanical reactance matrix $\underset{\sim}{X}_m$. However, in many practical situations neither the elements of these matrices nor the oscillation amplitudes can be chosen freely. This problem of power maximising with constraints is discussed later on. See section 5.3.

2.3 Latched non-sinusoidal motion.

So far we have assumed that all forces acting on a body are sinusoidal. Now we want to see whether the previous phenomenological formulation applies to a system acted upon by non-harmonic but periodic forces.

For simplicity we confine ourselves to a system of one oscillator only, say a heaving buoy. The exciting force $F'_e(t)$ - dashed symbols denote quantities which are real and time dependent - is balanced by a mechanical force $F'_m(t)$ and a hydrodynamical force $F'_r(t)$:

$$F'_m + F'_r = F'_e \tag{2.18}$$

Both F'_m and F'_r are forces which arise because of the buoy motion which is described by a displacement function $s'(t)$. Since these functions are periodic with the wave period $T = 2\pi/\omega$, they may be expressed by fourier series:

$$\dot{s}' \equiv \frac{ds'}{dt} = \mathrm{Re}\{\sum_{n=1}^{\infty} u^{(n)} e^{in\omega t}\} \tag{2.19}$$

$$F_e' = \mathrm{Re}\{\sum_{n=1}^{\infty} F^{(n)} e^{in\omega t}\} \tag{2.20}$$

$$F_r' = \mathrm{Re}\{\sum_{n=1}^{\infty} (-Z^{(n)} u^{(n)}) e^{in\omega t}\} \tag{2.21}$$

$$F_m' = \mathrm{Re}\{\sum_{n=1}^{\infty} (-Z_m^{(n)} u^{(n)}) e^{i\omega nt}\} \tag{2.22}$$

When the system is linear the expansion coefficient $F^{(n)}$ and the parameters $Z^{(n)}$ and $Z_m^{(n)}$ are independent of the displacement s'. Each frequency component, therefore, can be treated separately. That is

$$(Z^{(n)} + Z_m^{(n)}) u^{(n)} = F^{(n)} \tag{2.23}$$

for all $n \geq 1$. When $n = 1$ (2.23) is just the one-dimensional version of the matrix equation (2.1).

The power balance equation is obtained by multiplying the real force balance equation (2.18) by $\dot{s}'$ and taking the time average of the resulting equation. After some manipulations we arrive at

$$\sum_{n=1}^{\infty} P_r^{(n)} + \sum_{n=1}^{\infty} P_m^{(n)} = \sum_{n=1}^{\infty} P_e^{(n)} \tag{2.24}$$

where

$$P_r^{(n)} = \frac{1}{2} R^{(n)} |u^{(n)}|^2 \tag{2.25}$$

$$P_m^{(n)} = \frac{1}{2} R_m^{(n)} |u^{(n)}|^2 \tag{2.26}$$

$$P_e^{(n)} = \frac{1}{2} \mathrm{Re}\{F^{(n)*} u^{(n)}\} \tag{2.27}$$

and $R^{(n)}$ and $R_m^{(n)}$ are the real parts of the radiation impedance $Z^{(n)} \equiv Z(n\omega)$ and of the mechanical impedance $Z_m^{(n)}$, respectively.

As an illustrating and relevant example of application

we consider the phase-controlled wave power buoy proposed by Budal and Falnes[13] heaving in a monochromatic incident wave. See fig. 2. Because the mechanical force $F_m(t)$ is not known in detail, it is rather inconvenient to define $Z_m^{(1)}$ by the equation (2.22).

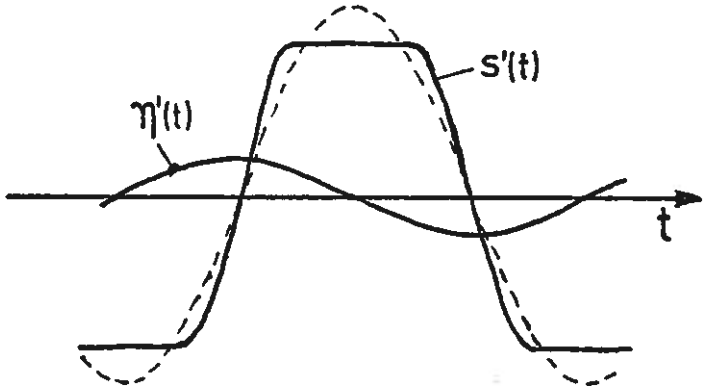

Fig. 2. Wave elevation $\eta'(t)$ and vertical displacement $s'(t)$ of a latched buoy as a function of time. The buoy is held fixed in certain intervals of each cycle so that the velocity $\dot{s}(t)$ is in phase with the exciting force. In that way one obtains "artificial" resonance condition even for a light buoy of eigenperiod T_o smaller than the wave period T. The dashed curve is the first harmonic fourier component of $s'(t)$.

However, it is possible to give meaningful physical interpretation for the mechanical resistance $R_m^{(1)}$ as well as the reactance $X_m^{(1)}$ without relating them to the mechanical force F_m'. This is seen by the following.

For the case of sinusoidal exciting force it is seen, by means of (2.23) and (2.24), that

$$\frac{1}{2} R_m^{(1)} |u^{(1)}|^2 = P_m + P_{r,loss} \qquad (2.28)$$

where P_m is the total mechanical converted power

$$P_m = \sum_{n=1}^{\infty} P_m^{(n)} \tag{2.29}$$

and $P_{r,loss}$ is the loss power due to radiation of higher harmonic waves:

$$P_{r,loss} = \sum_{n=2}^{\infty} P_r^{(n)} \tag{2.30}$$

If, therefore, the equation of motion (2.1) is applied to a system of latched buoys, the matrix $\underset{\sim}{R}_m$ has to be regarded as a generalised mechanical resistance matrix which includes the effect of higher harmonic wave radiation.

As indicated by the term "phase-controlled", the phase angle σ between the force $F^{(1)}$ and the first harmonic velocity component $u^{(1)}$ is a directly controlled parameter. That is

$$\sigma = \arg(F^{(1)}/u^{(1)}) \tag{2.31}$$

On the other hand, we have that σ is related to the imaginary and the real parts of $(Z^{(1)} + Z_m^{(1)})$ by

$$\operatorname{tg}\sigma = \frac{X^{(1)}+X_m^{(1)}}{R^{(1)}+R_m^{(1)}} \tag{2.32}$$

The total reactance $(X^{(1)}+X_m^{(1)})$, therefore, is a measure for the points of time when the buoy is released. Consequently, the diagonal elements of the radiation reactance matrix $\underset{\sim}{X}$ becomes of little or no significance for phase-controlled buoys.

3. APPROXIMATIONS FOR SMALL AXISYMMETRICAL HEAVING BUOYS

3.1 Presumptions.

We now want to leave the general description and consider the case when

i) the bodies are allowed to move in the heave mode, only. For convenience we adopt the following convention. Unless the mode superscript is explicitly indicated, the implied mode is heave. (Examples: $\kappa_i \equiv \kappa_i^3$, $Z_{ij} \equiv Z_{ij}^{33}$.)

ii) the bodies are vertical axisymmetrical buoys. The buoy radius a_i at the center of gravity (x_i, y_i, z_i) of buoy no. i is assumed to represent a characteristic buoy dimension. See fig. 3.

iii) the buoys are small compared to the wavelength. Because this is the definition of a point-absorber[14] we could call it the "point-absorber assumption". Its mathematical formulation is

$$\alpha_i \equiv ka_i << 1 \quad , \quad i = 1,..,N \tag{3.1}$$

iv) the buoys are widely separated so that the local field of a buoy is small compared to the corresponding far-field at the location of its nearest neighbour buoy. This far-field assumption may be formulated either by

$$kd_{ij} >> 1 \quad , \quad i \neq j \tag{3.2}$$

or by

$$d_{ij}/a_i >> 1 \quad , \quad i \neq j \tag{3.3}$$

d_{ij} being defined in fig. 3.

Although we confine ourselves to heaving buoys only, the next

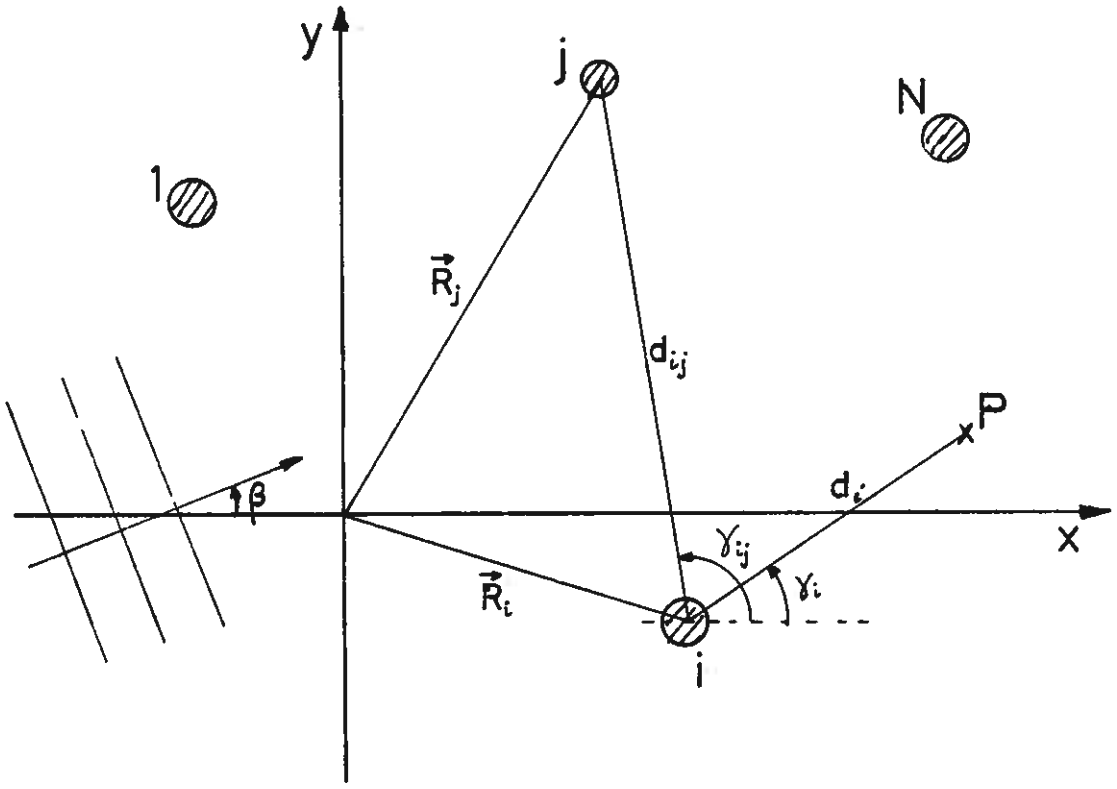

Fig. 3. Top view of a system of N axisymmetrical buoys.

$\vec{R}_i \equiv (x_i, y_i)$ - horizontal radius vector for the center of gravity of buoy no. i.

(d_i, γ_i) - local polar coordinates for an arbitrary point P. That is, $d_i = |\vec{R} - \vec{R}_i|$ and γ_i is the angle between $(\vec{R} - \vec{R}_i)$ and the x-axis.

$d_{ij} \equiv |\vec{R}_j - \vec{R}_i|$ - the horizontal distance between two different buoys i and j.

γ_{ij} - the angle between $(\vec{R}_j - \vec{R}_i)$ and the x-axis.

section concerns the surge and sway modes as well. The reason is that the surge force coefficients are used later on. See section 3.5.

3.2 Isolated buoy.

Far-field potentials for the translation modes

Consider the case of one isolated buoy (N = 1). For simplicity we assume the z-axis to coincide with the axis of symmetry. For reasons of symmetry the far-field parts of the normalised surge, sway or heave potential may be expressed by one single term of eq. (A.30). That is

$$\varphi_{\infty}^{p,o} = \begin{cases} A_1 e(kz) H_1(kR)\cos\theta & , \quad p = 1 \\ A_1 e(kz) H_1(kR)\sin\theta & , \quad p = 2 \\ A_o e(kz) H_o(kR) & , \quad p = 3 \end{cases} \qquad (3.4)$$

where the additional superscript ^{o} indicates that the quantity refers to an isolated buoy, and the subscript $_{\infty}$ indicates that the local field is not included. See (A.29). The exciting force coefficients for the translation modes are accordingly

$$\kappa^{p,o}(\beta) = \begin{cases} \kappa^{s}\cos\beta & , \quad p = 1 \\ \kappa^{s}\sin\beta & , \quad p = 2 \\ \kappa^{o} & , \quad p = 3 \end{cases} \qquad (3.5)$$

where κ^{s}, per definition, is the isolated surge force coefficient at normal incidence.
By means of (A.47), (A.48) and the asymptotic expression (A.28) for the Hankel functions H_n the coefficients A_1 and A_o in eq. (3.4) may be expressed by the exciting force coefficients κ^{s} and κ^{o}, respectively. Eq.(3.4) then becomes

$$\varphi_{\infty}^{p,o} = \begin{cases} \frac{k}{2\rho g D}\,\kappa^{s} e(kz) H_1(kR)\cos\theta & , \quad p = 1 \\ \frac{k}{2\rho g D}\,\kappa^{s} e(kz) H_1(kR)\sin\theta & , \quad p = 2 \\ -i\,\frac{k}{2\rho g D}\,\kappa^{o} e(kz) H_o(kR) & , \quad p = 3 \end{cases} \qquad (3.6)$$

The isolated far-field potentials $\varphi_{i,\infty}^{p,o}$ of an arbitrary buoy no. i is obtained by substituting the global coordinates (R,θ) by the local coordinates (d_i,γ_i) which are defined in fig. 3.

At present the exciting force coefficients κ^{s} and κ^{o} are unknown functions of wave frequency, buoy geometry, submergence and depth of water. Because these quantities are quite fundamental for the multi-buoy approximations presented later on, they will be subject of some investigation in the following.

Surge and heave force coefficients

We still consider an isolated buoy with its center of gravity at $\vec{r}_1 = (0,0,z_1)$. See fig. 4. In accordance with point-absorber assumption (3.1) the incident wave potential ϕ_o and its gradient are approximately constant on S_1. That is

$$\phi_o\Big|_{S_1} \approx \phi_o\Big|_{\vec{r}=\vec{r}_1} \qquad (3.7)$$

$$\frac{\partial\phi_o}{\partial x_p}\Big|_{S_1} \approx \frac{\partial\phi_o}{\partial x_p}\Big|_{\vec{r}=\vec{r}_1} \equiv v_p(1) \qquad , \quad p = 1,2,3 \qquad (3.8)$$

where $v_p(1)$ denotes the fluid velocity of the undisturbed wave at the center of gravity.

It can be shown[15] that this approximation leads to the following expressions for the Froude-Krylov force and the diffraction force

$$F_{FK}^{p} \approx \rho g A_w \eta_o(1)\delta_{3p} + i\omega V v_p(1), \quad p = 1,2,3 \qquad (3.9)$$

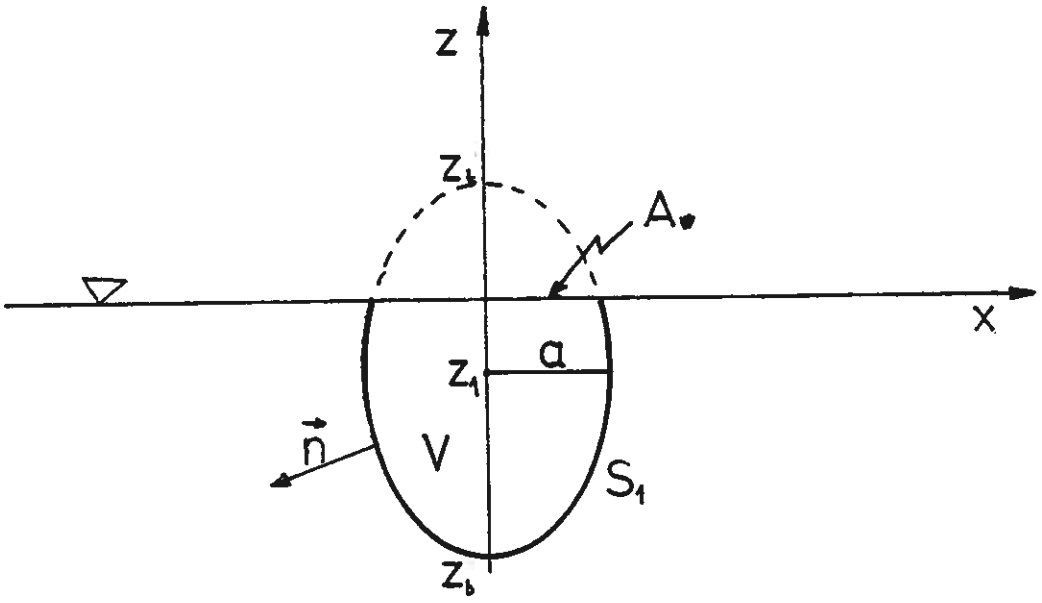

Fig. 4. Side view of an isolated axisymmetric buoy

a - buoy radius at the center of gravity.

z_t, z_1, z_b - vertical coordinates for top, center and base of the buoy, respectively.

S_1 - average wetted buoy surface.

A_w - water plane area (= 0 for a completely submerged buoy).

V - average displaced volum

$$F_d^P \approx \sum_{q=1}^{3} Z^{pq} v_q(1) \quad , \quad p = 1,2,3 \tag{3.10}$$

respectively, where δ_{3p} is the Kronecker delta symbol. Differentiating the incident wave potential (A.29) we find that

$$v_q(1) \equiv \left.\frac{\partial \phi_o}{\partial x_q}\right|_{\vec{r}=\vec{r}_1} = \begin{cases} f_1 \omega \eta_o \cos\beta & , \quad q = 1 \\ f_1 \omega \eta_o \sin\beta & , \quad q = 2 \\ i g_1 \omega \eta_o & , \quad q = 3 \end{cases} \qquad (3.11)$$

where f_1 and g_1 are submergence factors given by

$$f_1 = \frac{\cosh(kz_1 + kh)}{\sinh(kh)} \qquad (3.12)$$

$$g_1 = \frac{\sinh(kz_1 + kh)}{\sinh(kh)} \qquad (3.13)$$

(For half-immersed buoys on deep water $g_1 = f_1 = 1$.)

It is convenient to introduce the non-dimensional versions ε and μ of the radiation resistance and reactance, respectively, by

$$Z^{pq} = \omega \rho V (\varepsilon^{pq} + i\mu^{pq}) \qquad (3.14)$$

For reasons of symmetry there is no cross-coupling between different translation modes, that is, the radiation impedance matrix for the three translation modes $(p = 1,2,3)$ is diagonal.

$$Z^{pq} = Z^{pp}\delta_{pq} \quad , \quad p,q = 1,2,3 \qquad (3.15)$$

Also it may be realised[16] that for point absorbers

$$\varepsilon^{pp} << \mu^{pp} = O(1) \quad , \quad \alpha << 1 \qquad (3.16)$$

From the small-body equations (3.9) and (3.10) we obtain the exciting force coefficients

$$\kappa^s = \pi a^2 \rho g \{ i(1 + \mu^{11}) f_1 \frac{V}{\pi a^3} \alpha + O(\alpha^2) \} \qquad (3.17)$$

$$\kappa^o = \pi a^2 \rho g \left\{ \frac{A_w}{\pi a^2} - (1 + \mu^{33}) g_1 \frac{V}{\pi a^3} \alpha + O(\alpha^2) \right\} \qquad (3.18)$$

for the surge mode and the heave mode, respectively. Some

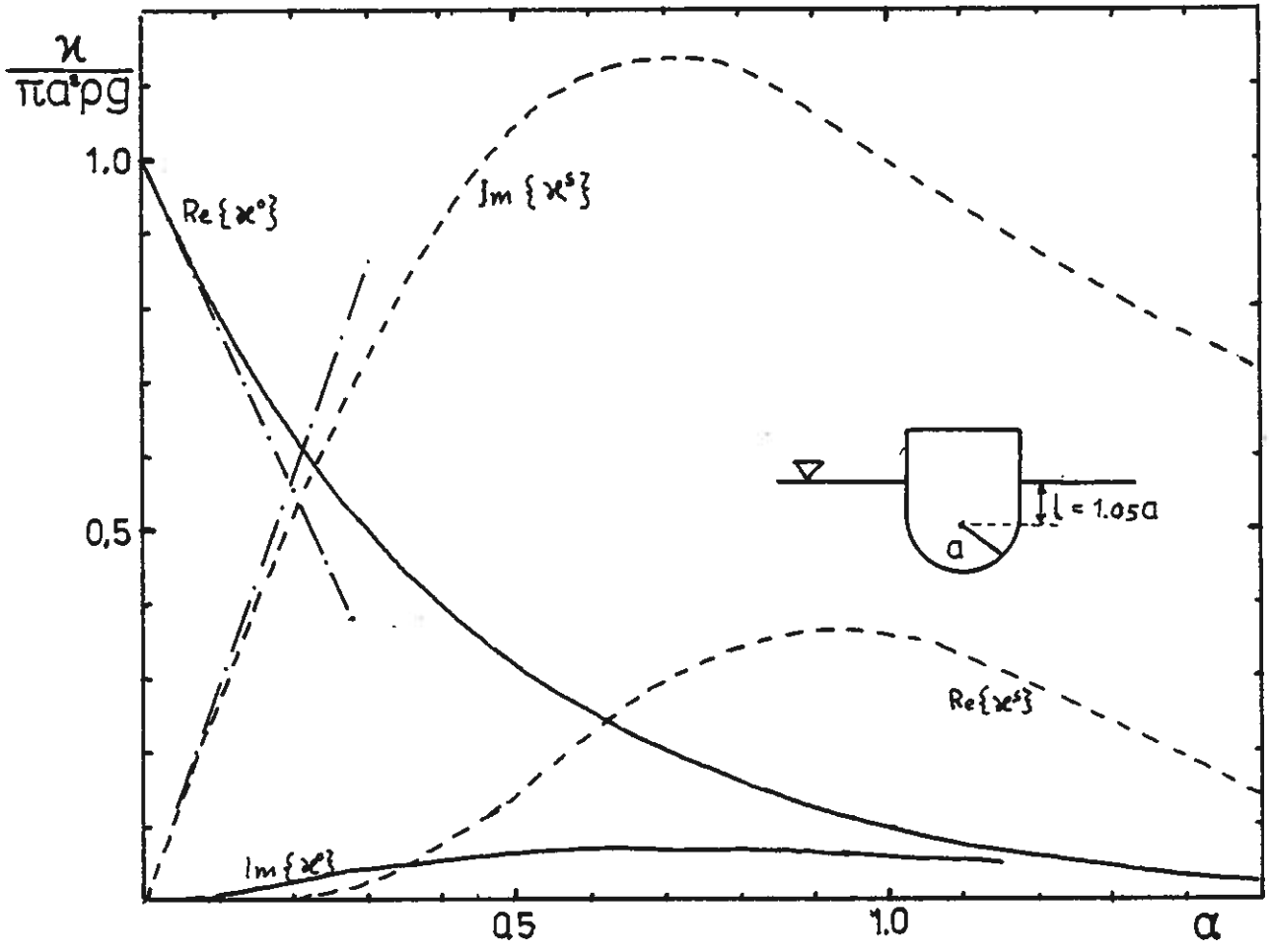

Fig. 5. Normalised exciting force coefficients for a semi-submerged vertical cylinder of hemispherical base on deep water.
The values ~~is~~ are calculated by a sink-source method using 87 buoy elements [17].
$\alpha \equiv ka$ - normalised buoy radius.
κ^o - heave force coefficient.
κ^s - surge force coefficient.
—•— small-body approximations according to (3.17) and (3.18).

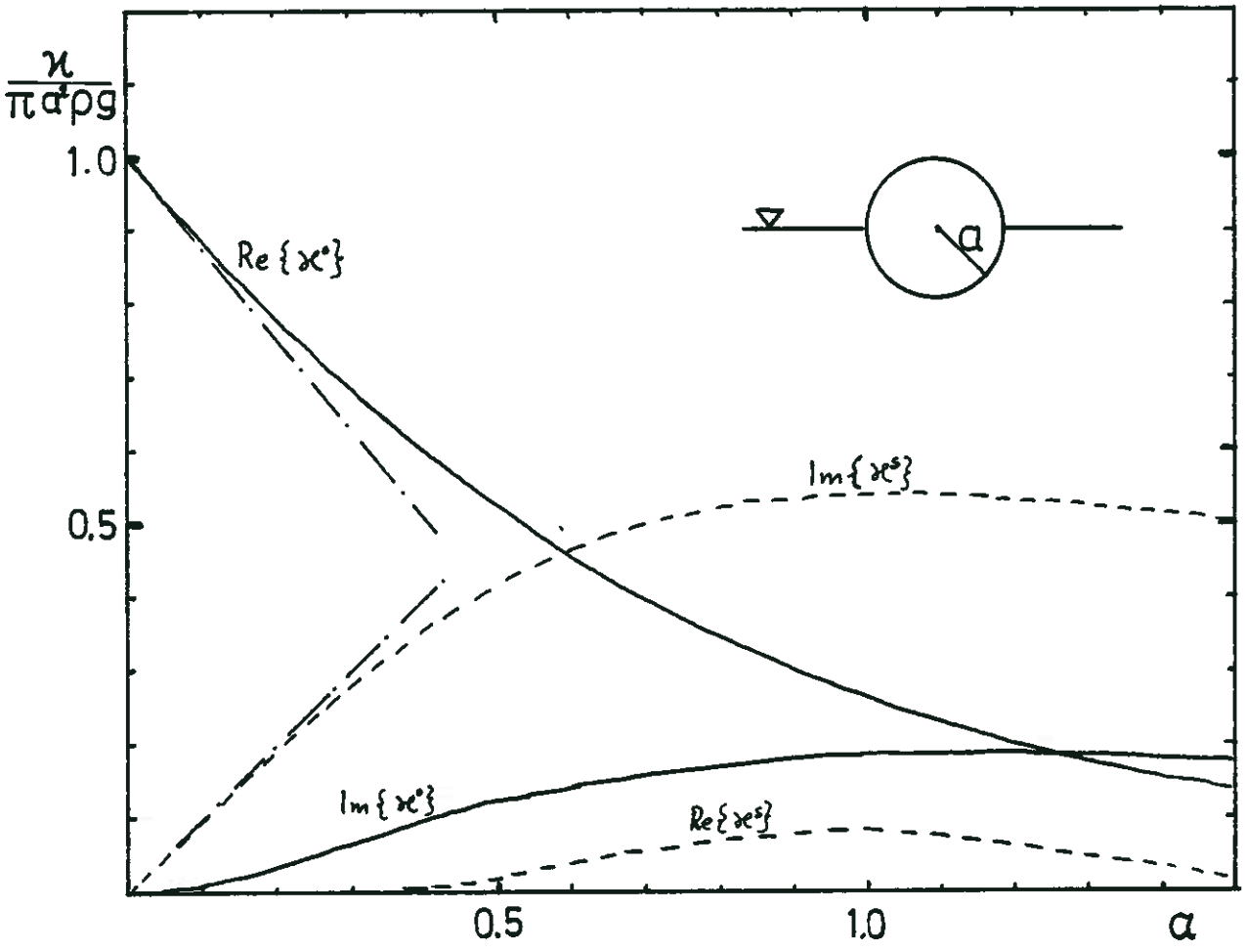

Fig. 6. Normalised exciting force coefficients for a semisubmerged sphere on deep water, calculated by a multi-pole expansion technic[18].

$\alpha \equiv ka$ - normalised buoy radius.

κ^o - heave force coefficient.

κ^s - surge force coefficient.

—·— small-body approximations according to (3.17) and (3.18).

comments on these formulae are listed below.

1) The diffraction force is of the same order as the Froude-Krylov force, except for floating buoys in heave where the latter dominates.

2) To the first order in α the surge force coefficient κ^s and the heave force coefficient κ^o are imaginary and real, respectively. Physically this means that the surge force is approximately 90^o out-of-phase and the heave force is approximately in-phase with the incident wave elevation $\eta_o(1)$.

3) Comparisons with more exact numerical values for κ^s and κ^o - see figs. 5 and 6 - indicate that the small-body approximations of (3.17) and (3.18) are quite accurate for non-dimensional buoy sizes less than $\alpha \sim 0.3$.

4) The significant phase difference between the heave force and the incident wave elevation goes like α^2 for small floating buoys. That is

$$\arg\{\kappa^o\} \approx O(\alpha^2) \tag{3.19}$$

provided that $A_w \sim \pi a^2$. Moreover, a quantitative expression for this phase shift is derived below.

Significant imaginary part of κ^o

It can be shown[19] that the Froude-Krylov force on a heaving axisymmetrical buoy is real, irrespective of buoy size α and depth of water kh. Any imaginary part, therefore, has to be found in the higher orders terms of the diffraction force F_d. See (A.36) and (A.37). In order to derive the second order term of F_d it is necessary to expand the gradient of ϕ_o to a higher order than what is done in (3.8). That is, we have to use the approximation

$$\left.\frac{\partial \phi_o}{\partial x_q}\right|_{S_1} \equiv v_q\big|_{S_1} \approx v_q(1) + \nabla v_q(1)\cdot(\vec{r} - \vec{r}_1) \qquad (3.20)$$

Without loss of generality we confine ourselves to the case of normal wave incidence ($\beta = 0$). From the incident wave potential of (A.19) we find that

$$\nabla v_q\big|_{S_1} = \begin{cases} (-i,0,\tanh(kz_1+kh))kv_1(1) & , \quad q = 1 \\ 0 & , \quad q = 2 \\ (-i,0,\tanh(kz_1+kh)+1/\cosh^2(kz_1+kh))kv_3(1) & , \quad q = 3 \end{cases} \qquad (3.21)$$

Eq. (3.20) then reads

$$v_q\big|_{S_1} = v_q(1)\{1 + (-i\xi + \zeta_q)\alpha + O(\alpha^2)\} \qquad (3.22)$$

where ξ and ζ_q are non-dimensional surface coordinates defined by

$$\xi = x/a$$

$$\zeta_q = \begin{cases} \tanh(kz_1+kh)z/a & , \quad q = 1 \\ \{\tanh(kz_1+kh)+1/\cosh^2(kz_1+kh)\}z/a & , \quad q = 3 \end{cases} \qquad (3.23)$$

Inserting (3.22) into the diffraction force expression (A.44) and using the expression (A.41) for the radiation impedance matrix it is seen that

$$F_d^p \approx \sum_{q=1}^{3} v_q(1)\left\{ Z^{pq} - i\omega\rho\alpha \iint_{S_1} \varphi^p(-i\xi+\zeta_q)n_q\,dS \right\} \qquad (3.24)$$

Taking the benefit of the symmetry for the problem and using (3.11), we finally get the diffraction part of the heave force coefficient:

$$\kappa_d^o \approx i\omega g_1 Z^o - \omega^2 \rho \alpha \iint_{S_1} \varphi^3 (f_1 \xi n_1 - g_1 \zeta_3 n_3) dS \qquad (3.25)$$

This expression is consistent to significant order of the normalised heave potential φ^3 that is for $\varphi^3(\alpha = 0)$. From the free surface condition (A.13), rewritten as

$$\frac{\partial \phi}{\partial (z/a)} = \alpha \tanh(kh)\phi \quad , \quad z = 0 \qquad (3.26)$$

it is realised that the degenerated "free" surface condition is just

$$\frac{\partial \phi}{\partial z} = 0 \quad , \quad z = 0 \ , \ \alpha = 0 \qquad (3.27)$$

Hence $(\partial \varphi^3 / \partial n)$ is real on all surfaces enclosing the fluid domain. See (A.14) and (A.15). It may then be realised - by the uniqueness theorem[20] and physical arguments - that φ^3 has to be real within the fluid. The significant imaginary part of the heave force coefficient is consequently

$$\mathrm{Im}\{\kappa^o\} = \mathrm{Im}\{\kappa_d^o\} \approx g_1 \omega R^o \qquad (3.28)$$

or - alternatively, by means of the relation (A.46) - :

$$\mathrm{Im}\{\kappa^o\} \approx \pi a^2 \rho g \ \{\tfrac{\pi}{2} g_1 \alpha^2 |\kappa^o / \pi a^2 \rho g|^2\} \qquad (3.29)$$

For half-immersed buoys $(z_1 = 0)$ the significant phase shift of the heave force coefficient κ^o is

$$\arg\{\kappa^o\} = \tfrac{\pi}{2} \alpha^2 + O(\alpha^3) \qquad (3.30)$$

To our knowledge the results of eqs. (3.29) and (3.30) are not previously published. They are, however, confirmed by numerical calculations. See fig. 7.

Because of the neglected terms of (3.25) - being of order $O(\alpha^3)$ - it should be noted that (3.29) is not consistent for completely submerged buoys.

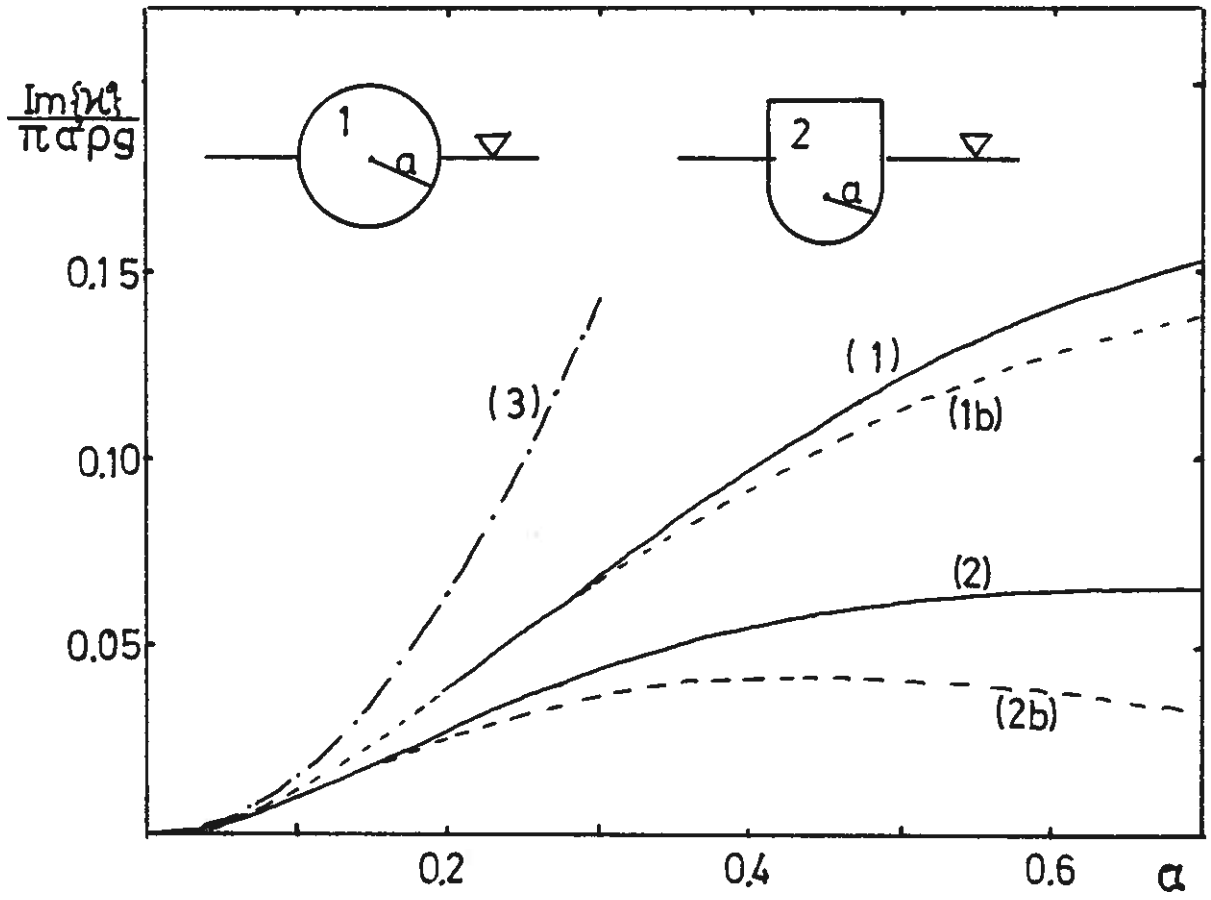

Fig. 7. Normalised imaginary part of the heave force coefficients for two different floating buoys, on deep water.

Curve (1) : Numerical values for buoy (1), according to Greenhow [18]. (Values are missing for $\alpha < 0.2$)

Curve (2) : Numerical values for buoy (2), according to Count [17].

Curve (3) : Lowest order term $\pi\alpha^2/2$ of eq. (3.29)

Curves (1b) and (2b): Approximations for the buoys (1) and (2), respectively, obtained by (3.29) when numerical values for $|\kappa^0|$ are used.

3.3 The non-scattering approximation.

It is intuitively evident that the scattering effects decrease as the dimension of the buoys decreases ($\alpha_i \to 0$). As a first approximation we therefore neglect the diffraction interaction forces, that is, the cross-coupling forces acting on a buoy due to the scattered waves from other buoys. Here we shall call this approximation the "non-scattering" (NS) approximation. For an arbitrary buoy no. i, then, neither the exciting force F_i nor the diagonal element Z_{ii} of the radiation impedance matrix are affected by the presence of other buoys. Consequently, we just have that

$$\kappa_i^{NS} = \kappa_i^o \tag{3.31}$$

$$Z_{ii}^{NS} = Z_{ii}^o \tag{3.32}$$

where the superscript ^{NS} refers to the non-scattering approximation. It should be noted that this approximation do not totally neglect the diffraction potential ϕ_d since κ_i^o includes both the Froude-Krylov force and the isolated diffraction force. See (A.34).

According to the NS assumption the potential due to heave motion u_j of buoy no. j is not disturbed by the other buoys. The corresponding wave elevation, see (3.6) and (A.18), is

$$\eta_j^o = -\frac{i\omega}{g} u_j \varphi_j^o \Big|_{z=0} \approx -\frac{\omega k}{2\rho g^2 D} \kappa_j^o H_o(kd_j) u_j \tag{3.33}$$

According to the far-field assumption (3.2) this radiated wave may be treated approximately as a plane wave at the site of another buoy. Thus the corresponding heave force acting upon another buoy no. i is

$$-Z_{ij}u_j \approx \kappa_i^o \eta_j^o(i) \quad , \quad i \neq j \tag{3.34}$$

The NS off-diagonal elements Z_{ij}^{NS} of the radiation impedance matrix are consequently

$$Z_{ij}^{NS} = \frac{\omega k}{2\rho g^2 D} \kappa_i^o \kappa_j^o H_o(kd_{ij}) \quad , \quad i \neq j \qquad (3.35)$$

Alternatively

$$Z_{ij}^{NS} = \frac{\kappa_i^o \kappa_j^o}{|\kappa_i^o \kappa_j^o|} \sqrt{R_{ii}^o R_{jj}^o}\, H_o(kd_{ij}) \quad , \quad i \neq j \qquad (3.36)$$

where the relation (A.46) has been used.
The right hand side of (3.36) is quite similar to a corresponding formula obtained by Falnes[21], except for the use of the Hankel function H_o and for the additional phase factor $\kappa_i^o \kappa_j^o / |\kappa_i^o \kappa_j^o|$.

An approximate value for the off-diagonal element R_{ij} of the radiation resistance matrix may also be derived from (A.45). Assuming isotropic heave force coefficients - that is, $\kappa_i \approx \kappa_i^o$, $i = 1,\ldots,N$ - (A.45) reduces to

$$R_{ij} \approx \frac{\omega k}{2\rho g^2 D} \kappa_i^{o*} \kappa_j^o J_o(kd_{ij}) \quad , \quad i \neq j \qquad (3.37)$$

where a well-known integral expression[22] for the Bessel function J_o has been used. It should be noted that this approximation is consistent with (3.35) only when the exciting force coefficients are real. Although either of the two approximate formulae (3.35) and (3.37) are based upon the assumption of isotropic heave force coefficients, the former seems to be the most accurate one. See fig.11.

3.4 Power invariance.

We have seen in section 3.2 that the heave force coefficient κ^o for a small axissymmetrical buoy is approximately real, irrespective of the buoy shape. Hereafter we shall use the term "ideal point absorber" for a buoy which has a real heave force coefficient and do not scatter waves. In the following we will show that the maximum power absorbed by a system of heaving ideal point absorbers is independent of the specific buoy shape.

We define the absorbed power P to be the sum of the useful P_c and the lost power P_l. According to (2.9) this total absorbed power is

$$P \equiv P_c + P_l = P_c(\underset{\sim}{R}_l = \underset{\sim}{0}) \tag{3.38}$$

From (2.15) and (2.14) we deduce that its maximum is just

$$P_{max} = \frac{1}{4}\,\underset{\sim}{\tilde{u}}^*\underset{\sim}{F}_i = \frac{1}{4}\sum u_i^* F_i \tag{3.39}$$

where the, otherwise unrestricted, velocity amplitudes u_i have to satisfy

$$\sum_{j=1}^{R} R_{ij}u_j = \frac{1}{2}F_i \tag{3.40}$$

Now, imagine that the geometry of buoy no. k is changed in a way so that κ_k is changed by a real factor, say c :

$$\kappa_i \to \kappa_i' = \begin{cases} c\kappa_i & , \quad i = k \\ \kappa_i & , \quad i \neq k \end{cases} \tag{3.41}$$

Because the NS approximation is an exact mathematical model for ideal point absorbers, eqs. (A.46), (3.31), (3.35) and (3.40) imply that

$$R_{ij} \to R_{ij}' = \begin{cases} c^2 R_{ii} & , \quad i = j = k \\ cR_{ij} & , \quad i = k \neq j \text{ or } i \neq k = j \\ R_{ij} & , \quad i \neq k \neq j \end{cases} \tag{3.42}$$

$$u_i \to u_i' = \begin{cases} \frac{1}{c}\,u_i & , \quad i = k \\ u_i & , \quad i \neq k \end{cases} \tag{3.43}$$

and finally from (2.4), (3.39) and (3.41)-(3.43)

$$P_{max} \to P'_{max} = P_{max} \tag{3.44}$$

Thus we have shown that the maximum power absorbed by a system

of unconstrained, heaving and ideal point absorbers is invariant to changes of the individual absorber geometry. Similar results are obtained previously by Budal[23] but his analysis is restricted to identical buoys and to special configurations.

Realising that the heave potential is approximately isotropic for small bodies even if they are not axisymmetrical, the statement above is valid even for arbitrary bodies provided that they are small enough.

3.5 The low-scattering approximation.

We now wish to look for an improvement to the NS approximation by taking also into account the interaction between bodies due to diffracted waves. This improvement leads to what we shall term the "low-scattering" (LS) approximation.

The first stage of this approximation involves writing the diffracted wave as a sum of elementary waves. That is

$$\phi_d \approx \sum_i \phi^o_{d,i} \qquad (3.45)$$

where $\phi^o_{d,i}$ represents the exact diffracted wave of buoy no. i if it were isolated. This approximation implies that multiple scattering is neglected. As opposed to the NS approximation the far-field parts of $\phi^o_{d,i}$ are now taken into account.

In general, an analytic solution of the single buoy diffraction problem does not exist. Fortunately, for small buoys it is possible to obtain good approximations for $\phi^o_{d,i}$ without solving the diffraction problem numerically. This is realised by the following.

A light and small body floating freely on surface waves does obviously not disturb the waves very much. This idea leads to a more general statement which is mathematically justified in appendix B. This statement is: When a small body, say buoy no. j, is moving in such a way that its

center of gravity (x_j,y_j,z_j) follows the orbit of the fluid particle of the incident wave, the disturbance of the incident wave is much smaller than the disturbance represented by the diffraction potential $\phi^o_{d,j}$. That is, the radiated wave potential $\phi^o_{r,j}$ due to the described motion approximately cancels the diffracted one. Hence

$$\phi^o_{d,j} \approx -\phi^o_{r,j} \equiv -\sum_{q=1}^{3} \varphi^{q,o}_j v_q(j) \tag{3.46}$$

By means of eq. (A.18), the far-field expressions for the normalised radiation potentials $\varphi^{p,o}_j$, see (3.6), and the explicit expressions for the undisturbed fluid velocity amplitudes $v_q(j)$, see (3.11), we deduce that the wave elevation associated with $\phi^o_{d,j}$ is approximately

$$\eta^o_{d,j} \approx i\frac{k^2 e(kz_j)}{2\rho g D}\left\{\tanh(kz_j+kh)\kappa^o_j H_o(kd_j) + \kappa^s_j H_1(kd_j)\cos(\gamma_j-\beta)\right\}\eta_o(j) \tag{3.47}$$

According to the far-field assumption this wave acts upon another buoy no. i by the force

$$\Delta F_i \approx \kappa^o_i \eta^o_{d,j}(i) = \kappa^o_i \eta_o(i)\Delta_{ij} \tag{3.48}$$

where the non-dimensional diffraction interaction term Δ_{ij} is given by

$$\Delta_{ij} = i\frac{k^2 e(kz_j)}{2\rho g D}\left\{\tanh(kz_j+kh)\kappa^o_j H_o(kd_{ij}) - \kappa^s_j H_1(kd_{ij})\cos(\gamma_{ij}-\beta)\right\}e^{-ikd_{ij}\cos(\gamma_{ij}-\beta)} \tag{3.49}$$

Because multiple scattering is neglected we simply obtain the LS heave force coefficient κ^{LS}_i by summing all such terms:

$$\kappa^{LS}_i = \kappa^o_i\left(1 + \sum_{\substack{j \\ j\neq i}} \Delta_{ij}\right) \tag{3.50}$$

Remember that the diffraction force $F^o_{d,i}$ due to $\phi^o_{d,i}$ is

already included in κ_i^o.

The LS radiation impedance matrix $\underset{\sim}{Z}^{LS}$ is derived in a similar way. The normalised radiated wave potential φ_j of buoy no. j is approximately

$$\varphi_j \approx \varphi_j^o + \sum_{\substack{k \\ k\neq j}} \varphi_{j,k} \tag{3.51}$$

where $\varphi_{j,k}$ represents the scattered wave on buoy no. k due to the undisturbed radiated wave from buoy no. j, represented by φ_j^o. In analogy with (3.46)

$$\varphi_{j,k} \approx - \sum_{q=1}^{3} \varphi_k^{q,o} \left. \frac{\partial \varphi_j^c}{\partial x_q} \right|_{\vec{r}=\vec{r}_k} \tag{3.52}$$

By means of (A.18), (3.6) and the fact[24] that

$$\frac{dH_o(x)}{dx} = -H_1(x) \tag{3.53}$$

it can be seen that the wave elevation $\eta_{j,k}$ corresponding to the velocity potential $\varphi_{j,k}u_j$ is

$$\eta_{j,k} \approx -i\frac{\omega k^3}{4\rho^2 g^3 D^2} \kappa_j^o e(kz_k)\Big\{\tanh(kz_k+kh)\kappa_k^o H_o(kd_{jk})H_o(kd_k) - i\kappa_k^s H_1(kd_{jk})H_1(kd_k)\cos(\gamma_k-\gamma_{jk})\Big\}u_j \tag{3.54}$$

The associating force acting upon another buoy no. i is approximately

$$-(\Delta Z_{ij})u_j \approx \kappa_i^o \eta_{j,k}(i) \quad , \quad i\neq k \tag{3.55}$$

This leads to the following expression for the LS radiation impedance matrix

$$Z_{ij}^{LS} = Z_{ij}^{NS} + \frac{\kappa_i^o \kappa_j^o}{|\kappa_i^o \kappa_j^o|} \sqrt{R_{ii}^o R_{jj}^o} \sum_{\substack{k \\ k\neq i,j}} \Delta_{ikj} \tag{3.56}$$

where the non-dimensional impedance correction term Δ_{ikj} is given by

$$\Delta_{ikj} = i\frac{k^2}{2\rho g D}\, e(kz_k)\Big\{\tanh(kz_k+kh)\kappa_k^o H_o(kd_{jk})H_o(kd_{ki}) - i\kappa_k^s H_1(kd_{jk})H_1(kd_{ki})\cos(\gamma_{ik}-\gamma_{kj})\Big\} \qquad (3.57)$$

An alternative expression

$$Z_{ij}^{LS} = \begin{cases} Z_{ii}^o + \dfrac{(\kappa_i^o)^2}{|\kappa_i^o|^2} R_{ii}^o \sum\limits_{\substack{k \\ k\neq i}} \Delta_{iki} & , \quad j = i \\ \dfrac{\kappa_i \kappa_j}{|\kappa_i^o \kappa_j^o|}\sqrt{R_{ii}^o R_{jj}^o}\Big\{H_o(kd_{ij}) + \sum\limits_{\substack{k \\ k\neq i,j}} \Delta_{ikj}\Big\} & , \quad j\neq i \end{cases} \qquad (3.58)$$

may be obtained by means of (3.32) and (3.36).

It is easily seen that $\Delta_{ikj} = \Delta_{jki}$. Consequently, the LS radiation impedance matrix $\underset{\sim}{Z}^{LS}$ is symmetrical and satisfies the resiprocity relation (A.42), as expected. Also it should be noted that for the special case N=2 we have that $Z_{12}^{LS} = Z_{12}^{NS}$.

4. DISCUSSION OF VALIDITY.

The main topic of this chapter is to see whether the NS and LS approximations are applicable to practical wave power buoys designed for typical ocean wave frequencies. In accordance to a suggestion made by Budal and Falnes[13] we concentrate our analysis about semisubmerged spherical buoys of diameter $2a = 10$ m. Operated in ocean waves of period $T = 6.5$ s - which represents the higher part of the energy spectrum - this is equivalent to a non-dimensional buoy radius $\alpha \approx 0.7$. See fig. 8. The pointabsorber assumption (3.1) is consequently not very well satisfied.

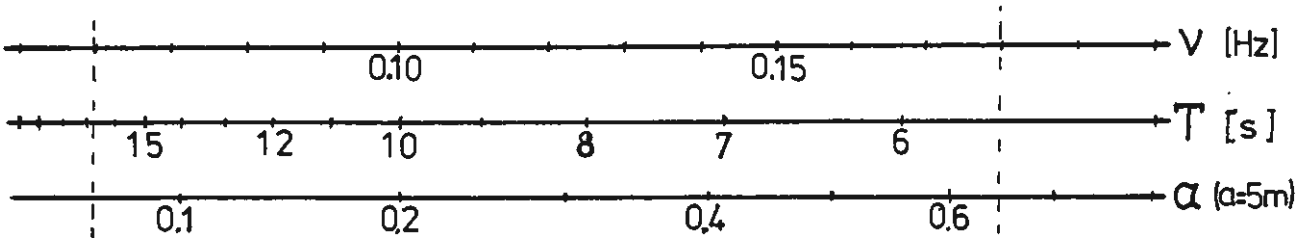

Fig. 8. Conversion scales for wave frequency ν, wave period T and non-dimensional buoy radius α. The buoy radius is $a = 5$ m and deep water conditons are assumed. The dashed bars indicate the limits of the wave energy spectrum of most interest[1].

As the suggested wave power plant involves buoy separation of as little as $d \approx 30$ m the neglected local fields may perhaps be of some importance. See assumption iv) of section 3.1. These facts, therefore, make it necessary to investigate the regimes of validity for our present approximations.

4.1 Comparison with numerical results for two-buoy systems.

The two-buoy system has already been numerically investigated by several authors[3-6]. Most of the methods used in the referred papers are general in the sense that they apply to bodies which need not satisfy the point-absorber assumption (3.1).

First, we compare our LS approximation with numerical results[17] for a pair of vertical floating cylinders with hemispherical bases. See fig. 5. The numerical method is a sink-source method and the two-buoy calculations has been carried out with 46 elements on each buoy. The associate discretisation errors are claimed to be less than 1-2%.

Results for the heave force ratio $|\kappa_1/\kappa^o|$, the radiation resistance ratios R_{11}/R^o and R_{12}/R^o are shown in figs. 9., 10 and 11, respectively. (As the buoys are identical we have, for convenience, omitted subscripts 1 or 2 on κ^o and R^o.) The LS values for the two-buoy system are, according to (3.50) and (3.58)

$$\left|\frac{\kappa_1^{LS}}{\kappa^o}\right| = |1 + \Delta_{12}| \approx 1 + \mathrm{Re}\{\Delta_{12}\} \tag{4.1}$$

$$\frac{R_{11}^{LS}}{R^o} = 1 + \mathrm{Re}\{(\kappa^o/|\kappa^o|)^2\Delta_{121}\} \tag{4.2}$$

and

$$\frac{R_{12}^{LS}}{R^o} = \mathrm{Re}\{(\kappa^o/|\kappa^o|)^2 H_o(kd)\} \tag{4.3}$$

where the non-dimensional correction terms Δ_{12} and Δ_{121} reduce to

$$\Delta_{12} = i\,\frac{k^2}{2\rho g}\{\kappa^o H_o(kd) - \kappa^s H_1(kd)\sin\beta\}e^{-ikd\sin\beta} \tag{4.4}$$

and

$$\Delta_{121} = i\,\frac{k^2}{2\rho g}\{\kappa^o (H_o(kd))^2 + i\kappa^s (H_1(kd))^2\} \tag{4.5}$$

when the buoys are situated along the y-axis and their centers coincide with the mean free surface.

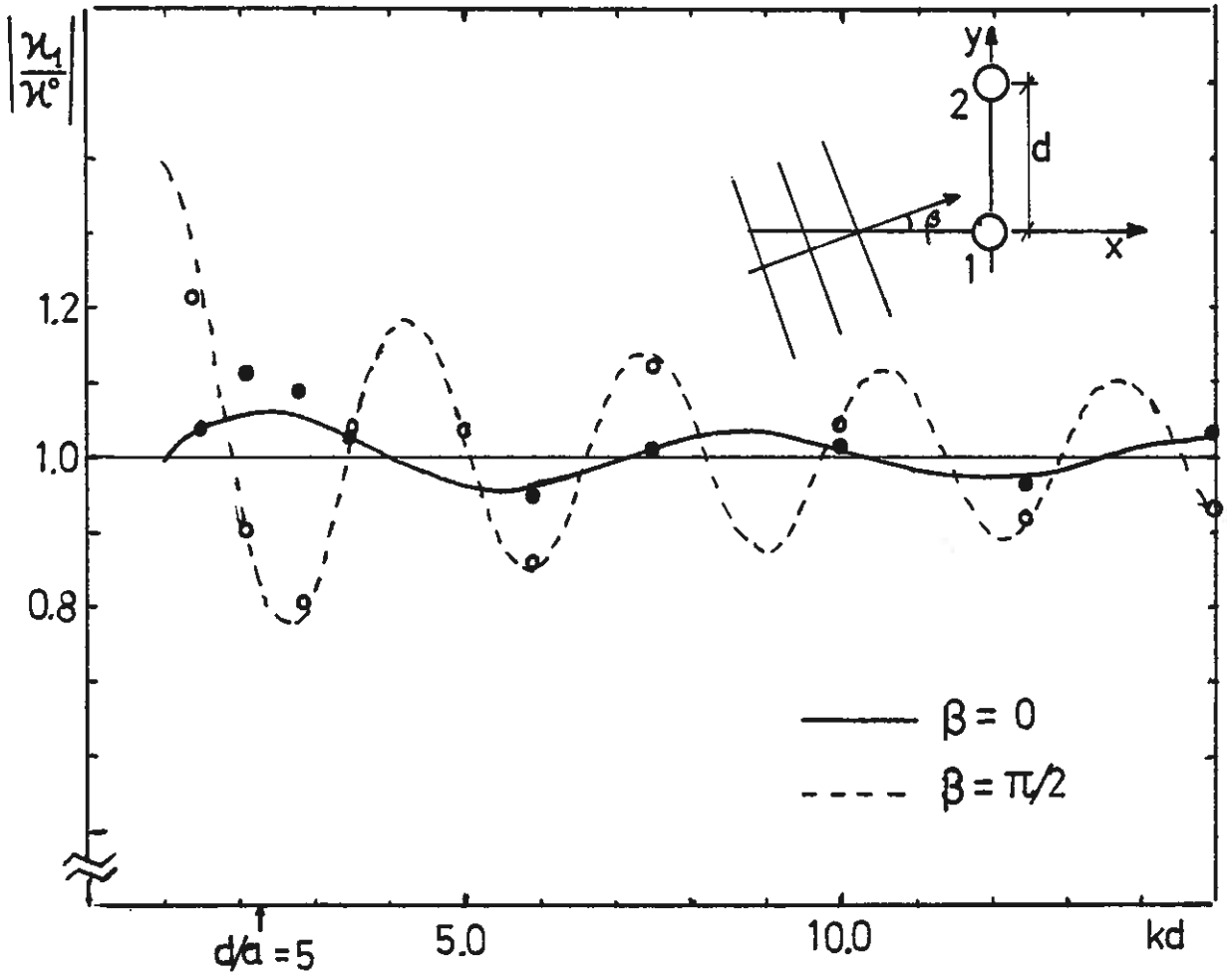

Fig. 9. Variation of heave force ratio $|\kappa_1/\kappa^o|$ with the normalised separation kd of two identical buoys. The buoys are vertical floating cylinders with hemispherical base and submergence L = 1.05a. See fig. 5.
Normalised buoy radius is $\alpha = 0.473$.
Curves (1) and (2): LS values according to (4.1) and (4.4) when numerical values for κ^o and κ^s are used. See fig.5.
• and o : Numerical values obtained by the sinc-source method[17].

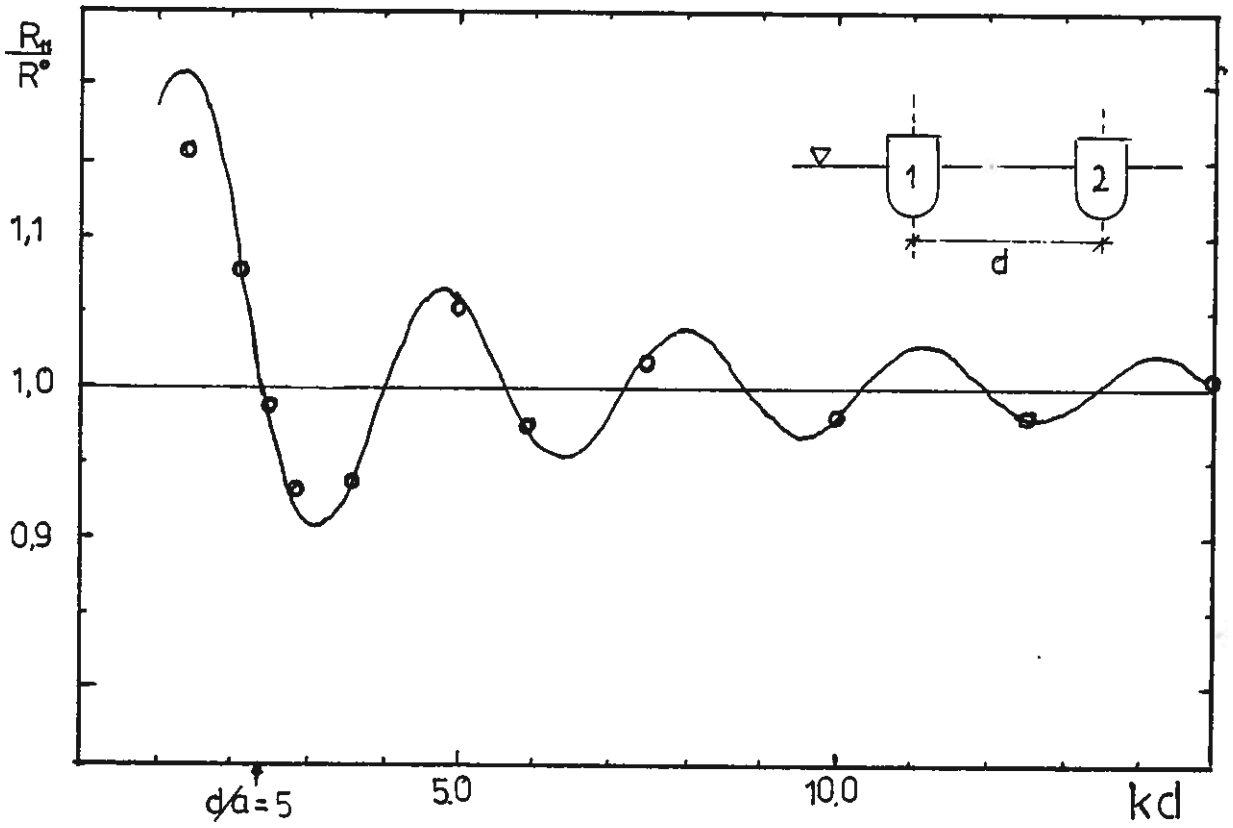

Fig. 10. Variation of the diagonal radiation resistance ratio R_{11}/R^{o} with the normalised separation kd of two identical buoys, as in fig. 9.

Solid curve: LS values according to (4.2) and (4.5) when numerical values for κ^{o} and κ^{s} are used. See fig. 5.

o : Numerical values obtained by the sink-source method[17].

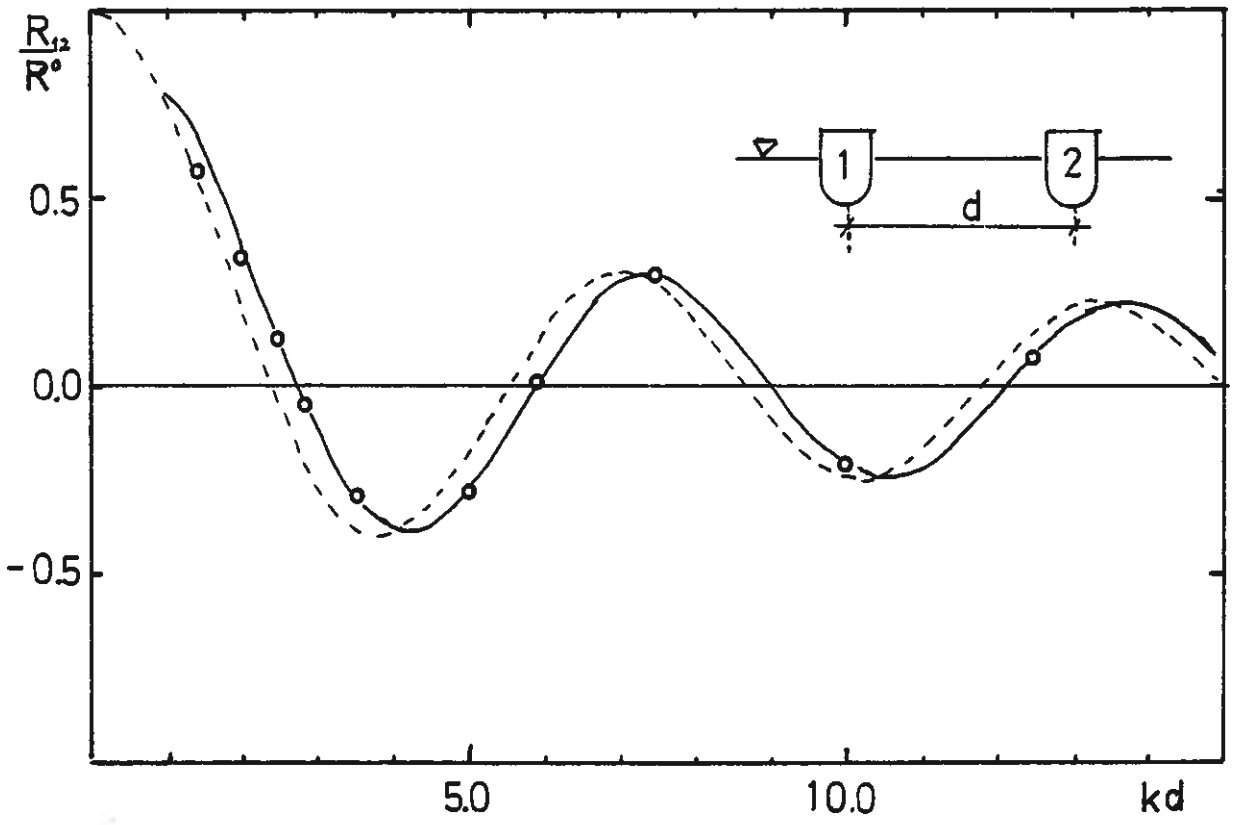

Fig. 11. Off-diagonal radiation resistance ratio R_{12}/R^{o} versus the normalised separation kd of two identical buoys as in fig. 9.

Curve (1): LS values according to (4.3) when numerical value for κ^{o} is used. See fig.5.

Curve (2): The Bessel function $J_{o}(kd)$.

o : Numerical values obtained by the sink-source method[17].

We see that the agreement between the LS approximations and the numerical results is excellent. For most cases the deviations are of the same order as the uncertainty of the numerical values, about 1-2%. However, we note that the filled and open rings in fig.9 tend to lie systematically outside and inside the solid and the dashed curve, respectively. This indicates that higher anisotropic terms - proportional to $\cos(n\gamma_i)$ and $\sin(n\gamma_i)$, $n \geq 2$ - of the exact scattered wave $\phi^o_{d,i}$ may be of some significance when $\alpha \gtrsim 0.5$. Nevertheless, the numerical results very well confirm the following:

1) The exciting force of buoy no. 1 is affected by another buoy in a way that causes κ_1 to oscillate about its isolated value κ^o. The oscillation is governed by the diffraction interaction term Δ_{12} which goes like

$$\Delta_{12} \propto (kd)^{-\frac{1}{2}} e^{-ikd(1+\sin\beta)} \qquad (4.6)$$

according to the asymptotic behaviour of the Hankel functions.

2) Also the radiation impedance Z_{11} of a buoy is substantially influenced by the scattering effect of a second buoy. The scattered wave from buoy no. 2 causes the diagonal radiation resistance R_{11} to be an oscillating function which tends towards R^o for large spacing. By means of the asymptotic behaviour of the correction term Δ_{121} :

$$\Delta_{121} \propto (kd)^{-1} e^{-i2kd} \qquad (4.7)$$

and of (4.6) it is realised that the scattering effects on the elements of the radiation impedance matrix decrease more rapidly with the spacing d than what is the case for the exciting forces.

3) The off-diagonal radiation impedance element Z_{12} is an

oscillation function proportional to the Hankel function. However, there is a significant phase shift between Z_{12}/R^{o} and H_{o}. This phase shift is associated with the complex phase factor $(\kappa_1^o\kappa_2^o/|\kappa_1^o\kappa_2^o|)$ and vanishes for ideal point-absorbers.

The excellent agreement between the LS values and the numerical values for κ_1 and R_{11} do, in fact, indicate that the approximations (3.46) and (3.51) are quite good even for relative large buoys not satisfying the point-absorber assumption (3.1) very well.

Next presented are some results concerning two floating vertical cylinders of flat bases and submergence $L = -Z_b = a/2$. Numerical results - obtained by Matsui and Tamaki[6] - as well as LS results are presented in figs. 12 and 13 for $|\kappa_1/\kappa^o|$ and R_{11}/R^o, respectively. As opposed to the previous two-buoy system the hydrodynamical parameters for this system have been evaluated as functions of frequency at the constant spacing/radius ratio $d/a = 5$. The method used for computing the numerical results take into account local fields as well as multiple scattering. Although the corresponding values are claimed to be quite accurate there is a substantial uncertainty associated with the solid curves of figs. 12 and 13. This is because they are redrawn from very small graphs in the published paper. For the highest frequencies corresponding to $\alpha \geq 0.5$ also the LS curves of figs 12 and 13 have to be treated with some caution. This is because the parametric approximations for κ^s and κ^o - used in the LS formulae - are based upon small graphs[26] for $|\kappa^s|$ and $|\kappa^o|$ and are consequently not quite reliable in this region. Nevertheless, the results shown in figs. 12 and 13 clairly demonstrate the applicability of the LS approximation.

Greenhow[3] has done calculations on two semisubmerged spheres. However, the heave force correction term due to scattering do not agree with our LS term Δ_{12}. It seems as if the orientation factor $e^{-ikdsin\beta}$ is missing in his correction term[27].

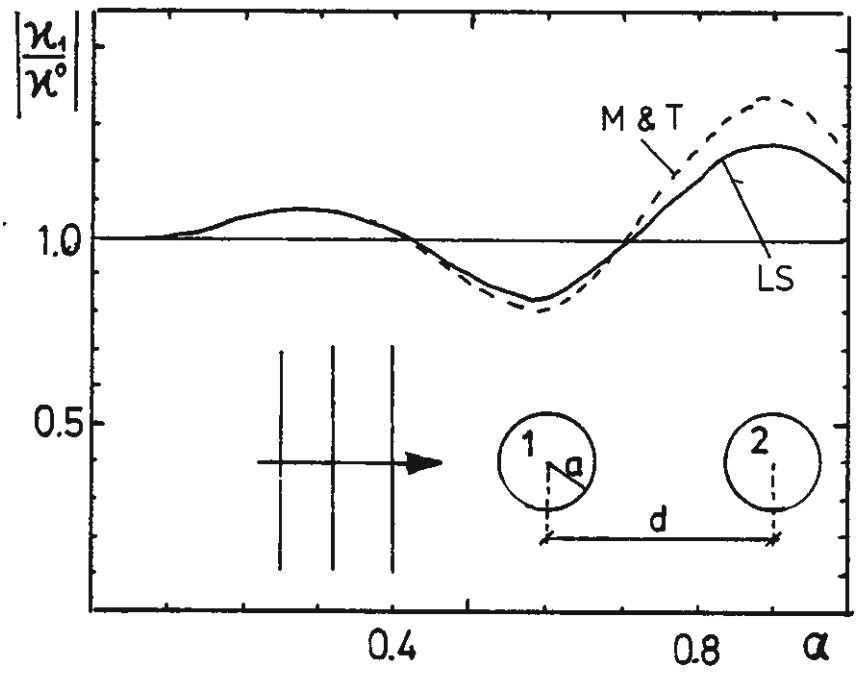

Fig. 12. Variation of the heave force ratio $|\kappa_1/\kappa^o|$ with the normalised frequency α for two identical buoys of spacing/radius ratio $d/a = 5$. The buoys are vertical cylinders with flat base. The submergence is $z_b = -a/2$.
Solid curve: LS values, according to (4.1) and (4.4) when approximate values for κ^o and κ^s are used.
Dashed curve: Numerical values according to Matsui and Tamaki[25].
The horizontal line $|\kappa_1/\kappa^o| = 1$ corresponds to the NS approximation.

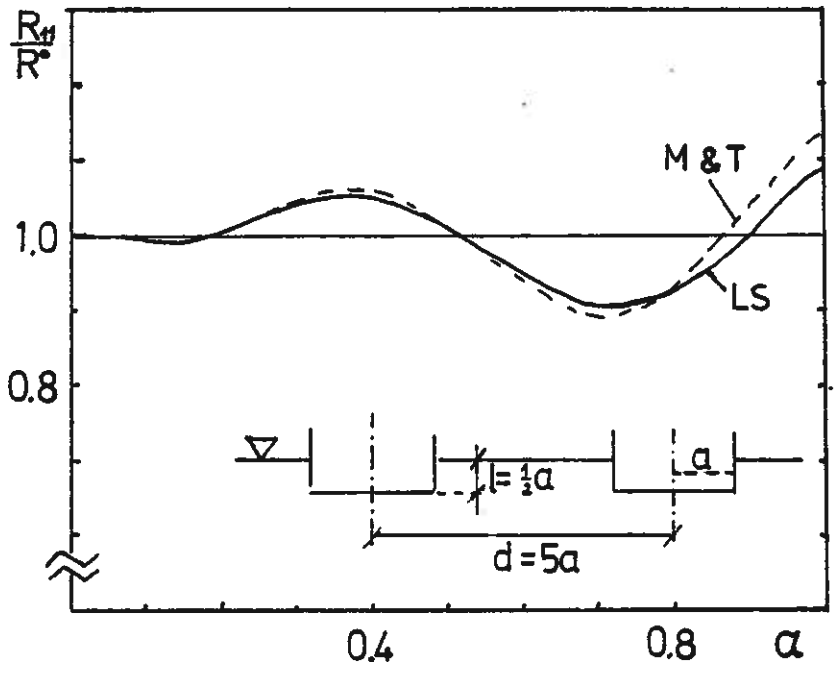

Fig. 13. Variation of the diagonal radiation resistance ratio R_{11}/R^{o} with the normalised frequency α for two identical buoys of spacing/radius ratio $d/a = 5$. The buoys are vertical cylinders with flat base. The submergence is $z_b = -a/2$.

Solid curve: LS values, according to (4.1) and (4.4) when approximate values for κ^{o} and κ^{s} are used.

Dashed curve: Numerical values according to Matsui and Tamaki[26].

The horisontal line $R_{11}/R^{o} = 1$ corresponds to the NS approximation.

4.2 Regimes of validity.

Now we are in the position of estimating the regimes of validity for the NS approximation as well as the LS approximation. The limits of these regimes are, of course, dependent on the requirement of precision. Here we choose the 5% relative error of the hydrodynamical parameter as a confidence criterion. First, we analyse our two approximations - the NS and the LS approximation - for systems of floating buoys. Next we will make some comments on the differences between such systems and systems of entirely submerged buoys.

The non-scattering approximation

Having seen that the LS approximation is quite good for $\alpha \sim 0.47$, we may analyse the NS model by means of the the LS parameters. For the heave force coefficient this is

$$\Delta\kappa_i^{NS} \equiv \kappa_i - \kappa_i^{NS} \approx \kappa_i^{LS} - \kappa_i^{o} \qquad (4.8)$$

This error is, of course, a function of buoy configuration and the specific buoy geometry as well as of α and separation kd. Confining ourselves to the case of two semi-submerged buoys we get a rough estimate of the relative error by using the lowest order term of (4.4)

$$\frac{\Delta\kappa^{NS}}{\kappa^{o}} \approx \Delta_{12} \approx \sqrt{\frac{\pi}{2}}\,\alpha^2 (kd)^{-\frac{1}{2}} e^{-i[kd(1+\sin\beta)-3\pi/4]} \qquad (4.9)$$

It should be emphasised that the expression above is based upon the far-field assumption. See (3.2) and (3.3). Ohkusu[4] has done calculations on wave forces on vertical cylinders and he claims that the local fields are negligible when

$$d/a \gtrsim 5 \qquad (4.10)$$

This far-field criterion is, in fact, confirmed by the the results of figs. 9, 10 and 11, too. Except for quite special buoy geometries, therefore, we assume our error analysis to be valid for $d/a \gtrsim 5$. In fig. 14 is tried to visualise the

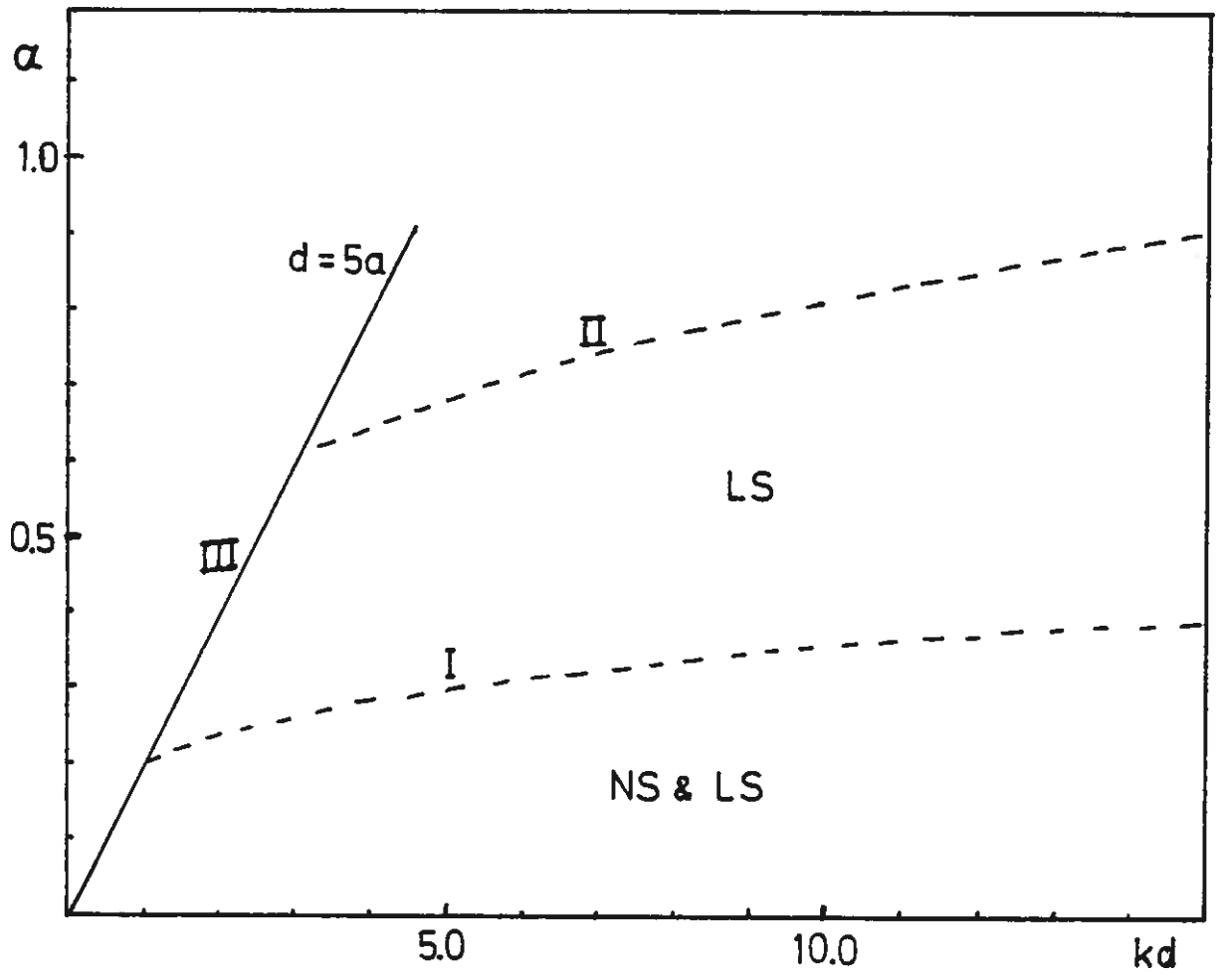

Fig. 14. A visualisation of the limitations for the NS and the LS approximations when applied to floating buoy systems. Neither of these two approximation is assumed to be valid for buoy spacings less than $d = 5\,a$, which corresponds to the domain to the left of curve III. The domain below curve I corresponds to the situations when the NS approximation is reliable. Accordingly, the curve II indicates the limit of validity for the LS approximation.

situations for which the NS approximation is applicable. Curve I is the limiting case when the modulus of the right hand side of (4.9) equals 0.05. Although the present analysis concerns the two-buoy system we expect that the regime of validity is almost the same for a multi-body system. For most configurations and frequencies the phases of the scattered waves will be distributed in such a way that they, to some extent, cancel each other. That is

$$\left|\sum_{\substack{j \\ j\neq i}} \Delta_{ij}\right| << \sum_{\substack{j \\ j\neq i}} |\Delta_{ij}| \qquad N >> 1 \qquad (4.11)$$

and

$$\left|\sum_{\substack{k \\ k\neq i,j}} \Delta_{ikj}\right| << \sum_{\substack{k \\ k\neq i,j}} |\Delta_{ikj}| \qquad N >> 1 \qquad (4.12)$$

Caution, however, has to be taken for some special configurations, for example a line of equidistant buoys of spacing $d = n \cdot \lambda$. Then the scattered waves will interfere constructively, and the resulting correction terms may become rather large.

See section 6.3 for further comments on the NS approximation.

The low-scattering approximation

Because accurate numerical results are missing for $\alpha > 0.5$, it is difficult to fix the regime for which the errors of the LS parameters are less than 5%. Nevertheless, knowing that the errors are less than 1-2% for $\alpha = 0.47$ even when $d/a = 5$, it is reasonable to suppose the LS approximation to be valid for $\alpha \approx 0.7$. The results of figs. 12 and 13 do in fact, support this assumption. The correction terms decrease with separation so we have chosen the domain of confidence to be as indicated in fig. 14. Because the local-field effects are not investigated in detail we, for sure, adopt $d = 5a$ as being one of the limitations for the LS approximation, too. In many cases the errors of the NS parameters are probably less than 5% even for shorter spacings.

The regime of validity of the LS approximation is less

sensitive to the configuration and the number of buoys than what is the case for the NS approximation. This is because all the first order scattered waves are taken into account and the errors may not accumulate in the same way as in the NS model. On the other hand, the regime of validity is very much affected by the accuracy of the coefficients κ^s and κ^o entering the LS formulae. Curve II of fig.14 would, for instance, be substantially lowered if the small-body approximations (3.17) and (3.18) were used instead of the "exact" coefficients.

The results of the LS model itself justify the neglection of multiple scattering. From the results of section 3.5 it may be deduced that

$$\left|\frac{\eta_{d,ij}}{\eta_{d,i}}\right| \approx |\Delta_{ij}| << 1 \qquad (4.13)$$

where $\eta_{d,ij}$ denotes the second order scattered wave on buoy no. j due to the first order scattered wave $\eta_{d,i}$. Thus, if multiple scattering were included in the LS model, the added terms would hardly be of any significance. It should, however, be noticed that inclusion of higher order scattered waves in the LS approximation would be inconsistent. This is because the first order scattering terms Δ_{ij} and Δ_{ikj} represent approximations which neglect terms of the same order in magnitude as the twice scattered waves.

One should at last notice that the correction terms Δ_{ij} and Δ_{ikj} are of order $O(1/\sqrt{kd})$ and $O(1/kd)$, respectively. For large separations, therefore, it is consistent to put $\underset{\sim}{Z}^{LS} \approx \underset{\sim}{Z}^{NS}$ while retaining the LS exciting force vector $\underset{\sim}{F}^{LS}$. With reference to fig. 10 such an approximation would not be reliable unless the more restricted far-field assumption (3.2) is satisfied, that is for kd greater than, say, 10.

Submerged buoy systems

It is instructive to study the asymptotic behaviour of the scattering terms Δ_{ij} and Δ_{ikj} as $\alpha \to 0$. Assuming deep

water condition it can be seen from (3.17), (3.18), (3.49) and (3.57) that

$$|\Delta_{ij}| \propto \begin{cases} \alpha^2/\sqrt{kd_{ij}} & \text{for half-immersed buoys} \\ e^{-2k|z_i|}\alpha^3/\sqrt{kd_{ij}} & \text{for submerged buoys} \end{cases}$$

and

$$|\Delta_{ikj}| \propto \begin{cases} \alpha^2/k\sqrt{d_{ik}d_{jk}} & \text{for half-immersed buoys} \\ e^{-2k|z_k|}\alpha^3/k\sqrt{d_{ik}d_{jk}} & \text{for submerged buoys} \end{cases}$$

The lessons to be learned from these asymptotic expressions are

1) The scattering effects are less for small submerged buoys than for floating buoys of corresponding size.

2) The depth factor, $\exp(-2k|z_i|)$ causes the scattering effects to stay small for submerged buoys even when α is not much less than unity.

From this we deduce that the NS approximation is more precise for submerged systems than for systems of floating buoys. The regime of NS validity is consequently larger for submerged buoys than what is indicated by curve I in fig. 14. Probably, the regime of validity for the LS approximation, too, is larger than what is indiated by curve II of the same figure.

4.3 Conclusions.

1) It has been justified that the scattering effect may be neglected provided that the buoys are small enough and that they are not too closely spaced. The relative significance of the scattering correction terms go like α^2 and α^3 for floating and submerged buoys, respectively.

2) The approximation of the isolated diffraction wave $\phi^o_{d,i}$ by the composite radiation wave $-\phi_r$ seems to be pretty good even for floating buoys of normalised radius as

large as $\alpha \approx 0.5$.

3) Except for buoys of quite special geometry the far-field assumption seems to be pretty well satisfied when the buoy spacings d is larger than $5a$.

4) A consequence of 2) and 3) is that the LS approximation applies for most of the ocean wave frequencies of interest even for buoys of diameter as large as $2a = 10$ m and spaced as closely as $d = 25$ m.

5) The LS approximation is a simple analytic model for interacting buoys. Its hydrodynamical parameters are expressed by the isolated exciting force coefficients only, and the execution times needed for computing the LS parameters are probably significantly less than what is needed by the methods used in the above cited references[3-6]. See table 1, page 48.

5. COMPUTING METHODS.

In order to gain knowledge of the dynamical behaviour and the power absorption properties of specific many-buoy systems, our mathematical model has to be implemented on a computer. The present chapter concerns assumptions and brief descriptions of the methods used in the computer program[27b].

5.1 Computing the hydrodynamical parameters.

The fundamental quantities of the LS approximation as well as the NS approximation, are the surge and heave force coefficients κ^s and κ^o. Because their small-body approximations (3.17) and (3.18) are not valid unless $\alpha \lesssim 0.3$ it is preferable to use more accurate values, for instance, parametric approximations based on numerical results. The parametric expressions used for evaluating the exiting force coefficients of the two buoy types shown in figs.5 and 6 contain enough fitting parameters to ensure quite correct coefficients for $\alpha < 1.0$.

The remaining hydrodynamical parameters- κ_i^{LS} , Z_{ij}^{NS} or Z_{ij}^{LS} - are evaluated according to (A.46), (3.36), (3.50) and (3.58). It should be noted that the diagonal radiation reactances $X_{ii}^o \equiv \omega m_{ii}^o$ are not considered since the model is intended for applications to phase-controlled buoys only.

The use of fast and accurate standard routines for evaluating the Hankel functions implies that no significant computer errors are attached to the output figures. The execution time needed for computing all the hydrodynamical parameters increases rapidly with the numbers of buoys. See the table 1 below. Of course, the resiprocity relation (2.44) is used so that only half of the off-diagonal elements of $\underset{\sim}{Z}$ are explicitly evaluated.

N	$\tau^{NS}(s)$	$\tau^{LS}(s)$
5	0.018	0.083
10	0.067	0.561
15	0.150	1.699
20	0.272	3.827
25	0.430	7.436

Table 1. Typical execution times τ for computing all the hydrodynamical parameters $\{\kappa_i\}$ and $\{Z_{ij}\}$

N - number of buoys

τ^{NS} - execution time when the non-scattering approximation is used

τ^{LS} - execution time when the low-scattering approximation is used.

5.2 Unconstrained power maximisation.

Hereafter we confine ourselves to multi-buoy systems where

i) all buoys are identical, that is

$$\left.\begin{aligned} \kappa_i^S &= \kappa^S \\ \kappa_i^O &= \kappa^O \\ Z_{ii}^O &= Z^O \end{aligned}\right\} \quad i = 1, .., N \qquad (5.1)$$

ii) the buoys are mechanically decoupled, that is

$$Z_{m,ij} = Z_{m,ii}\delta_{ij} \equiv (R_{c,ii} + R_{l,ii} + X_{m,ii})\delta_{ij} \qquad (5.2)$$

iii) the loss resistance matrix is a constant diagonal matrix, that is

$$\underset{\sim}{R}_1 = R_1 \underset{\sim}{I} \qquad (5.3)$$

$\underset{\sim}{I}$ being the $N \times N$ matrix of identity.

Because we consider phase-controlled buoys it is convenient to write the diagonal elements of the total impedance matrix in the following way

$$Z_{t,ii} \equiv Z_{ii} + Z_{m,ii} = R_{ii} + R_1 + Z_i \qquad (5.4)$$

where the conversion impedance elements Z_i are defined by

$$Z_i = R_i + iX_i \equiv R_{c,ii} + i(X_{ii} + X_{m,ii}) \qquad (5.5)$$

(We use a single index i on Z_i in order to avoid confusion with the radiation impedance element Z_{ii}.)

A consequence of the assumption ii) is that the useful absorbed power by a system of N buoys equals the sum of absorbed power in each buoy:

$$P_c = \sum_{i=1}^{N} P_{c,i} = \frac{1}{2} \sum_{i=1}^{N} R_i |u_i|^2 \qquad (5.6)$$

Now, let us turn to the power maximisation problem. If there are neither bounds on the elements Z_i nor restrictions on the heave amplitudes $|u_i|$ the maximum power is found by the following three steps.

1) Find the optimal velocity vector u_{opt} by solving the matrix equation (2.15). Use $u = u_{opt}$ in the following steps.
2) Find the corresponding optimal conversion impedance elements Z_i from the equations of motion which may be written in the following way

$$(R_{ii} + R_1 + Z_i)u_i = F_i - \sum_{\substack{j \\ j \neq i}} Z_{ij} u_j \qquad (5.7)$$

3) Find P_c by using (5.6).

Although the complex matrix equation of (2.15) may be split into two real equations, a general routine for solving complex linear equations is applied. The routine is a single precision one, but several checkings of the solutions did not reveal any rounding errors of significance. However, the execution times become seriously long for large N. See table 2.

N	τ(s)
5	0.022
10	0.097
15	0.251
20	0.517
25	0.915

Table 2. Typical execution times τ for solving a set of N linear complex equations.

5.3 Power maximisation under motion constraints.

In many practical situations it is difficult or even practically impossible to achieve optimum buoy motion as described by (2.15). For instance, the heave amplitude for a floating buoy cannot be larger than its physical dimension. This leads to the problem of power absorption under motion constraints. This problem is recently studied by Evans[28] and by Falnes and Budal[29]. We here present a computer implemented technique for solving a quite general problem of constrained power maximisation.

We distinguish between the following kinds of constraints.

a) Bounds on the variables, which are the real and imaginary parts of Z_i.

b) Amplitude constraints.

The first kind is generally of the form

$$x^{min} \leq x \leq x^{max} \qquad (5.8)$$

where x represents one of the variables. Resonant buoy condition is a special case of this:

$$X_i^{max} = X_i^{min} = 0 \quad , \quad i = 1,... \qquad (5.9)$$

For non-absorbing reflecting buoys the appropriate bounds on R_i are

$$R_i^{max} = R_i^{min} = 0 \qquad (5.10)$$

The resistance bounds for practical absorbing buoys depend on the specific turbine and generator characteristics.

For simplicity we shall here confine ourselves to the case when the variables are either fixed or unbounded. It is then convenient to introduce a new real vector $\underset{\sim}{x}$ containing those resistance elements R_i and reactance elements X_i which are not fixed. The dimension of $\underset{\sim}{x}$ thus equals the number of unbounded real variables in the conversion impedance matrix and is denoted by n_{max}. For instance, if each buoy is resonant and possesses an adjustable power take-off equipment, then $\underset{\sim}{x}$ contains the resistance elements, only, and $n_{max} = N$.

While a) represents a special type of linear constraints, the amplitude restrictions of b) are non-linear. This is because the velocity amplitude $|u_i|$ is not a linear function of the variables of $\underset{\sim}{x}$. It is usual to write the non-linear constraints as inequality constraints; in our case we set

$$c_i(\underset{\sim}{x}) \equiv 1 - |u_i|/\omega s_{max} \geq 0 \quad , \quad i = 1,...,N \qquad (5.11)$$

These constraints are said to be active if c_i are negative.

The mathematical formulation of the simplified maximisation problem we term "P1", and it reads

$$\text{P1:} \qquad \underset{\underset{\sim}{x}}{\text{Maximise}} \ \{P_c(\underset{\sim}{x}) | c_i(\underset{\sim}{x}) \geq 0 \quad , \quad i = 1,...,N\}$$

The problem of unconstrained power maximisation - hereafter called P0 - is a special case the problem of P1 if $s_{max} \to \infty$. In this case $\underset{\sim}{x}$ contains all the 2N real parameters of R_i and X_i and all the amplitude constraints (5.11) are inactive. However, the general problem P1 is by far much more complicated to solve than P0. Firstly, the constrained optimum velocity vector $\underset{\sim}{u}_{opt}$ cannot be found by any simple relation. Secondly, analytic expressions for neither the first nor the second order derivatives of P_c - with respect to the variables x_i - are available. The reason is that $P_c = P_c(\underset{\sim}{u}(\underset{\sim}{Z}_m(\underset{\sim}{x})))$ is an implicit function of $\underset{\sim}{x}$. See (2.10), (2.1) and (2.7).

Although computer routines for non-linear constrained minimisation problems are available, none of them were used for solving P1. The reasons for that are: 1) the routines are very general so that a lot of programming work is required, 2) it is feared that execution times due to frequent function evaluations will be large, and finally 3) an alternative simple procedure did work for most cases of interest. This procedure is outlined in the following.
Motivated by the Langrangian method[30] we consider a related but simpler problem

P2: $\underset{\underset{\sim}{x}}{\text{Minimise}} \{F(\underset{\sim}{x})\}$

where $F(\underset{\sim}{x})$ is an objective function chosen so that the solution of the problem P2 is approximately equal to the solution of P1. In the computer program we have chosen one of the following three forms of $F(\underset{\sim}{x})$

$$F(\underset{\sim}{x}) = \begin{cases} F_1(\underset{\sim}{x}) = -P_c(\underset{\sim}{x}) \\ F_2(\underset{\sim}{x}) = -P_c(\underset{\sim}{x}) + W(\underset{\sim}{x}) \\ F_3(\underset{\sim}{x}) = -P_c(\underset{\sim}{x}) + W'(\underset{\sim}{x}) \end{cases} \qquad (5.12)$$

where

$$W = C \sum_{i=1}^{N} (\min(0, c_i(\underset{\sim}{x})))^2 \qquad (5.13)$$

is a smooth barrier function, and

$$W' = C \sum_{i=1}^{N} (c_i(\underset{\sim}{x}))^2 \qquad (5.14)$$

is a smooth well function. C is a positive constant or variable. The functions W and W' are illustrated in fig. 15. The splitting up into three different cases has been done

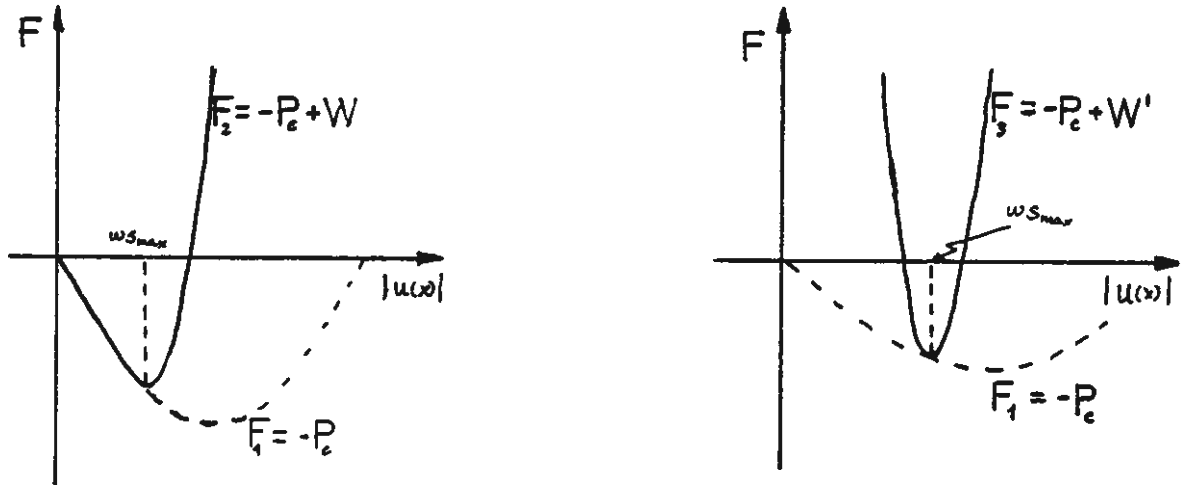

Fig. 15. Schematical drawings which show the effects of using a barrier function W and a well function W'. Minimisation of the objective functions F_2 and F_3 ensure that the inequality constraint $|u| \leq ws_{max}$ and the equality constraint $|u| = ws_{max}$, respectively, are approximately satisfied.

for computational reasons. Because the second order derivatives of the barrier function $W(\underset{\sim}{x})$ are not continuous when $c_i(\underset{\sim}{x}) = 0$, it causes some troubles in the minimisation procedure. Therefore, at low incident waves when none of the constraints (5.11) are active, the first objective function F_1 is used, whereas the last one, F_3, is used when the waves are so large that all of the constraints are active. Supported by the illustrations in fig. 15 it is realised that the solution of P2 approximates the solution of the original constrained problem P1 when the constant C becomes large, that is, when $C/P_c \to \infty$.

The routine written for solving the problem P2 is based upon the following simplified algorithm

i) Select an objective function $F(\underset{\sim}{x})$, a convergence criterion and a starting variable vector $\underset{\sim}{x}^{(o)}$

ii) Set $n = 1$

iii) Minimise $\{F(\underset{\sim}{x})\}$. Update the variable x_n.
x_n

iv) Repeat iii) for $n = 2,\ldots,n_{max}$

v) Return to ii) if the convergence criterion is not satisfied.

The convergence criterion used in the computer program is

$$|\Delta F^{(i)}| \equiv |F^{(i)} - F^{(i-1)}| < |F^{(i)}|\epsilon \qquad (5.15)$$

where $F^{(i)}$ denotes the objective function after running through the loop ii)-iv) i times and ϵ is a convergence parameter. Step no. iii) is a one-dimensional optimisation problem because all the remaining variables $\{x_i | i \neq n\}$ are regarded as being constant parameters. The method used for executing the step no. iii) is illustated in fig.16. It is based upon the assumption that the objective function $F(x_n)$ in a certain neighbourhood of the minimum may be approximated by a second order polynomial in x_n. Because each evaluation of F involves solving the N-dimensional complex equation of motion (2.1) the total execution time for the optimisation routine critically depends on the efficiency of step no. iii). See table 2. In order to combine the requirements of solving this one-dimensional minimisation problem by a minimum of steps and to an acceptable accuracy the subroutine possesses some refinements not shown in fig.15: 1) the initial step length is adjusted according to the convergence parameter ϵ and to the curvature of $F(x_n)$, and 2) a special procedure handles the cases when the second order derivative $(\partial^2 F/\partial x_n^2)$ is non-positive.

5.4 Comments on the computer efficiency.

The results exhibited in table 1 tell us that the execution times for computing the hydrodynamical parameters may become seriously long for large systems. However, it is not believed that these times can be drastically reduced by any programming tricks. Evaluations of the Hankel functions $H_o(kd_{ij})$ and $H_1(kd_{ij})$ probably represent the major part of these execution times, but the applied single precision

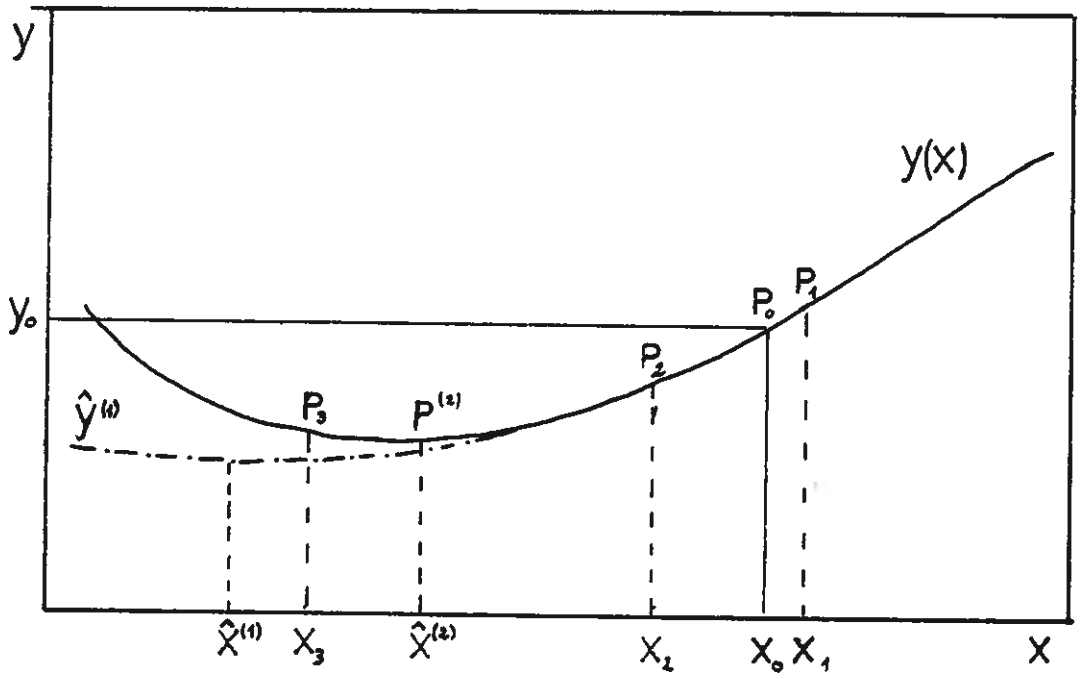

Fig. 16. An example which illustrates the method applied for solving a one-dimensional optimisation problem. The objective function and an arbitrary variable are denoted by y and x, respectively. Explanation of the successive steps:

1) A point $P_1 \equiv (x_1, y_1)$ is evaluated beside the starting point P_o.
2) Evaluate the second point P_2 in the direction of negative slope.
3) A parabola $\hat{y}^{(1)}$ (dashed curve) is fitted to P_o, P_1 and P_2, and $\hat{x}^{(1)}$, which minimises $\hat{y}^{(1)}$, is found analytically.
4) Because $\hat{x}^{(1)}$ is outside the region defined by x_1 and x_2, a new point P_3 is evaluated.
5) Another parabola $\hat{y}^{(2)}$ is fitted to the points P_3, P_2, P_o, and $\hat{x}^{(2)}$ is derived.
6) Because $\hat{x}^{(2)}$ lies within the region defined by x_3 and x_o we assume that $y(\hat{x}^{(2)}) \approx y_{min}$.

routines proved to be very fast, even compared to a self-supplied and less accurate Hankel function routine.

The execution time for solving the unconstrained optimisation problem would probably be reduced by rewriting (2.15) as two real $N \times N$ matrix equations. This is because it is faster solving a real matrix equation of two right hand side vectors - $\mathrm{Re}\{\underset{\sim}{F}\}$ and $\mathrm{Im}\{\underset{\sim}{F}\}$ - than solving a general complex matrix equation with a sigle right hand vector. In the actual computer program the equation (2.15) was, for convenience, solved by the same routine as used for solving the equation of motion (2.1).

The greatest problems and challenges to improvements are, however, to be found in the problem of constrained optimisation. Difficulties tend to pile up when

1) the couplings between the buoys are strong, for example when lightly loaded buoys are closely spaced.
2) the barrier function W is used.
3) the number n_{max} of variables is large.

The typical problem of case 1) is slow convergence. See the illustration in fig. 17. Bad or missing convergence is the problem of the case 2) as well, but now the reason is probably that the quatratic approximation of the objective function F_2 fails when the constraints are active. This is realised from the fact that second order devivatives $\partial^2 W/\partial x_n^2$ are discontinous when $c_i(\underset{\sim}{x}) = 0$. A common problem associated with case 3) is that the objective function possesses local minima. Not unexpectedly, this problem is most pronounced when the reactances X_i are variables of optimisation. When the optimal phase or relative reactance $(X_i/R_{t,ii})$ is large, the corresponding buoy motion is small, implying that a sign flip $X_i \rightarrow -X_i$ will affect the power P_c to a small extent. See the illustration in fig.18. Consequently, it is difficult to optimise the power with respect to the reactances for large systems, especially if the buoys are lightly loaded and strongly coupled.

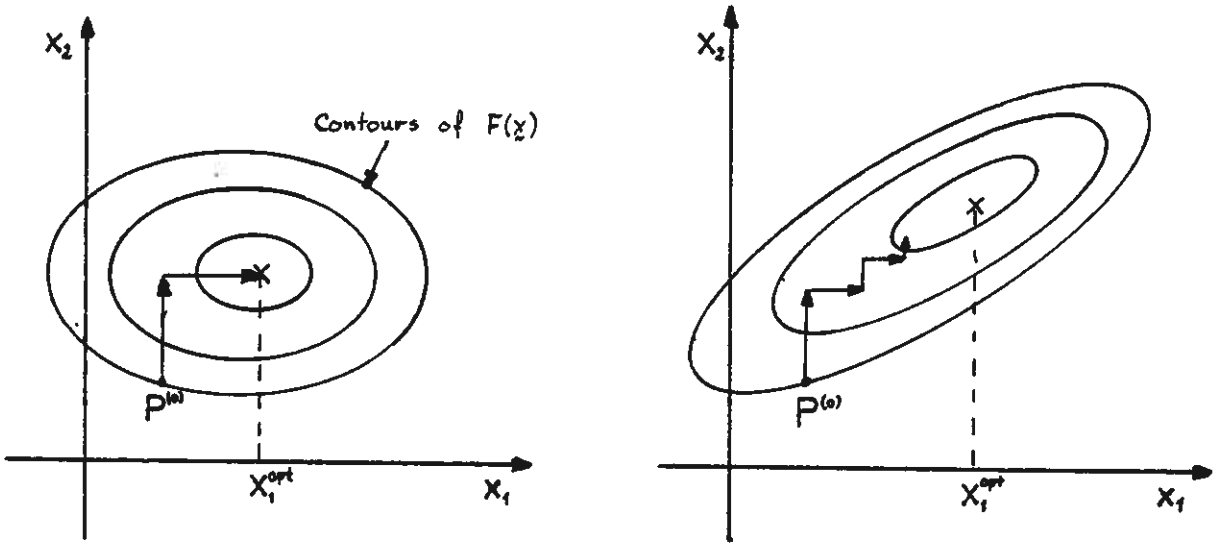

Fig. 17. Geometrical interpretation of the optimisation procedure for two different cases:
1) the coupling terms between the variables are small.
2) the coupling terms are strong.
While the the minimum of F is found in a few steps for the first case, the zigzagging path of the latter case implies slow convergence.

Some of the mentioned convergence problems would probably be reduced by using a more sophisticated optimisation procedure. With reference to fig. 17 a sort of directional descent method[30] would probably be more efficient for systems where the couplings are relatively important. However, a thorough outline of an improved method in constrained optimisation is beyond the scope of this thesis. We are content to point out that there is room for considerable improvements.

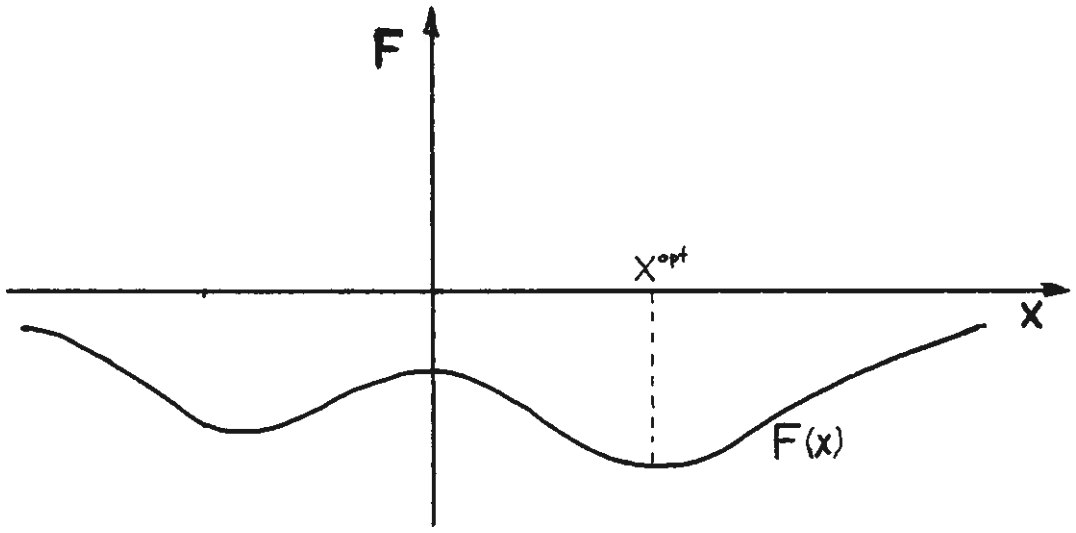

Fig. 18. Illustration of a situation which causes troubles in the procedure for constrained optimisation. The objective function possesses a local minimum in addition to the global one. This is a typical situation when x represent a reactance and the number of optimisation variables, n_{max}, is large.

6. APPLICATONS.

6.1 Definitions and some results for an isolated buoy.

A main topic of this chapter is to investigate the interaction effect within groups of equal wave-power buoys. Therefore, it is reasonable to study the ratio Q defined by

$$Q = P_{c,max}/NP_c^o \qquad (6.1)$$

Here $P_{c,max}$ is the maximum useful power converted by the whole system. Further, P_c^o is the maximum useful power convertable by one isolated buoy. Both $P_{c,max}$ and P_c^o are, in general, functions of a lot of factors, included the loss resistance R_1 and, if any, the imposed constraints. Hereafter we shall term Q the "interaction factor". Its value gives some information of how the wave-power buoys within a given configuration are interacting. If the interaction forces between different buoys are relatively small, Q will be approximately equal to unity. It should be noted that Q, in general, differs from the interaction factors used by Budal[23], Falnes[7] and Evans[10]. Their expressions for the interaction factor are based upon the assumptions of 1) real exciting force coefficients, 2) no losses and 3) no amplitude constraints. (Budal also assumed equal heave amplitudes.) Denoting the interaction factor used by Falnes and Evans by Q^E, we thus have that Q^E is a special case of the more general interaction factor Q:

$$Q^E = \lim_{a \to 0} Q(R_1 = 0) \quad , \text{ no constraints} \qquad (6.2)$$

The interaction factor Q does not give any information of how the power is distributed among the individual buoys. In order to study this distribution, therefore, it is convenient to define an individual interaction factor Q_i by

$$Q_i \equiv P_{c,i}/P_c^o = \frac{1}{2} R_i |u_i|^2 / P_c^o \qquad (6.3)$$

where $P_{c,i} = \frac{1}{2} R_i |u_i|^2$ is the actual useful power converted by buoy no. i. Hence Q is simply the mean value of all Q_i. In the special case of dynamical focusing, see section 6.2, where all the reflecting buoys are non-absorbing ($R_i = 0$, $i = 2,..,N$), we have that $Q = Q_1/N$.

Next it is convenient to introduce a critical wave amplitude $|\eta_{cr}|$ defined by

$$\text{Max}\left\{|u_i^{opt}| : i = 1,\ldots,N\right\} = \omega s_{max}, \quad |\eta_o| = |\eta_{cr}| \qquad (6.4)$$

where u_i^{opt} is the unconstrained optimum of the velocity amplitude of buoy no. i. Hence $|\eta_{cr}|$ represents the largest incident wave for which all amplitude constraints are passive. Strictly speaking, one should multiply ωs_{max} in (6.4) by a frequency dependent factor because the first harmonic component $|u_i|/\omega$ of a latched buoy motion is slightly greater than the physical maximum s_{max}. See fig. 2. However, it is assumed that this correction factor will affect the absorption characteristics very little.

In fig. 19 is shown how the critical wave amplitude $|\eta_{cr}^o|$ for an absorbing, isolated and semi-submerged sphere varies with the wave frequency ν. The depth of water used throughout is $h = 500$ m which ensures deep water condition for all frequencies considered. We see that $|\eta_{cr}^o|$ increases very rapidly with the wave frequency ν. This fact is easily derived from (2.1), (3.18) and (A.46), showing that buoy/wave amplitude ratio is

$$\left|\frac{u^{opt}}{\omega\eta_o}\right| = \left(\frac{R^o}{R^o+R_1+R_c}\right) \cdot \frac{|\kappa^o|}{\omega R^o} = O(\alpha^{-2}) = O(\omega^{-4}) \qquad (6.5)$$

in the low-frequency limit $\omega \to 0$. Another feature indicated by the different curves of fig. 19 is that the critical wave amplitude increases as the total load resistance $(R_c + R_1)$ increases.

Most of the results in this chapter are presented in normalised form. In order to get a feeling of what is the

absolute value of the absorbed power we have plotted the constrained maximum power P_c^o in fig. 20 for some frequencies. We see that P_c^o is a quadratic or a linear function of $|\eta_o|$ for $|\eta_o| < |\eta_{cr}^o|$ or $|\eta_o| > |\eta_{cr}^o|$, respectively.

The results of figures 19 and 20 should be treated with some caution because they are derived from linear theory. For buoy amplitudes as large as s_{max} the exciting force is obviously not independent of the buoy elevation as assumed in linear theory. Especially, we expect that non-linearities become significant when the actual water-plane area is not a constant. Nevertheless, we assume that the results of fig. 19 and 20 represent reasonable estimates of the true values for $|\eta_{cr}^o|$ and P_c^o, respectively.

For later use it is convenient to give a precise definition of the following terms:

1)	resonant buoy:	a buoy, say no. i, for which the diagonal reactance is fixed and equals zero, that is, $\chi_i = 0$.
2)	phase-optimisation:	optimisation of power with respect to the principal reactance elements χ_i.
3)	non-absorbing buoy:	a buoy of no power take-off equipment, also called a reflecting buoy.
4)	beam seas:	incident waves with wave crests parallel to a linear row of buoys.
5)	head seas:	incident waves which have their direction of propagation parallel to a linear row of buoys.

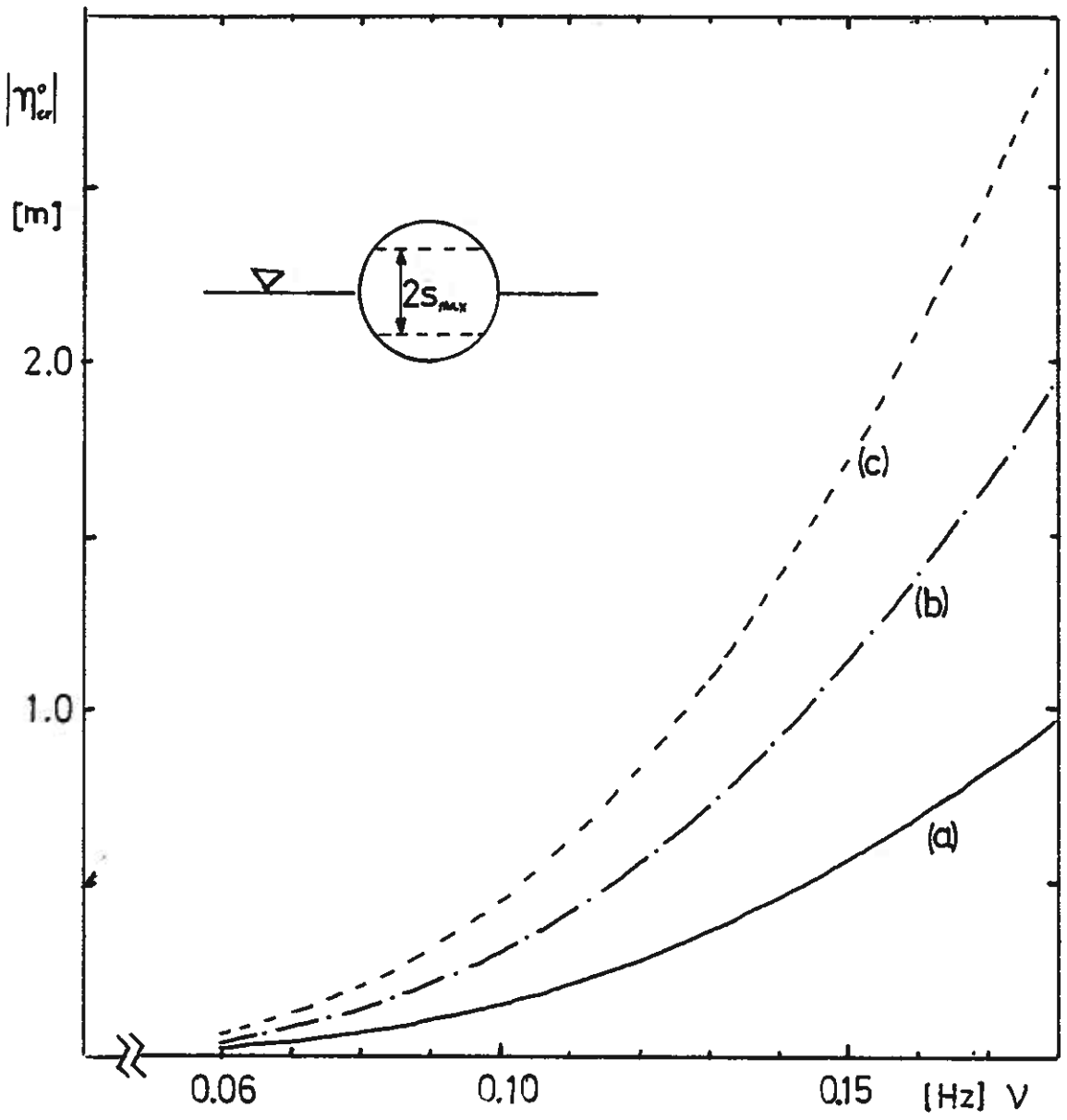

Fig. 19 Critical wave amplitude $|\eta^o_{cr}|$ versus wave frequency ν for an isolated semi-submerged sphere of radius $a = 5$ m and maximum heave amplitude $|u/\omega|_{max} = s_{max} = 3$ m.

Curve (a): Unloaded buoy of no loss resistance.

Curve (b): Optimally absorbing buoy of no loss resistance.

Curve (c): Optimally absorbing buoy with loss resistance $R_1 = \frac{1}{2} R^o(\nu)$.

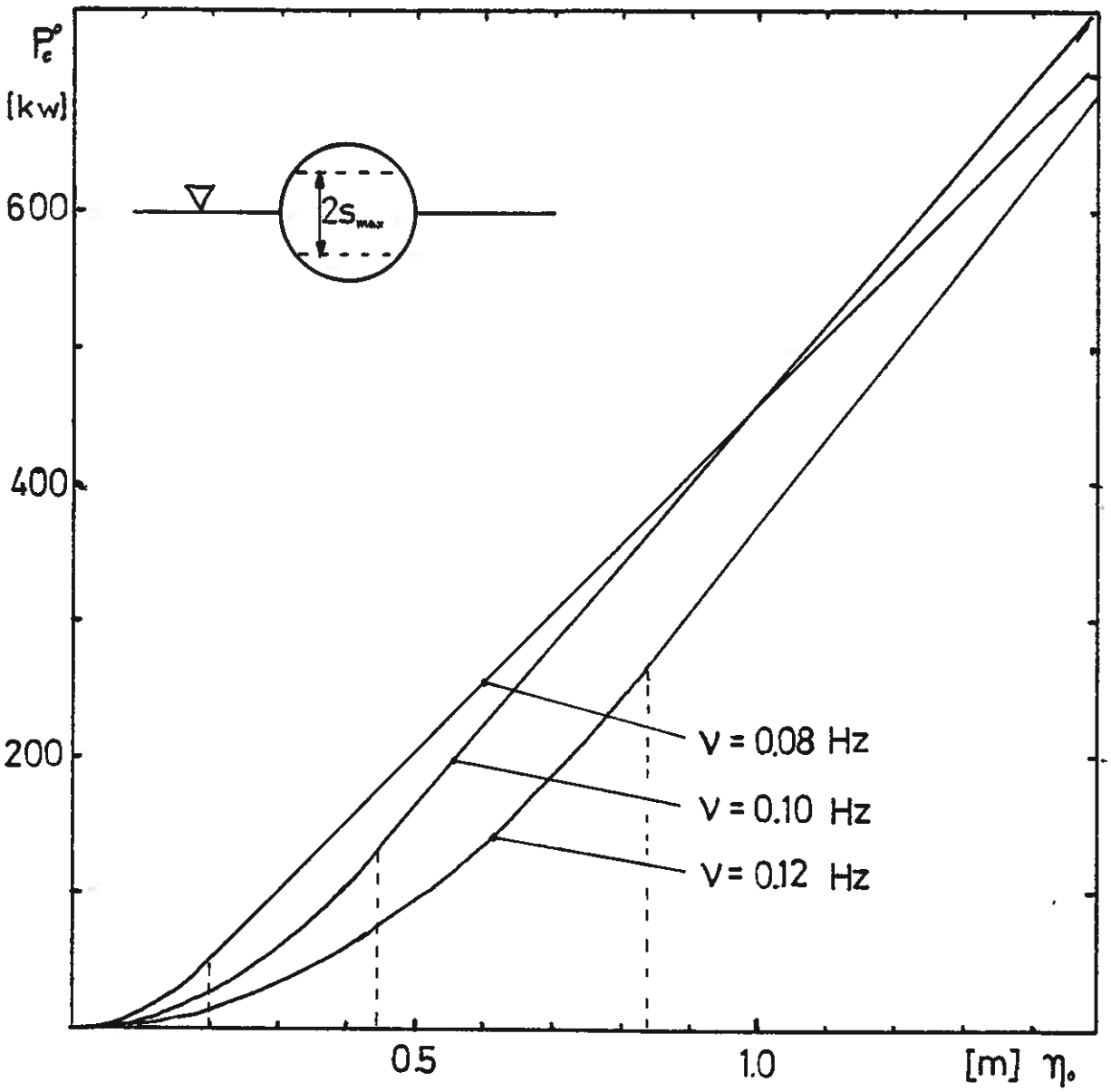

Fig. 20. Maximum absorbed power P_c^o versus incident wave amplitude $|\eta_o|$ for an isolated semi-submerged sphere of radius $a = 5$ m and maximum heave amplitude $|u/\omega|_{max} = s_{max} = 3$ m. A loss resistance $R_1 = \frac{1}{2} R^o(\nu)$ is assumed for all curves.
The dashed vertical bars indicate the critical wave amplitudes as given by the curve (c) of fig. 19.

6.2 Dynamical focusing.

It has been demonstrated[31] that a linear row of equidistant resonant buoys is acting as a dynamic reflector provided that the interspacing is below a certain limit (which is one wavelength at normal incidence). This fact leads to an interesting question: Is it possible to focus ocean waves by reflecting buoys analogous to focusing acustical waves or visible light by parabolic mirrors? In order to answer this question we investigate the system shown in fig. 21. The buoy no. 1 - hereafter referred to as the "focal buoy" - is the only absorbing buoy. The other ones are non-absorbing reflecting buoys positioned along a parabolic curve given by

$$x = d_f - y^2/4d_f \qquad (6.6)$$

Here d_f is the distance - termed the "focal length" - between the focal buoy and the point where the parabola intersects the x-axis. The y-coordinates of the reflecting buoys are chosen to be

$$y_i = d_w/2 - (N - i)d \quad , \quad 2 \leq i \leq N \qquad (6.7)$$

where d is the lateral buoy spacing and d_w is the mirror width. Hereafter d_w is called the "aperture", in analogy to optical systems. It just equals the distance between buoy no. 2 and buoy no. N.

$$d_w = (N - 2)d \qquad (6.8)$$

Although the basic idea - to concentrate the wave energy in a small area - is the same, the focusing system described above is quite different from the focusing system proposed by Mehlum[8]. The latter is a forward focusing system based upon refraction on fixed submerged plates or lens elements while our system is a backward reflection focusing system. Also the conversion unit proposed by Mehlum is quite different from the absorbing heaving buoy. Further, the focal length of Mehlum's "lens" is dependent on wave frequency, while the dynamical mirror - provided that the interspacing d is small enough -

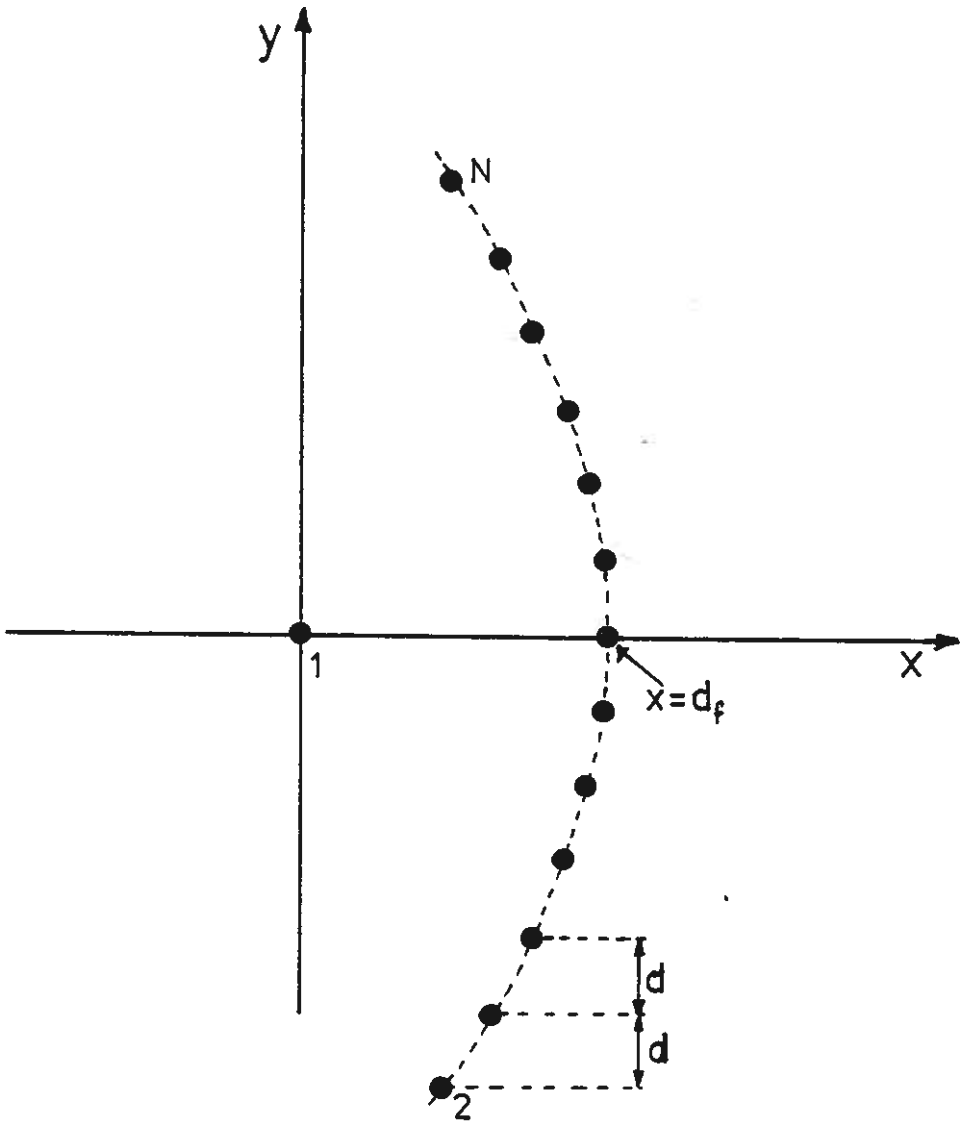

Fig. 21. Schematical top view of a dynamically focusing wave-power system. The dashed curve going through the centers of the reflecting buoys (no. 2,3,...,N) is a parabola which has its focal point at origin. See eq. (6.6). The only absorbing unit is the buoy no. 1, called the "focal buoy".

is expected to have a focal length independent of the frequency.

Results for relatively small systems are shown in figures 22 to 27. "Small" in this context means that the focal length d_f and the aperture d_w are of the same order of magnitude as the wavelength. Because merely low and moderate wave frequencies ($\nu < 0.11$ Hz) are used and because qualitative characteristics are of more interest than very accurate results, the mathematical model used in this section is the simplest possible one: the NS approximation for small buoys having real heave force coefficients. From these results, although they concern one special configuration, we deduce that following features are typical for small dynamically wave focusing systems:

1) The power absorbed by the focal buoy is very much affected by the phase of the focused wave, that is, whether it interferes constructively with the incident wave or not.

2) The power absorption for oblique wave incidence ($\beta \neq 0$) is poor.

3) The absorbed power is increased if the phases of the reflectors are optimalised. Especially the performance for oblique waves is much improved by phase-optimisation. See fig. 23.

4) Losses in the reflectors very much reduce the absorbed power.

In fig. 24, it is shown how the amplitude of the focused wave increases with increasing aperture or number reflecting resonant buoys. When the focused wave $|\eta_f|$ is of the same order as the incident wave $|\eta_o|$, one may expect that for some frequencies these two waves will interfere destructively and cause the power to be less than for an isolated buoy! In fact, this is just what is happening for $N = 10$ and $R_1 = \frac{1}{2} R^o$ (when the curves pass below $Q = 0.1$ in figs. 22 and 23). The results of fig. 25 and additional calculation (not shown here) indicate that the focused wave amplitude $|\eta_f|$ is more affected by the aperture d_w than by the lateral interspacing d, provided that $kd \lesssim 4$. The power absorption, therefore, is probably not much improved by using

more but less spaced buoys. However, this argument is valid only if the reflecting buoys are not restricted in their amplitudes. The heave amplitude distributions for the two cases when $d = 100$ m and $d = 50$ m are shown in figs. 26 and 27, respectively. From these results we deduce the critical wave amplitude $|\eta_{cr}|$ increases as the interspacing d decreases. Consequently, if the reflecting buoys have to be amplitude restricted, the efficiency of a dynamical reflector will increase with increasing buoy "density" $(N - 1)/d_w$.

The sudden decrease of the interaction factor Q for relative small angles of incidence β (see fig. 25) is explained by the fact that the effective focus will not coincide with the site of the absorbing buoy. (With "effective focus" is meant the position where the focused or reflected wave has its maximum amplitude.) Calculations, not presented here, indicate that the lateral shift of the effective focus is approximately

$$\Delta y \approx d_f \tan\beta \qquad (6.9)$$

Thus we deduce that the longer the focal length d_f the narrower band of the angular wave distribution can be absorbed. The physical interpretation of the improvement due to phase-optimising the reflecting buoys is that the effective focus, to some extent, is directed or steered back to the focal buoy.

It should be emphasised that the the presented results concern small systems. For large systems, say $d_f \approx d_w \approx 10^4$ m, the situation will be more comparable to geometrical optics where the linear dimensions are much larger than the wavelength. Although numerical calculations have not been carried of for such large systems - the computer program would be very expensive to use when $N \approx 100$ - we may expect the following. The focused wave at normal incidence will be much larger than the incident one, making the interaction factor less sensitive to the phase difference between the respective waves. However, the focused wave may become so large that linear hydrodynamics will not apply in the focal region.

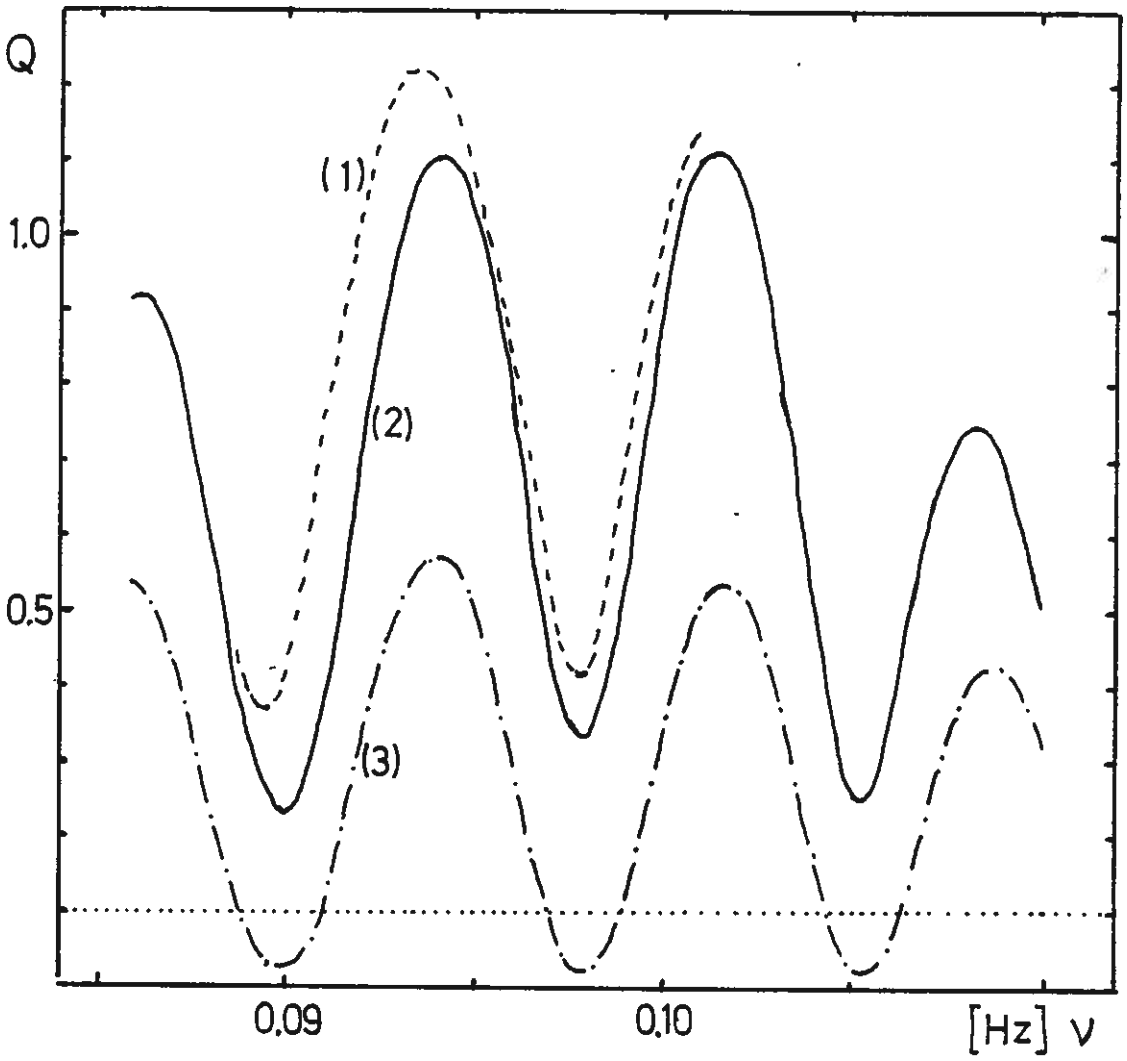

Fig. 22. Interaction factor Q versus wave frequency ν for a dynamically focusing system.

- Number of buoys (including the focal buoy): N = 10.
- Focal length: d_f = 500 m.
- Aperture: d_w = 800 m. (Lateral spacing: d = 100 m.)
- Angle of incidence: β = 0.

Curve (1): Each non-absorbing buoy is phase-optimised. The loss resistance is $R_1 = 0$

Curve (2): All buoys are resonant. The loss resistance is $R_1 = 0$.

Curve (3): All buoys are resonant. The loss resistance is $R_1 = \frac{1}{2} R^{\circ}(\nu)$.

The horizontal dotted line Q = 0.1 (= Q_1/N) represents the maximum power when all of the (N-1) reflecting buoys are held fixed.

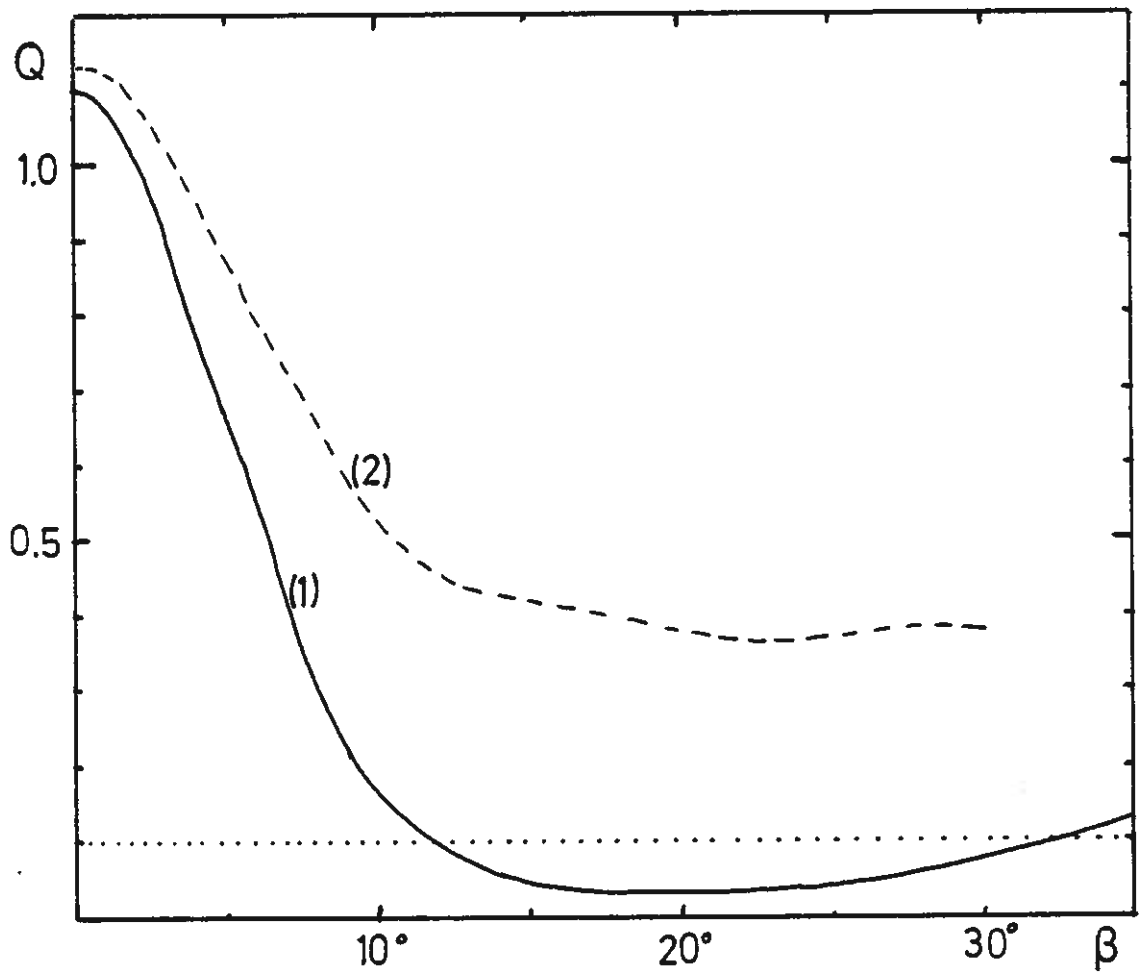

Fig. 23. Interaction factor Q versus incident wave angle β for the focusing system described in fig. 22.
- Wave frequency: $\nu = 0.101$ Hz.
- Loss resistance: $R_1 = 0$

Curve (1): All buoys are resonant.
Curve (2): The non-absorbing buoys are phase-optimised.
The horizontal dotted line $Q = 0.1$ represents the maximum power absorbed by the focal buoy when all the remaining buoys are held fixed.

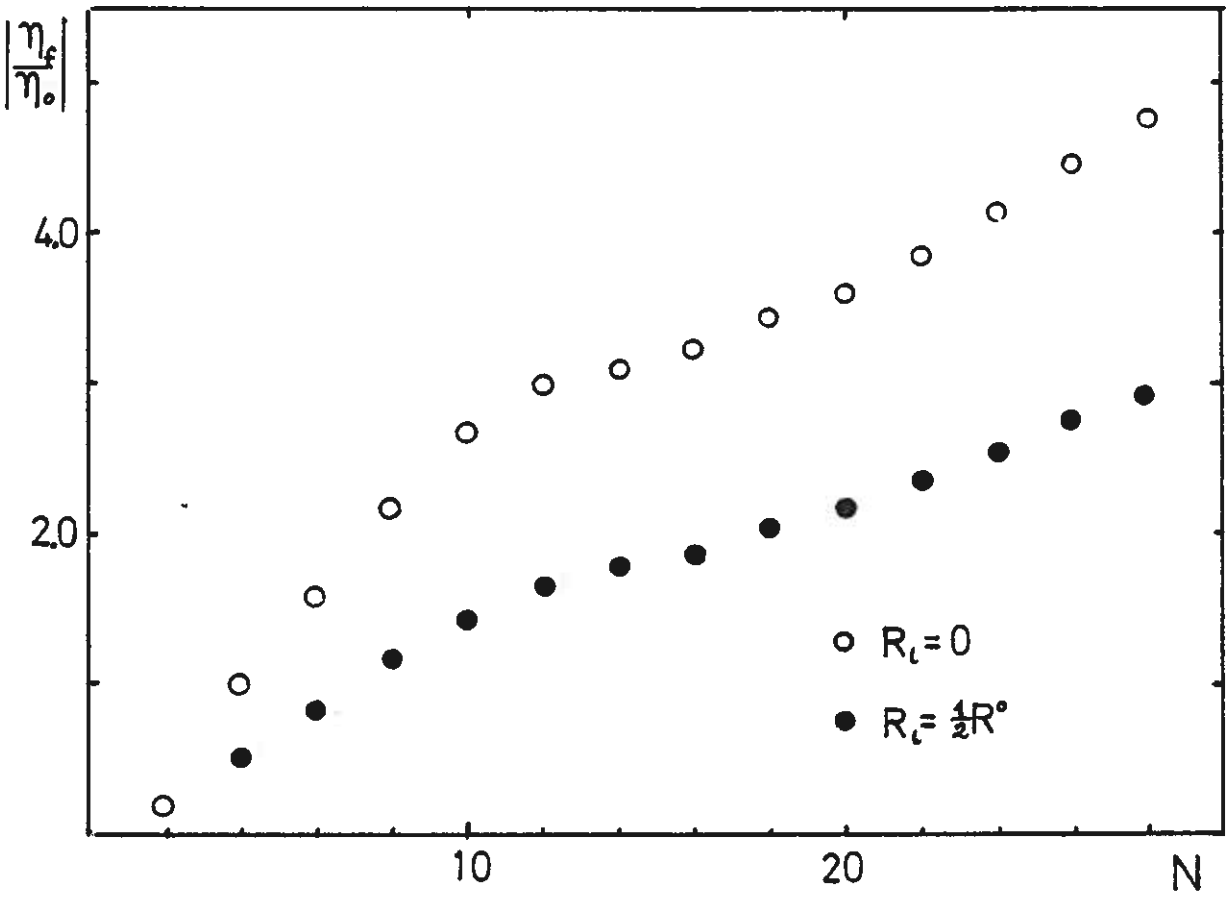

Fig.24. Focused wave amplitude ratio $|\eta_f/\eta_o|$ versus the aperture d_w or the number of buoys N. η_f is the wave elevation at the fixed focal buoy due to the motion of the remaining $(N-1)$ resonant and reflecting buoys.

- Focal length: d_f = 500 m.
- Lateral buoy spacing: d = 100 m
- Incident wave frequency: ν = 0.100 Hz.
- Angle of incidence: β = 0.

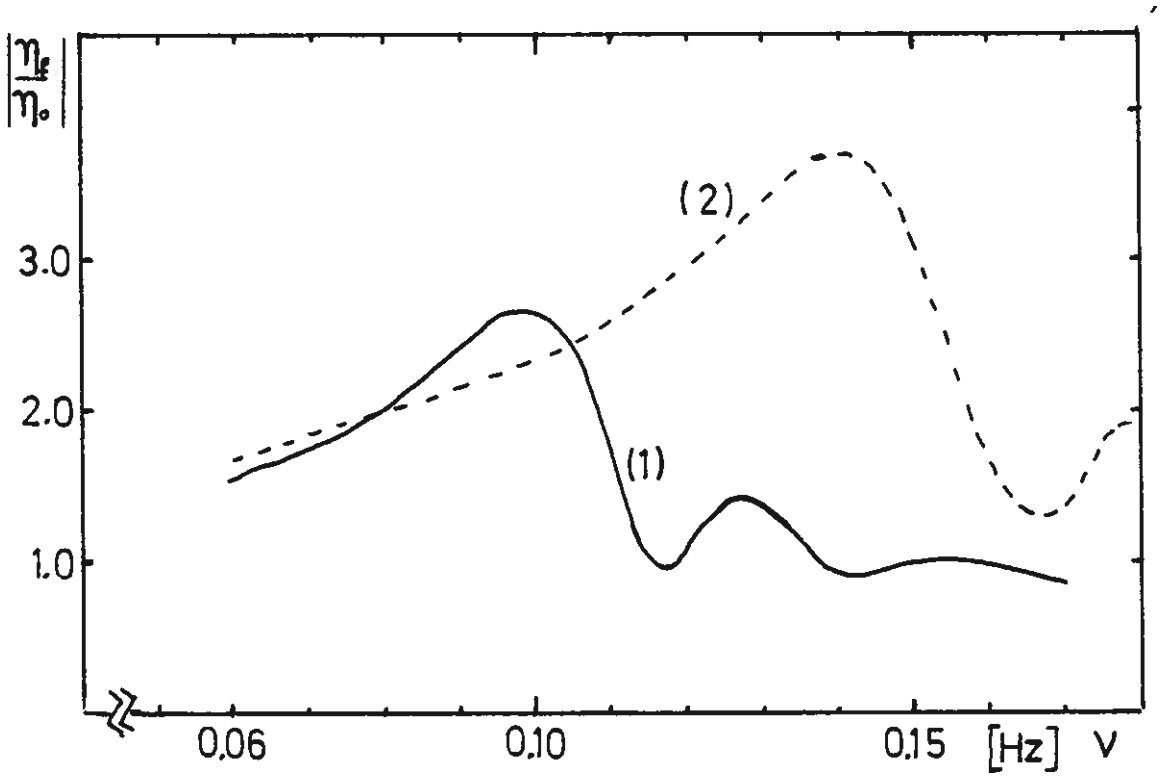

Fig. 25. Focused wave amplitude ratio $|\eta_f/\eta_o|$ versus wave frequency ν. η_f is the wave elevation at the fixed focal buoy due to the motion of the remaining (N - 1) resonant and reflecting buoys.

- Focal length: d_f = 500 m.
- Aperture: d_w = 800 m.
- Angle of incidence: β = 0.
- Loss resistance: R_l = 0.

Curve (1): N = 10, d = 100 m.

Curve (2): N = 18, d = 50 m.

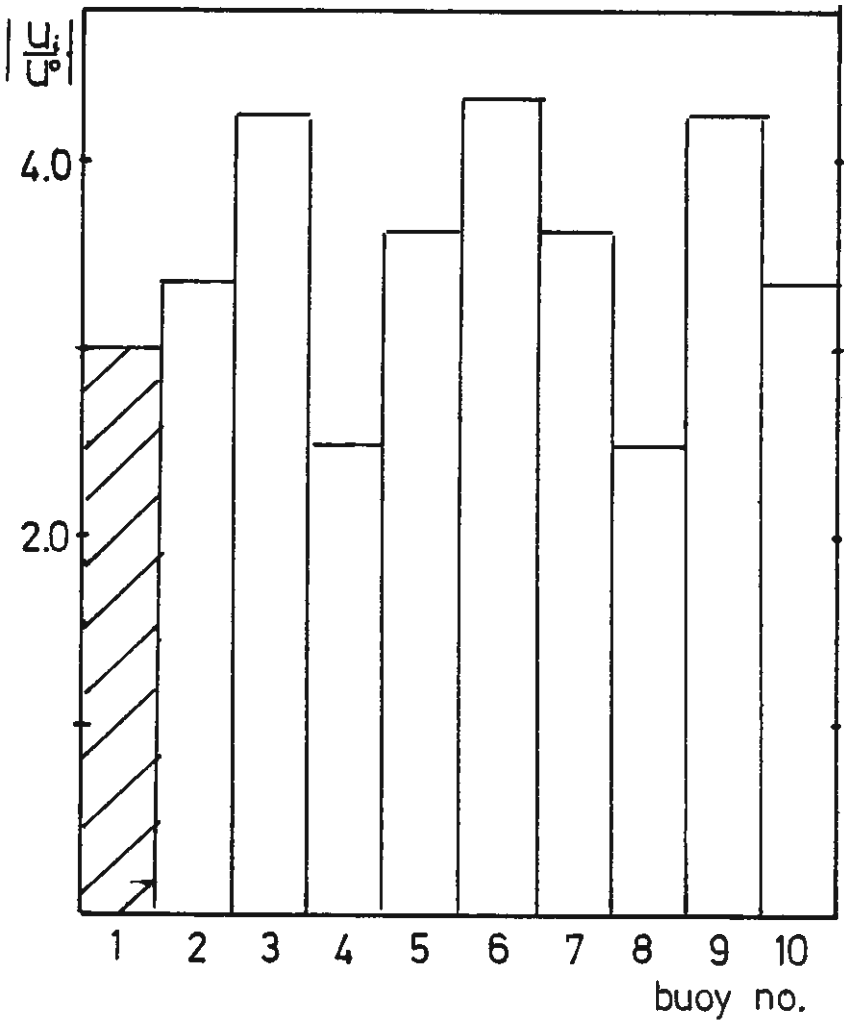

Fig. 26. Histogram showing the distribution of heave amplitude ratios $|u_i/u^\circ|$ for a ten-buoy focusing system. (u° is optimal velocity amplitude for one absorbing isolated buoy.) The hatching of post no. 1 indicates that this buoy is the only absorbing one.

- Wave frequency: $\nu = 0.10$ Hz.
- Angle of incidence: $\beta = 0$.
- Loss resistance: $R_1 = 0$.
- Aperture $d_w = 800$ m.
- Lateral buoy spacing $d = 100$ m.

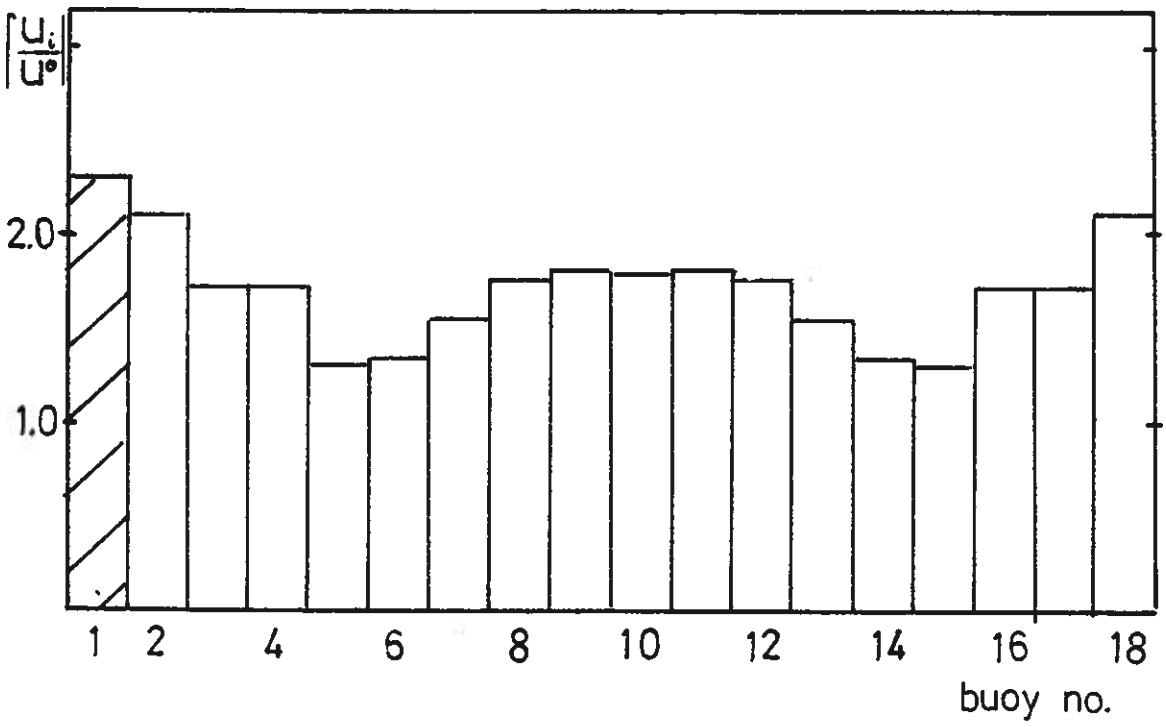

Fig. 27. Histogram showing the distribution of heave amplitudes $|u_i|$ for a focusing system of N = 18 buoys. (u^o is the optimal velocity amplitude for one absorbing isolated buoy.) The hatched post indicates the absorbing focal buoy.

- Wave frequency: ν = 0.10 Hz.
- Angle of incidence: β = 0.
- Loss resistance: R_1 = 0.
- Aperture: d_w = 800 m.
- Lateral buoy spacing: d = 50 m.

6.3 Systems of absorbing buoys.

As opposed to the previous section we now consider wave power systems of absorbing buoys only. That is, each buoy is assumed to have a power take-off equipment. We also assume that the power take-off has a linear characteristic, that is, the effective conversion resistance R_i is independent of the heave amplitudes. The results of the previous section on dynamical focusing are not attached to any special buoy geometry because the approximation for ideal point absorbers was used. In contrast to this, the results presented throughout this section concern semi-submerged spheres of radius $a = 5$ m. The implied mathematical model is the LS approximation.

The results shown in fig. 28 concern rows of equidistant buoys lined up along the x-axis. With a loss resistance of $R_1 = \frac{1}{2} R^o(\nu)$ and a buoy interspacing of $d = 30$ m the results indicate that the interaction factor Q decreases with increasing buoy number N. Figure 29 shows that the interaction factor Q also depends quite a lot on the angle of incidence β.

The results of figs. 30 and 31 try to reveal the effects of losses and amplitude constraints, respectively. Although the results concern a special two-buoy system, the following features are probably quite general:

1) The interaction effects become less significant, that is, Q approaches unity when a) the loss resistance increases or b) the incident wave amplitude exceeds the critical value $|\eta_{cr}|$ which means that the amplitude constraints become active.

2) Resonance conditions do not, in general, represent the optimal phases for the buoy motion, a result previously pointed out by Falnes[7].

The former point is simply explained by the fact that the diagonal elements of the total impedance matrix $(\underset{\sim}{Z} + \underset{\sim}{Z}_m)$ in either case become larger. Thus the hydrodynamical coupling forces become of less relative importance. As for the latter

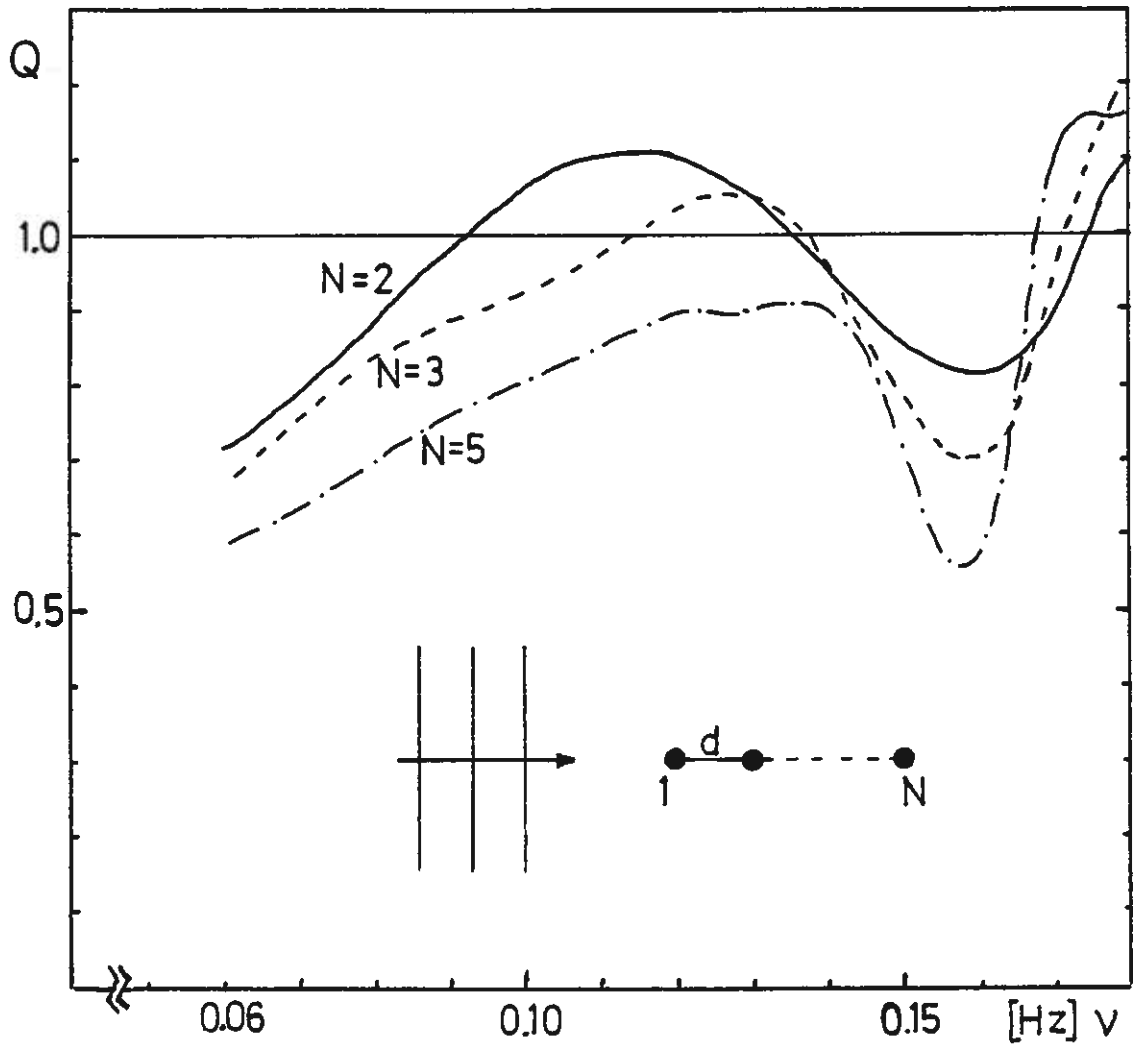

Fig. 28. The interaction factor Q versus wave frequency ν for one linear row of equidistant unconstrained buoys in head seas. N = 2, 3 or 5 buoys in the row.
- Buoy interspacing: d = 30 m.
- Loss resistance: $R_1 = \frac{1}{2} R^o(\nu)$.

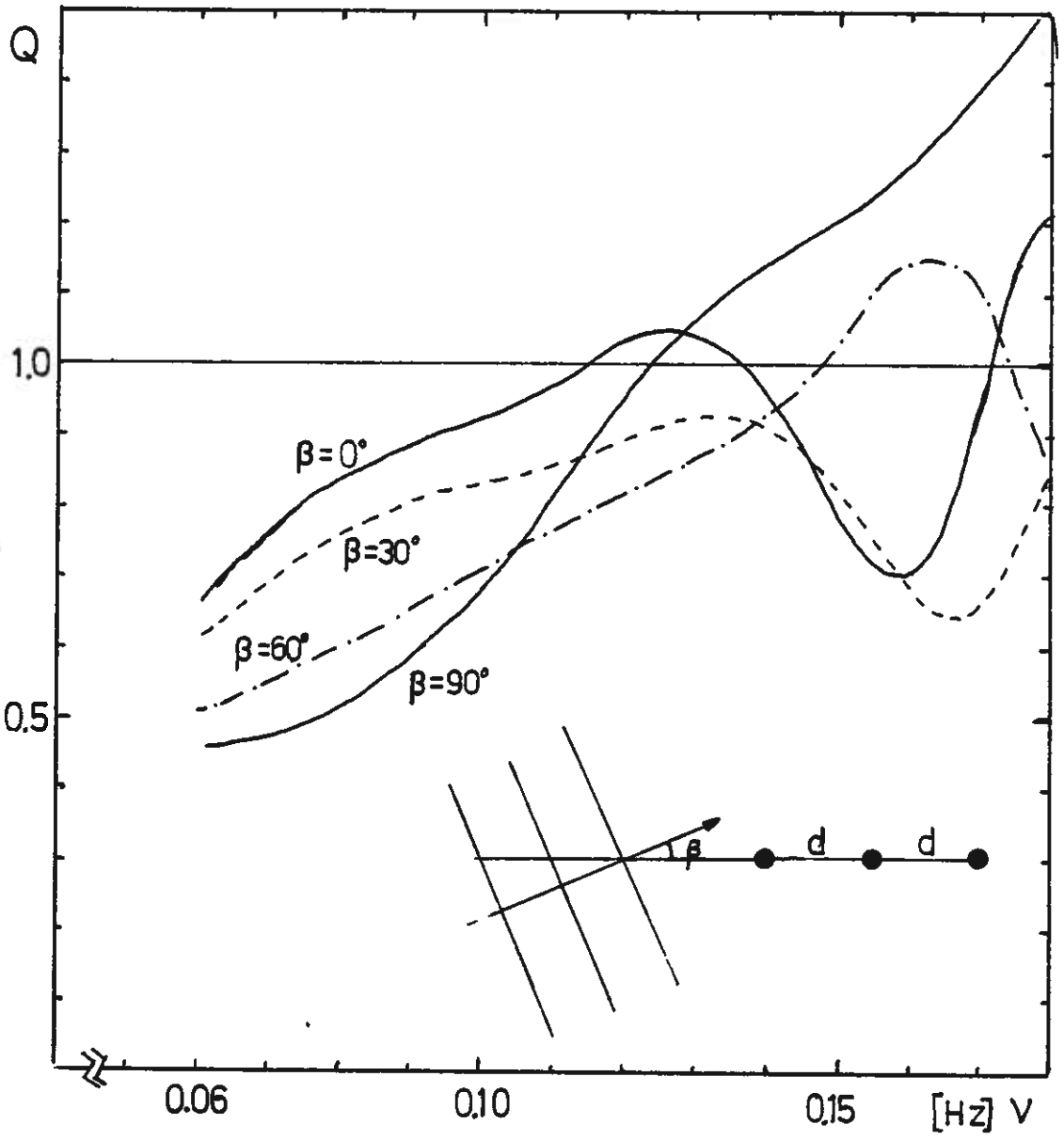

Fig. 29. The interaction factor Q versus the wave frequency ν for a system of three unconstrained buoys at various angles of incidence.
- Buoy spacing: d = 30 m.
- Loss resistance: $R_1 = \frac{1}{2} R^o(\nu)$.

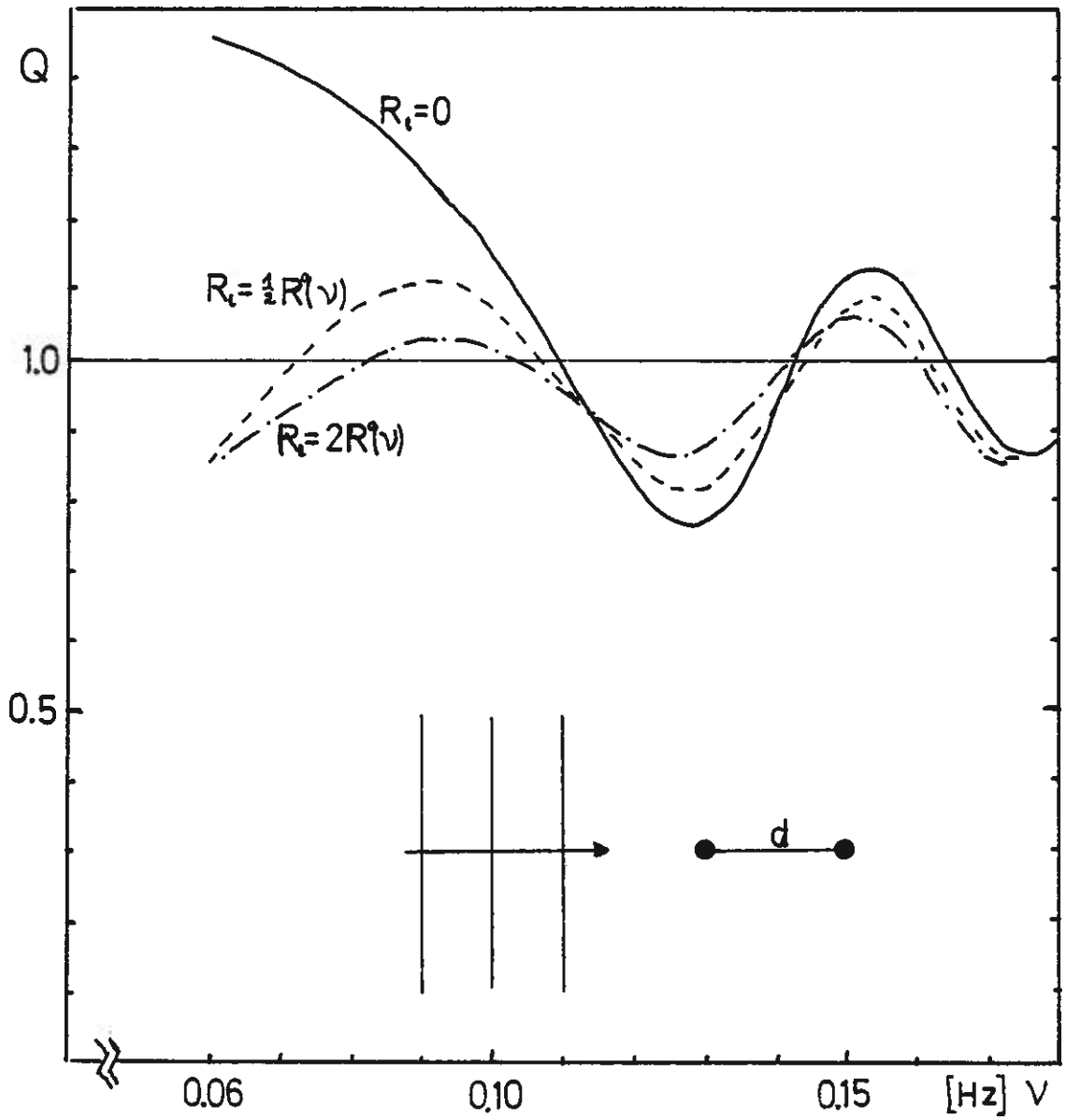

Fig. 30. The interaction factor Q versus the wave frequency for an unconstrained two-buoy system in head seas with various loss resistances R_l.
- Buoy interspacing: d = 50 m.

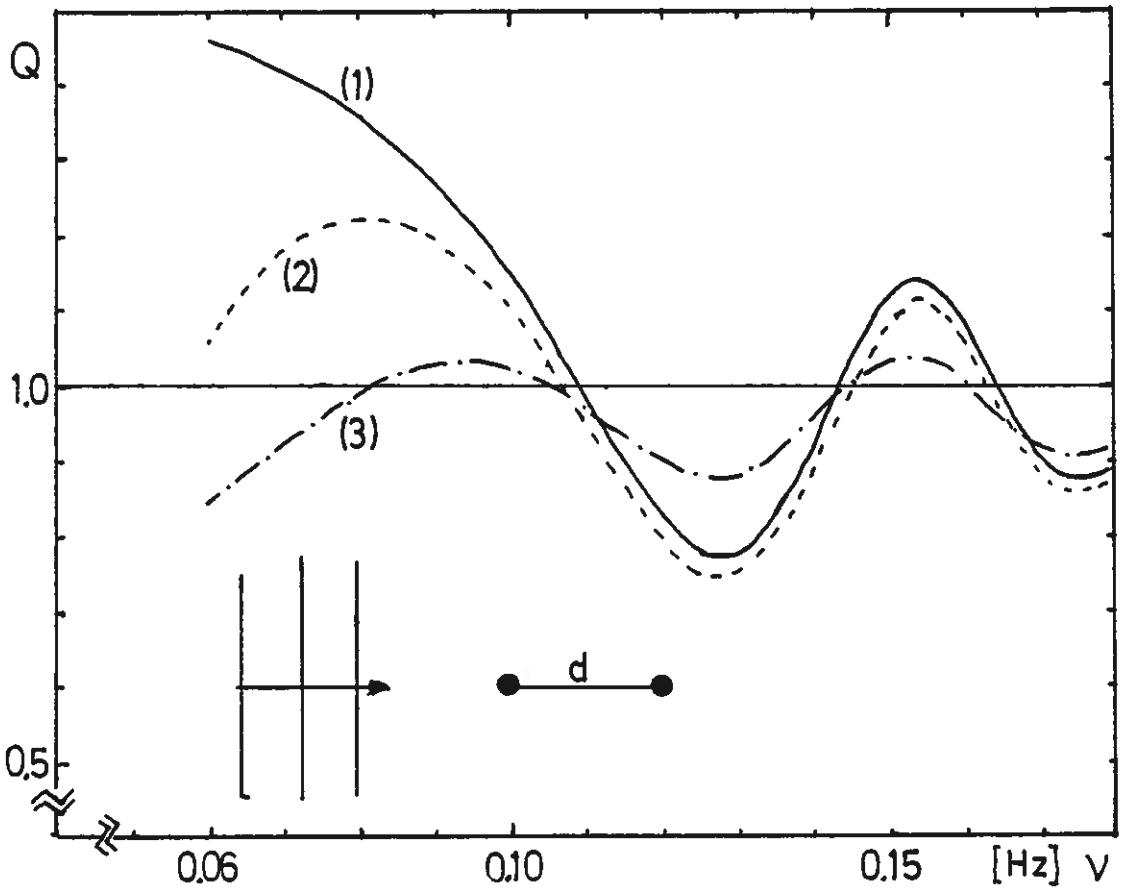

Fig. 31. The interaction factor Q versus the wave frequency ν for a two-buoy system in head seas.
- Buoy interspacing: d = 50 m.
- Loss resistance: $R_1 = 0$.
Curve (1): Unconstrained and phase-optimised buoys.
Curve (2): Unconstrained and resonant buoys.
Curve (3): Constrained and resonant buoys.
Incident wave amplitude: $|\eta_o| = 2|\eta^o_{cr}(\nu)|$.

point it should be noted that the increase of the power P_c due to phase-optimisation is quite small in most cases. In fact, the interaction factor of curve (3) in fig. 31 would not be detectably enhanced if the constrained and heavily loaded buoys were phase-optimised.

The relatively large difference between curve (1) and curves (2) and (3) in fig. 31 for the lowest frequencies is explained by the following. As the frequency ν tends towards zero, the optimum motion for the two buoys without loss resistance approaches that of an ideal dipol radiator. That is, the front and the rear buoy move with large amplitudes but with opposite phases. When losses are included this dipol behaviour will be ceased and the maximum power will be substantially reduced.

While the figs. 28-31 mainly concern linear rows in head seas, the fig. 32 shows some results for a linear row in beam seas. Although losses are included we see that these results qualitatively confirm what is previously indicated by Budal[23] and by Evans[10]: 1) the interaction factor Q changes rapidly at the frequency corresponding to $kd \approx 2\pi$ and 2) the changes are more pronounced with increasing number of buoys. The results in fig. 33 show the effect of placing additional rows of absorbing buoys behind the first row. They indicate that the drop in $Q(\nu)$ at the frequency ν corresponding to $\lambda \approx d$ becomes less distinct when the number of rows, N_r, increases. This is not unexpected for the following reason. The radiated waves from the buoys within one group - the configurations in fig. 3 may alternatively be regarded as five groups, each consisting of N_r buoys - will have different phases and partly cancel each other at the site of another group.

In order to compare with the dynamically focusing system we present the heave amplitude distribution for a ten-buoy system with no loss resistance. See fig. 34. Comparing these results with those in fig. 26 it is seen that the optimal heave amplitudes at beam seas are approximately one half of the corresponding values for the focusing system. Despite of the large amplitudes the absorbed power is substantially less for the focusing system. This illustrates a feature which is probably quite general: The

absorbed power per unit volume of displacement, P_c/V_d, is larger for systems of absorbing buoys than for system where the major part of the buoys are reflecting or non-absorbing. The volume of displacement V_d is here defined by

$$V_d = \pi a^2 \cdot \sum_{i=1}^{N} 2|u_i|/\omega$$

Additional calculations, not shown here, indicate that the optimal buoy amplitudes in beam seas are roughly proportional to the normalised buoy interspacing kd, provided that $kd < 2\pi$. For the particular frequency $\nu = 0.10$ Hz the results of fig.34 show that the optimal heave amplitudes as well as the absorbed power are substantially reduced at head seas relative to beam seas. However, at frequencies $\nu < 0.07$ Hz the conditions are quite different. Provided that there are neither losses nor amplitude constraints, the head sea orientation then represents the greatest amount of power and the largest heave amplitudes as well. This low frequency behaviour is previously predicted by Evans[10].

In chapter 4, the validity of the NS and the LS approximation was discussed on the basis of their hydrodynamical parameters. It is, however, of interest to compare the interaction factors for these approximations with the interaction factor Q^E used by Evans[10]. We firstly present some results for a two-buoy system of neither losses nor constraints. See fig. 35. These results surprisingly indicate that the interaction factor Q^E fits better to Q^{LS} than what is the case for Q^{NS}. (Q^{LS} and Q^{NS} denote the interaction factors according to the LS and NS approximations, respectively.) The difference between Q^{NS} and Q^E must be ascribed to the "phase" shift of R_{12}^{NS} ($\equiv R_{12}^{LS}$ for the two-buoy system) relative to $R^o J_o(kd_{12})$. Although R_{12}^{NS} is a better approximation than its limit $\lim_{a\to 0} R_{12}^{NS} = R^o J_o(kd_{12})$, the results of fig. 35 need not represent a paradox. See Appendix C for an explanation. However, the curves in fig. 35 and their analytical counterparts (C.13)-(C.15) indicate that the NS approximation is not consistent

unless the exciting force coefficients κ_i^o entering the NS formulae are real. On the other hand, the results increases the confidence of the ideal point absorber approximation. Probably, it gives reliable values for the absorbed power even for frequencies or buoy sizes corresponding to the region above the curve I in fig. 14.

Finally, in fig. 36 are shown some results for a five-buoy system. In contrast to most of the graphical presentations in this section the interaction factors in fig. 36 are shown versus the normalised buoy spacing kd and at a constant wave frequency. This is done in order to facilitate the comparison with previously known results[23,33]. The relative high frequency, corresponding to $\alpha = 0.5$, is chosen in order to display a significant difference between the curves (1) and (2). However, it also corresponds to an incident wave amplitude - implied in curve (4) - which is rather unphysical. See curve (c) of fig. 19. Nevertheless, the curve (4) clearly demonstrates the effect of amplitude constraints at lower frequencies.

The curves in fig. 36, in fact, display our main original contributions to a more thorough knowledge about interacting wave power buoys. The simple mathematical model for ideal point absorbers (curve (2)) is improved by the LS approximation which applies for relatively large buoys. Secondly, the power absorption has been made more realistic by the inclusion of conversion losses. And finally, a method for power maximising under quite general motion constraints has been developed.

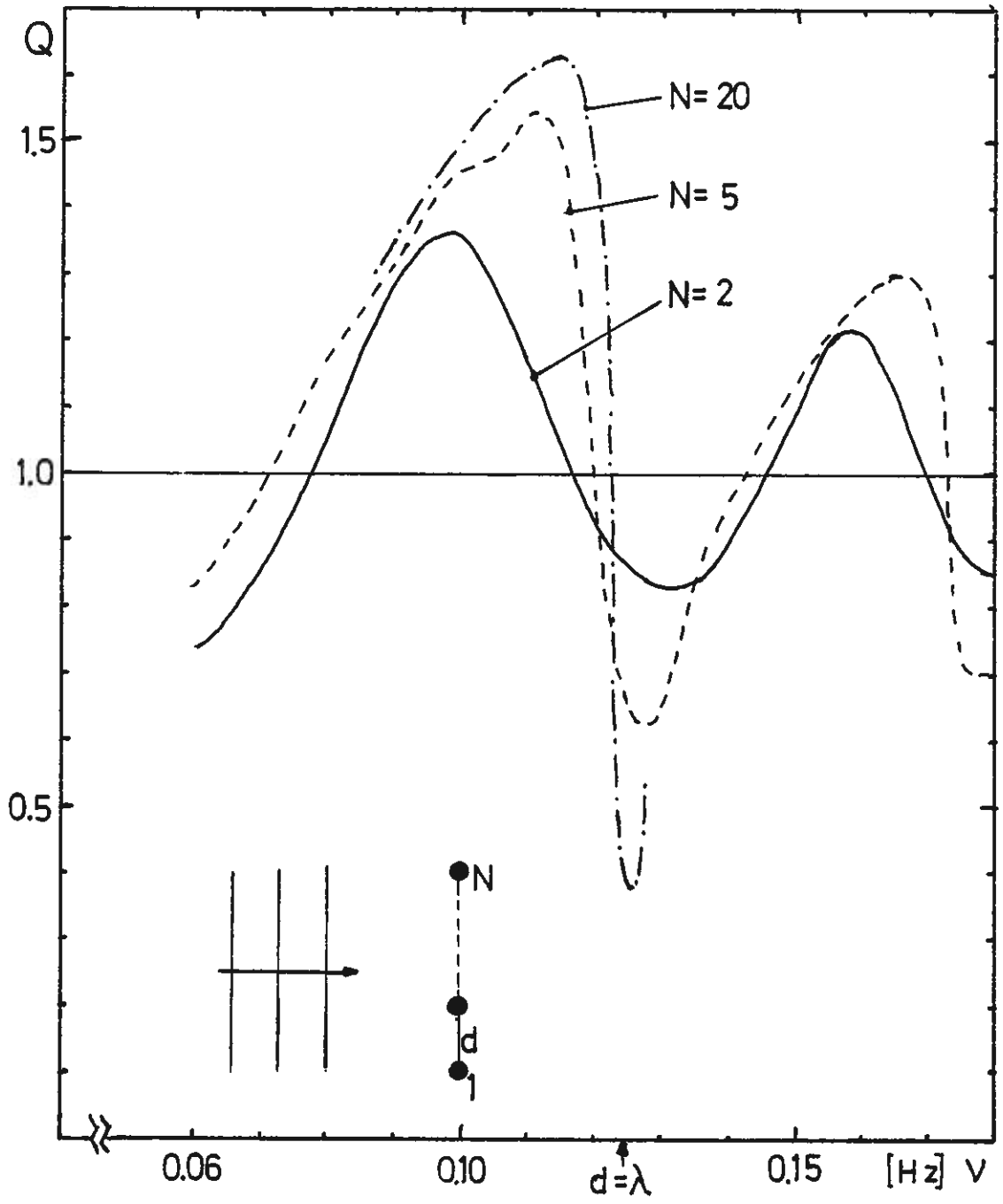

Fig. 32. The interaction factor Q versus the wave frequency ν for a finite row of unconstrained absorbing buoys in beam seas.

- Buoy interspacing: d = 100 m.
- Loss resistance: $R_1 = \frac{1}{2} R^o(\nu)$.

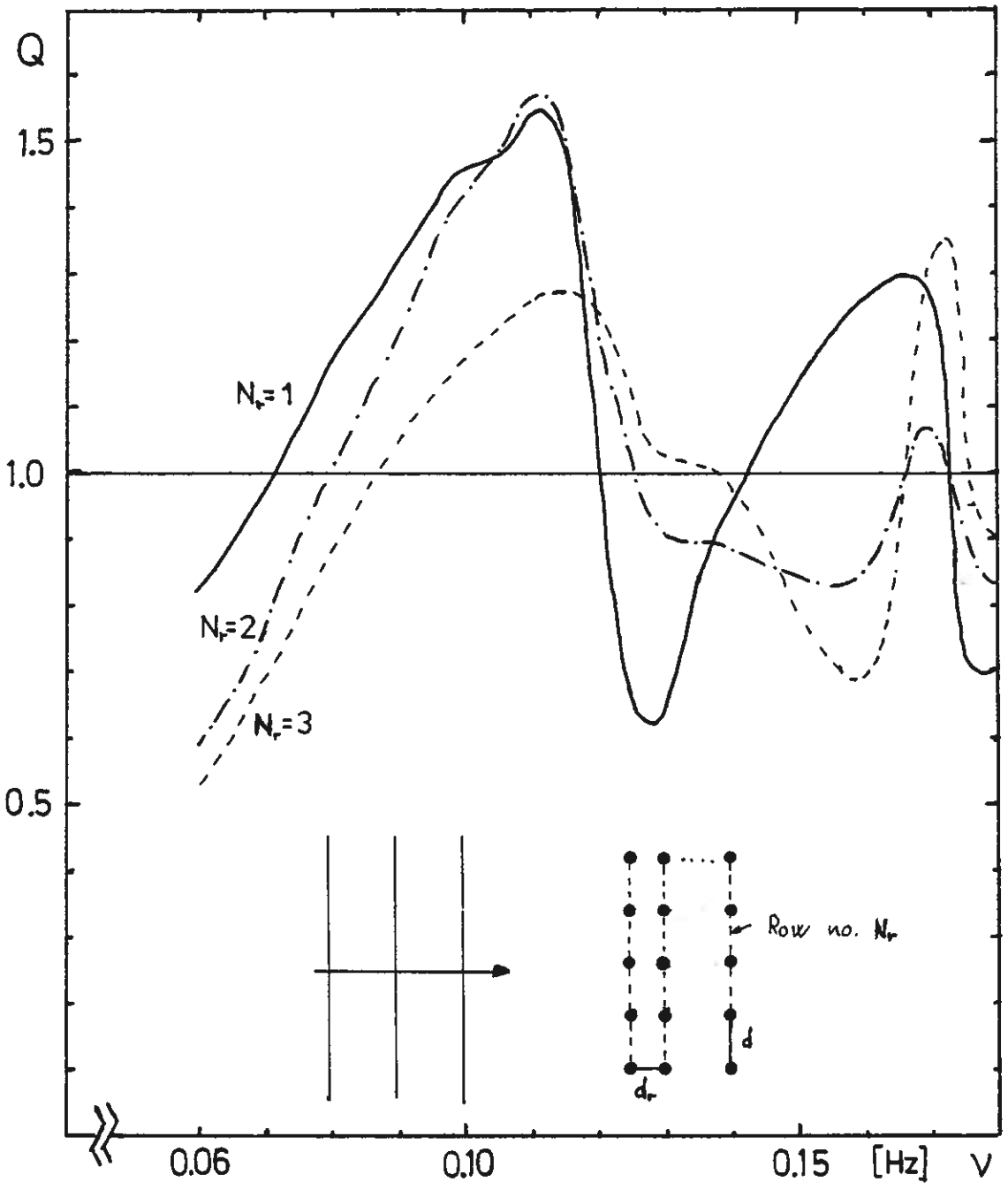

Fig. 33. The interaction factor Q versus the wave frequency ν for one, two and three parallel rows of five equidistant buoys. N_r is the number of rows.

- Buoy spacing within one row: d = 100 m.
- Row spacing: d_r = 30 m.
- Angle of incidence: $\beta = 0$.
- Loss resistance: $R_l = \frac{1}{2} R^{\circ}(\nu)$.

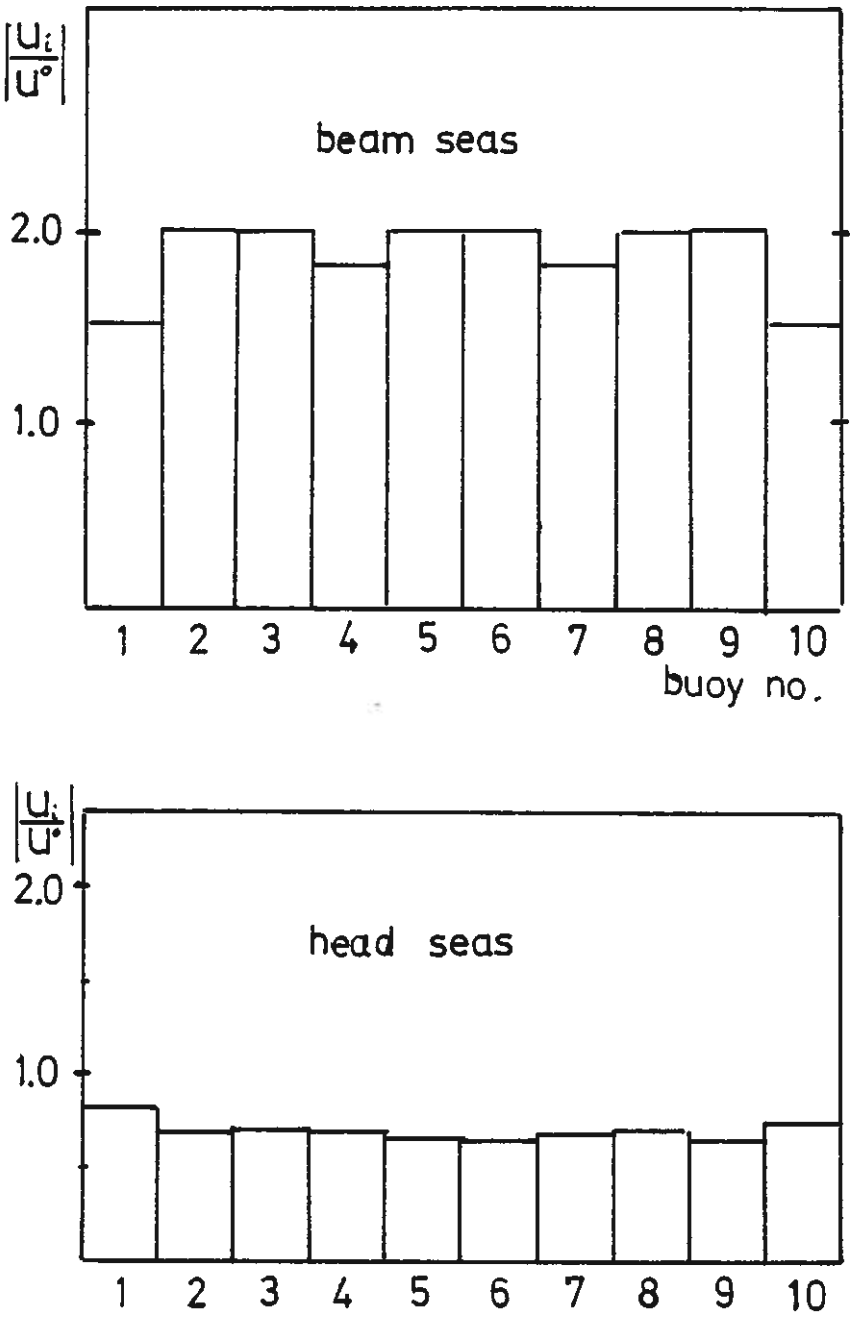

Fig. 34. Histograms showing the optimum heave amplitudes $|u_i/u^o|$ for of a ten-buoy system. (u^o is defined in fig. 26)

- Configuration: linear row of equidistant buoys.
- Buoy spacing: d = 100 m.
- Wave frequency: ν = 0.10 Hz.
- Loss resistance: R_l = 0.
- Interaction factors: Q = 1,95 at beam seas.
  Q = 0,63 at head seas.

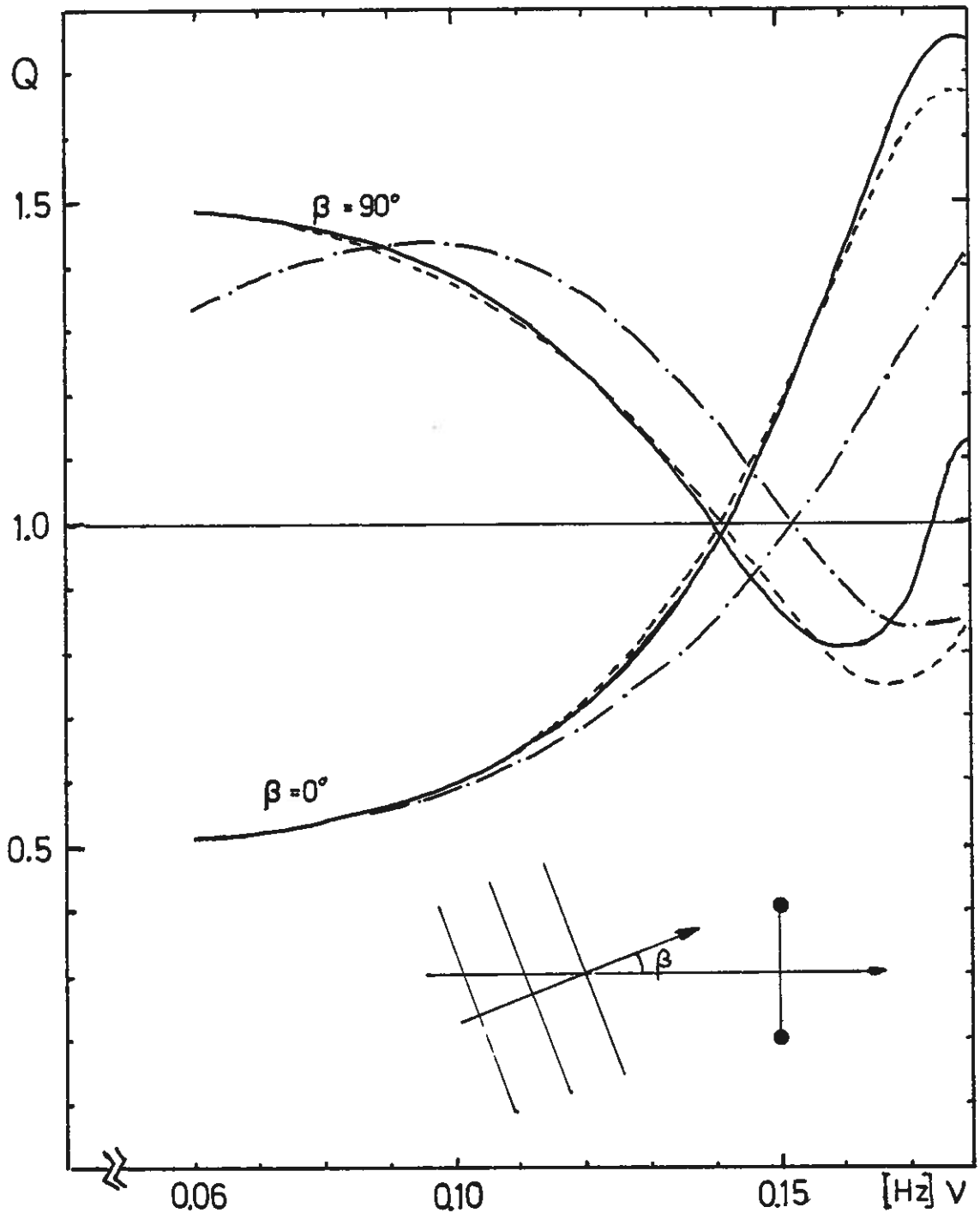

Fig. 35. Interaction factors for two identical buoys versus the wave frequency ν for different mathematical approximations.

- Buoy interspacing: d = 50 m.
- Loss resistance: $R_1 = 0$.
- Constraints: no.

———— Q^{LS}.

——·—— Q^{NS}.

---------- Q^{E}. See eq. (6.2).

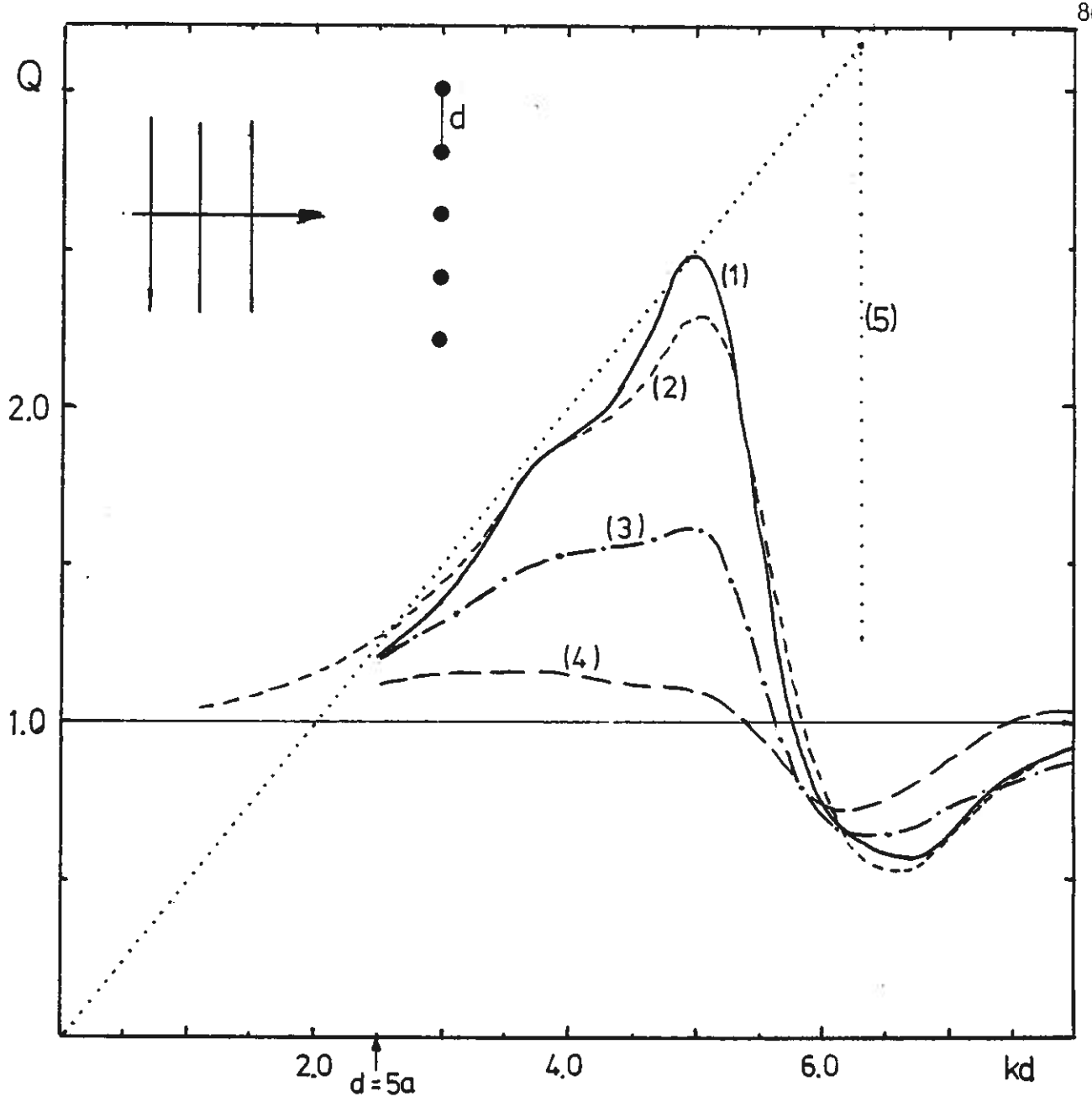

Fig. 36. Interaction factor Q versus the non-dimensional buoy spacing kd for a linear row of N = 5 equidistant buoys in beam seas. The wave frequency is $\nu = 0.1577$ Hz, corresponding to $k = 0.1\ m^{-1}$ and $\alpha = 0.5$.

Curve (1): $Q^{LS}(R_1=0)$. Constraints: no.

Curve (2): Q^{E}, originally calculated by Evans[33]. See also (6.2).

Curve (3): $Q^{LS}(R_1=\frac{1}{2}R^{o})$. Constraints: no.

Curve (4): $Q^{LS}(R_1=\frac{1}{2}R^{o})$. Constraints: 1) resonant buoys and 2) amplitude constraints corresponding to an incident wave $|\eta_o| = 2|\eta_{cr}^{o}|$

Curve (5): $\lim_{N\to\infty} Q^{E}$, according to Budal[23].

6.4 Concluding remarks.

The results presented in this chapter provide a lot of valuable information about the absorption characteristics for some wave power buoy configurations. It is, however, useful to give a short summary and to make some supplying comments on the results.

As for dynamical focusing systems we have demonstrated the following.

1) It is possible, by means of a parabolic line of non-absorbing heaving buoys to concentrate a substantial part of the incident wave energy in a small focal area.

2) Unless the dynamical mirror is very wide and consists of numerous buoys, the power take-off by the focal buoy very much depends on the phase of the focused wave relative to the incident one.

3) The wave focusing ability will be reduced if there are losses in the non-absorbing buoys or if the amplitude constraints become active.

4) The power absorption rapidly falls off in oblique waves, especially when the reflecting buoys are resonant. Phase-optimisation substantially improves the performance at normal as well as oblique incidence.

The possibilities of phase-optimising in practical situations depend on the actual wave spectrum. It is obviously very difficult to perform phase-optimising by means of buoy latching when the sea condition is represented by a number of waves of different frequencies and angles of incidence. At wide angular wave spectra, therefore, the possibility of steering the effective focus are perhaps practically limited. Also it should be noted that at large incident waves ($|\eta_0| > |\eta_{cr}|$) the possibility of phase-optimisation is reduced because "distuning" or steering "out-of-phase" is the only way of performing amplitude restriction. A suggestion for improving the bad angular band-width for the dynamical focusing system is to apply more absorbing devices on either sides of the

focal buoy. At oblique incidence the effective focus then would hit one or two of the other absorbing devices. This idea is based upon a proposal previously made by Mehlum[32].

As for wave power systems consisting of merely absorbing buoys we have demonstrated the following:

1) The interaction forces between different wave power buoys have substantial influence on the power absorption in each buoy. Consequently, the maximum power available for the whole system depends on the buoy configuratuon and on the angle of incidence.

2) Inclusion of power losses in the buoys reduces the maximum useful power convertable by the system. Also the interaction effects decreases when the loss resistance increases.

3) Constraints on the heave amplitudes have somewhat the same effect as a loss resistance. That is, the interaction effects are reduced relative to an unconstrained system.

4) Compared to buoys which are always resonant, phase-optimisation does not increase the power significantly when the absorbing buoys are heavily loaded.

5) The power absorption is pretty good for all angles of incidence.

The greatest advantages of such systems in preference to focusing systems are i) the absorbed power per displacement volume is much larger, ii) the absorption characteristics in oblique incident waves is better. Another advantage, not mentioned yet, is that the power output from many absorber units will be more smooth than from a single one. Unless non-absorbing buoys are much cheaper than absorbing ones, the dynamically focusing systems probably are economically disfavourable.

7. CONCLUSION

The preceding chapters provide a lot of interesting and useful knowledge about wave-power buoys and, in particular, the interaction effects arising in multi-buoy systems. Some of the results represent well-known knowledge, but the thesis also contains some new and original results not published previously. It is, therefore, appropriate to give a short summary of what is new in this field. Finally we give some recommendations and suggestions for further progress.

The summary comprises the following points:

1) The phenomenological formulation of a general multi-body system includes a loss resistance matrix $\underset{\sim}{R}_1$ which takes care of all the inevitable power losses in a practical system. The expression (2.16) for the maximum useful part $P_{c,max}$ of the total absorbed power, therefore, represents an extension of a similar result obtained by Evans[10] and Falnes[11].

2) We have explicitly shown that the maximum total power $P_{c,max}(\underset{\sim}{R}_1 = 0)$ for a system of unconstrained, heaving and ideal point absorbers is independent of the specific buoy geometry.

3) By extenting the well-known small-body theory to second order in α we have derived the following interesting result. The significant imaginary part of the heave force coefficient κ^o for a floating semisubmerged buoy is

$$\lim_{\alpha \to o} \{\kappa^o\} = \pi a^2 \rho g \cdot \frac{\pi}{2}\alpha^2$$

irrespective of the buoy geometry.

4) An analytic approximation for the far-field scattered wave of an isolated buoy is derived. This approximation is composed of two terms: one isotropic term proportional to $\kappa^o H_o(kd)$ and one anisotropic term proportional to $\kappa^s H_1(kd) \cos(\theta-\beta)$.

5) On the basis of this scattered wave approximation a mathematical model for interacting heaving buoys is formulated. This model - which is termed the LS approximation - takes care of first order scattering effects but neglects multiple scattering effects as well as the influence of the local fields. It therefore represents a large simplification relative to more accurate methods solving the differential equations numerically. The corresponding reduction of the execution times is of vital importance in studying systems of numerous interacting buoys. On the other hand, the LS approximation represents a substantial improvement or sophistication of the ideal point-absorber approximation. Comparison with accurate numerical results indicates that the LS approximation is reasonably good for floating buoys even for diameters 2a as large as 1/5 of the wavelength and for buoy spacings d as small as 5 buoy radii.

6) A method for calculating the maximum useful power under motion constraints is described and implemented on a computer. The constraints are of two different types: 1) restricted heave amplitudes and 2) fixed values for the load resistances R_i or the reactances X_i. These constraints are more general than the simple global constraint ($\tilde{u}^* \underset{\sim}{u} \leq$ Const.) used by Evans[28] or the equality constraints ($|u_i| = \omega s_{max}$) discussed by Falnes and Budal[29].

7) Quantitative results from the written computer program have demonstrated the possibility of dynamically focusing of ocean waves by a parabolic line of reflecting non-absorbing buoys. With the proviso that the analysis concerns a small system we have,however, found that dynamically focusing systems have many disadvantages in preferance to systems of merely absorbing buoys.

8) In addition to the focusing system a lot of practically interesting buoy configurations have been analysed. For some of these systems the effects of power losses and of motion constraints have been demonstrated. Not unexpectedly, these quantitative examples show that the hydrodynamical interaction forces become less influent on the power

absorption when the loss resistance increases and when the waves are high so that the buoy amplitudes have to be restricted.

9) Finally, we have noticed that the interaction factor for two interacting ideal point absorbers surprisingly well coincides with the LS interaction factor even for frequencies corresponding to non-dimensional buoy sizes as large as $\alpha \approx 0.5$. Moreover, an analytic investigation provides a plausible explanation to this: the scattering effects are smaller on the absorbed power than on the hydrodynamical parameters because the different scattering terms - to the lowest order in α - cancel each other.

It is hoped that this thesis provides increased understanding in the field of wave power conversion. Also it is hoped that the presented results will be valuable and useful in the process of determining the optimal buoy configuration of a practical wave power plant. Nevertheless, more work ought to be done in this field. In the following we shortly mention some recommendations or suggestions for how to make further progress.

Clearly, an important aspect of optimising the buoy configuration is to maximise the average power enhancement due to the interaction effects. Better than using the simple interaction factor shown in the figures of chapter 6, therefore, is to study an effective interaction factor, for instance

$$Q_{eff} = \iint \hat{Q}(\nu,\beta)\ E(\nu,\beta)\ d\beta d\nu$$

where $\hat{Q}$ denotes the interaction factor at a typical wave $\eta_o(\nu,\beta)$ and E is the energy spectrum or another suitable weight function. However, this sophistication requires some knowledge of the wave climate at the site of the actual wave power plant.

Also the mathematical model may be improved. Firstly, the LS model may be further improved, for instance, by including additional and more accurate terms in the expression for the scattered waves $\eta^o_{d,i}$. Secondly, a more realistic loss resistance $R_1(\nu)$ than $R_1 = \frac{1}{2} R^o(\nu)$ should be used in the calculations. The ratio R_1/R^o for a practical wave power buoy

probably depends on the frequency ν as well as the conversion resistance R_c (non-linear losses). It is, indeed, of great importance to investigate the non-linearities because it may turn out that they play an important role at large waves. Inclusion of non-linearities, however, implies that the equations of motion must be solved by iterative methods.

APPENDIX A. BASIC HYDRODYNAMICS FOR SURFACE WAVES.

The subject matter presented in this appendix represents well-known theory available in books of hydrodynamics[16,34]. For completeness and convenience of reference, however, some fundamental equations and useful relations are here briefly reproduced in our notation.

A.1 Basic equations.

For irrotational flow of an non-viscous and incompressible fluid the velocity field $\vec{v}'(\vec{r},t)$ always can be written as a gradient

$$\vec{v}' = \nabla\cdot\phi' \qquad (A.1)$$

where $\phi'(\vec{r},t)$ is a scalar field - termed the velocity potential - satisfying the Laplace equation:

$$\nabla^2\phi' = 0 \qquad (A.2)$$

The absolute pressure $p'_{tot}(\vec{r},t)$ within the water is related to ϕ' through the Bernoulli equation:

$$\frac{\partial\phi'}{\partial t} + \frac{1}{2}(\nabla\phi')^2 + \frac{p'_{tot}}{\rho} + gz = C = \frac{p'_{air}}{\rho} \qquad (A.3)$$

where ρ is the density of water, g is the acceleration of gravity and C is an arbitrary function of time, chosen so that the absolute pressure p'_{tot} equals the atmospherical pressure at the free surface.

The boundary condition at rigid surfaces is

$$\frac{\partial\phi'}{\partial n} \equiv \vec{n}\cdot\nabla\phi' = u'_n \qquad (A.4)$$

where $\vec{n}$ is the normal vector pointing inwards the fluid domain (see fig. 1), and u'_n is the normal component of the surface velocity.

The free surface condition is a bit more complicated. It may, however, be derived from the fact that a water particle on the free surface will stay on the free surface. That is

$$\frac{D\eta'}{Dt} \equiv \frac{\partial \eta'}{\partial t} + (\nabla \phi') \cdot \nabla \eta' = \frac{\partial \phi'}{\partial z} \quad , \quad z = \eta' \qquad (A.5)$$

where $\eta'(x,y,t)$ is the wave elevation. The Bernoulli equation (A.3) gives

$$\frac{\partial \phi'}{\partial t} + \frac{1}{2} (\nabla \phi')^2 + g\eta' = 0 \quad , \quad z = \eta' \qquad (A.6)$$

Combining these two last equations, evaluating them at the the mean free surface, $z = 0$, and dropping all second and higher order terms in ϕ', we arrive at the linearised free surface condition

$$\frac{\partial^2 \phi'}{\partial t^2} + g \frac{\partial \phi'}{\partial z} = 0 \quad , \quad z = 0 \qquad (A.7)$$

The linearised expressions for the wave elevation η' and the hydrodynamical pressure p' are

$$\eta' = - \frac{1}{g} \frac{\partial \phi'}{\partial z} \quad , \quad z = 0 \qquad (A.8)$$

and

$$p' \equiv p'_{tot} + \rho g z - p_{air} = \rho \frac{\partial \phi'}{\partial t} \qquad (A.9)$$

From now on we assume harmonical time variation. However, in linear theory this does not imply any loss of generality since a large class of time-varying functions can be decomposed into harmonical components which can be treated independently. For convenience we use complex representation. Any time-dependent physical quantity represented by a primed symbol, say A', is related to a corresponding complex amplitude A by

$$A'(t) = \mathrm{Re}\{Ae^{i\omega t}\} \qquad (A.10)$$

where i is the imaginary unity and ω is the angular frequency related to the wave period T by

$$\omega = 2\pi/T \tag{A.11}$$

The complex versions of the Laplace equation (A.2) and the free surface condition (A.3) are just

$$\nabla^2\phi = 0 \tag{A.12}$$

and

$$\frac{\partial\phi}{\partial z} - \frac{\omega^2}{g}\phi = 0 \quad , \quad z = 0 \tag{A.13}$$

Assuming constant depth of water h the boundary condition (A.4) is conveniently split into two terms:

$$\frac{\partial\phi}{\partial z} = 0 \quad , \quad z = -h \tag{A.14}$$

and

$$\frac{\partial\phi}{\partial n} = u_n \quad , \quad \text{on body surfaces.} \tag{A.15}$$

The complex amplitudes of velocity, hydrodynamical pressure and wave elevation are

$$v_i = \frac{\partial\phi}{\partial x_i} \quad , \quad i = 1,2,3 \quad , \tag{A.16}$$

$$p = -i\omega\rho\phi \tag{A.17}$$

and

$$\eta = -\frac{i\omega}{g}\phi \quad , \quad z = 0 \tag{A.18}$$

respectively.

A.2 Plane and circular waves.

A solution of the boundary value problem (A.12)-(A.14) which represents a progressive plane wave is

$$\phi_o = -\frac{g}{i\omega}\eta_o\, e(kz)e^{-ik(x\cos\beta+y\sin\beta)} \qquad (A.19)$$

where η_o is the complex wave elevation amplitude at origin, k is the wave number related to the wave length λ by

$$k = 2\pi/\lambda \qquad (A.20)$$

Further, β is the angle of incidence and $e(kz)$ is the depth function

$$e(kz) = \frac{\cosh(kz+kh)}{\cosh(kh)} \qquad (A.21)$$

approximating $\exp(kz)$ for deep water $(kh>>1)$. Inserting ϕ_o into the free surface condition (A.13) we get the dispersion relation for surface waves

$$\omega^2 = gk\tanh(kh) \qquad (A.22)$$

It can be shown that the wave ϕ_o is carrying a mean power of

$$K = \frac{\rho g^2 D}{4\omega}|\eta_o|^2 \qquad (A.23)$$

pr. unit length of the wave crest, D being a non-dimensional depth factor given by

$$D = \tanh(kh)\{1 + 2kh/\sinh(2kh)\} \qquad (A.24)$$

It is easily seen that $D = 1$ on deep water.

Before presenting circular waves we introduce an additional condition which has to be satisfied by potentials representing scattered or radiated waves. This is the so-called radiation condition

$$\lim_{kR\to\infty}\phi = b(\theta)e(kz)(kR)^{-\frac{1}{2}}e^{-ikR} \qquad (A.25)$$

where b is a function of the azimuthal angle θ. The physical interpretation of this condition is that ϕ has to represent an outgoing progressive wave.

Two linearly independent solutions of the boundary value problem (A.12)-(A.14) which represent outgoing circular waves are

$$\psi_n^c = e(kz)H_n(kR)\cos(n\theta) \tag{A.26}$$

$$\psi_n^s = e(kz)H_n(kR)\sin(n\theta) \tag{A.27}$$

where H_n is the Hankel function of order n and second kind. (The commonly used superscript (2) is omitted, for convenience.) The fact that these eigenfunctions satisfy the radiation condition (A.25) is seen from the large argument expansion [35] for H_n :

$$H_n(x) = (\pi/2x)^{\frac{1}{2}}e^{-i(x-\pi/4-n\pi/2)}\{1 + O(x^{-1})\} \tag{A.28}$$

Because H_n tends to infinity as the argument $x \to 0$ it is realised that neither ψ_n^c nor ψ_n^s are regular at the z-axis. In general we may decompose a potential ϕ - satisfying the boundary value problem, including also the body condition (A.15) and the radiation condition (A.55) - into two parts

$$\phi = \phi_{loc} + \phi_\infty \tag{A.29}$$

The far-field potential ϕ_∞ may be expanded in terms of the eigenfunctions ψ_n^c and ψ_n^s, that is

$$\phi_\infty = \sum_{n=0}^{\infty} \{A_n\psi_n^c + B_n\psi_n^s\} \tag{A.30}$$

A_n and B_n being complex coefficients. The local field potential ϕ_{loc} has to be added in order to 1) make ϕ being regular at the z-axis and 2) make ϕ satisfying the body condition (A.15). In some special cases the local field potential ϕ_{loc} may be expanded into wave-free eigenfunctions of the boundary value problem (A.12)-(A.14), but in general analytic expressions do not exist. Anyway, ϕ_{loc} represents

a local standing wave of no average energy transport. We therefore have that

$$\phi_{loc} = O(1/kR) \quad , \quad kR>>1 \tag{A.31}$$

A.3 The hydrodynamical parameters.

By the hydrodynamical parameters are meant the exciting force coefficients κ_i^p and the radiation impedance elements Z_{ij}^{pq}. Their physical meaning is explained in section 2.1. Knowing the geometry of each body and their position it is - in principle at least - possible to calculate these parameters for an arbitrary wave frequency ω. The exciting force coefficients are determined from the

diffraction problem:

Consider the case when all bodies are fixed and the incident wave is represented by the plane wave potential ϕ_o as given by (A.19). The total potential then is

$$\phi = \phi_o + \phi_d \tag{A.32}$$

where ϕ_d is the diffraction potential satisfying the Laplace equation (A.12), the free surface condition (A.13), the bottom condition (A.14), the radiation condition (A.25) and finally the body conditions

$$\frac{\partial \phi_d}{\partial n} = - \frac{\partial \phi_o}{\partial n} \quad \text{on} \quad S_i \quad , \quad i = 1,..,N \tag{A.33}$$

S_i representing the average wetted surface of body no. i. The exciting force F_i^p corresponding to the mode p(i) is given by the integrated hydrodynamical pressure p

$$F_i^p = -\iint_{S_i} p n_p dS = i\omega\rho \iint_{S_i} (\phi_o + \phi_d) n_p dS \tag{A.34}$$

where the normal component n_p is

$$n_p = \begin{cases} \vec{e}_p \cdot \vec{n} & p = 1,2,3 \\ \vec{e}_{(p-3)} (\vec{\rho}_i \times \vec{n}) & p = 4,5,6 \end{cases} \tag{A.35}$$

Here $\vec{e}_1$, $\vec{e}_2$, $\vec{e}_3$ are the unit vectors in x-, y- and z-direction, respectively, and the radius vector $\vec{\rho}_i$ is referred to the center of rotation. The exciting force is conveniently decomposed into two terms: 1) the so-called Froude-Krylov force

$$F^p_{i,FK} = i\omega\rho \iint_{S_i} \phi_o n_p dS \tag{A.36}$$

and 2) the diffraction force

$$F^p_{i,d} = i\omega\rho \iint_{S_i} \phi_d n_p dS \tag{A.37}$$

The radiation impedance matrix elements are determined by the

radiation problem:

Consider the case of no incident wave and body no. j oscillating in mode q , all other modes being fixed. The potential then is

$$\phi = \varphi^q_j u^q_j \tag{A.38}$$

where u^q_j is the generalised velocity amplitude and φ^q_j is the normalised radiation potential for the oscillating mode q(j). This normalised potential has to satisfy the same equations as the diffraction potential, with exception of the body condition which takes the form

$$\frac{\partial \varphi^q_j}{\partial n} = \begin{cases} n_q & \text{on } S_j \\ 0 & \text{on } S_k,\ k \neq j \end{cases} \tag{A.39}$$

The force component corresponding to mode p(i) due to the motion in mode q(j) is

$$-Z_{ij}^{pq}u_j^q = i\omega\rho \iint_{S_i} \varphi_j^q u_j^q n_p dS \qquad (A.40)$$

Thus we have that

$$Z_{ij}^{pq} = -i\omega\rho \iint_{S_i} \varphi_j^q n_p dS \qquad (A.41)$$

It also can be shown[36] that the radiation impedance matrix $\underset{\sim}{Z}$ is symmetric:

$$Z_{ij}^{pq} = Z_{ji}^{qp} \qquad (A.42)$$

which is the so-called resiprocity relation.

Some other useful relations are presented below.

1) The Froude-Krylov force and the diffraction force may alternatively be expressed by

$$F_{i,FK}^p = -i\omega\rho \iint_{S_\infty} \phi_o \frac{\partial\varphi_i^p}{\partial n} dS \qquad (A.43)$$

and

$$F_{i,d}^p = -i\omega\rho \sum_{q=1}^{3} \iint_{S_i} \varphi_i^p \frac{\partial\phi_o}{\partial x_q} n_q dS \quad , \qquad (A.44)$$

respectively.

2) The radiation resistance element $R_{ij}^{pq} \equiv \mathrm{Re}\{Z_{ij}^{pq}\}$ may be expressed[37] by the exciting force coefficients for the modes p(i) and q(j) :

$$R_{ij}^{pq} = \frac{\omega k}{2\rho g^2 D} \cdot \frac{1}{2\pi} \int_0^{2\pi} \kappa_i^p(\beta)^* \kappa_j^q(\beta) e^{-ikd_{ij}\cos(\gamma_{ij}-\beta)} d\beta \qquad (A.45)$$

where the distance d_{ij} and the angle γ_{ij} are defined

in fig. 3. As a special case of (A.45) we get the radiation resistance R^o for an isolated heaving buoy

$$R^o = \frac{\omega k}{2\rho g^2 D} |\kappa^o|^2 \qquad (A.46)$$

κ^o being the isolated exciting force coefficient in heave.

3) The far-field coefficient $b_i^p(\gamma_i)$ defined by

$$\lim_{kd_i \to \infty} \varphi_i^p = b_i^p(\gamma_i) e(kz)(kd_i)^{-\frac{1}{2}} e^{-ikd_i} \qquad (A.47)$$

is related to the exciting force coefficient κ_i^p by

$$\kappa_i^p(\gamma_i + \pi) = \frac{\rho g D}{k} \sqrt{2\pi} e^{i\pi/4} b_i^p(\gamma_i) \qquad (A.48)$$

where (d_i, γ_i, z) are local cylinder coordinates. See fig.1.

APPENDIX B. ANALYTICAL APPROXIMATION OF THE DIFFRACTED WAVE POTENTIAL

In this appendix it will be shown that the diffracted wave of a small isolated buoy is approximately equal to a certain composite radiation potential. The analysis below is not restricted to symmetrical bodies. We therefore let "a" be a characteristic buoy dimension. The body may be floating or submerged and its mean center for gravity is $\vec{r}_1 = (x_1, y_1, z_1)$.

Suppose the body is moving in such a way that its center of gravity follows the orbit of a fluid particle of the undisturbed incident wave ϕ_o. Let the resulting wave potential be ϕ. The perturbing potential $\Delta\phi$ then is

$$\Delta\phi \equiv \phi - \phi_o = \phi_d + \phi_r \tag{B.1}$$

where ϕ_d is the diffracted wave potential and ϕ_r is the radiation potential due to the prescribed motion. That is

$$\phi_r = \sum_{p=1}^{3} \varphi^p \left.\frac{\partial \phi_o}{\partial x_p}\right|_{\vec{r}_1} \tag{B.2}$$

since rotary motion of the body is neglected. According to (A.39) and (A.33) the boundary conditions for ϕ_r and ϕ_d at the body surface S ($\equiv S_1$) are

$$\left.\frac{\partial \phi_r}{\partial n}\right|_S = \sum_{p=1}^{3} n_q \left.\frac{\partial \phi_o}{\partial x_p}\right|_{\vec{r}_1} \tag{B.3}$$

and

$$\left.\frac{\partial \phi_d}{\partial n}\right|_S = -\sum_{p=1}^{3} n_q \left.\frac{\partial \phi_o}{\partial x_p}\right|_S = -\sum_{p=1}^{3} n_q \left.\frac{\partial \phi_o}{\partial x_p}\right|_{\vec{r}_1} \{1 + O(\alpha)\} \tag{B.4}$$

respectively. The boundary condition for the perturbing potential is consequently

$$\left.\frac{\partial(\Delta\phi)}{\partial n}\right|_S = -\sum n_p \left.\frac{\partial \phi_o}{\partial x_p}\right|_{\vec{r}_1} O(\alpha) = -\left.\frac{\partial \phi_r}{\partial n}\right|_S O(\alpha) \qquad (B.5)$$

From this we deduce that

$$\frac{\Delta\phi}{\phi_r} = O(\alpha) \qquad (B.6)$$

or, equivalent

$$\phi_d = -\phi_r(1 + O(\alpha)) \approx -\phi_r \quad , \alpha << 1 \qquad (B.7)$$

A few comments on this result are listed below.

1) This approximation is built-in in the small-body formula (3.10) for the diffraction force F_d^p. The approximation above is, however, valid not only at the body surface S, but in the far-field region as well.

2) From eqs. (3.6), (3.17) and (3.18) it is realised that the heave potential φ^o is the dominant one for floating small buoys. In the long-wave limit $(\alpha \to 0)$, therefore, floating bodies scatter waves isotropically.

3) For a floating body the neglected term $\Delta\phi$ of the diffracted wave potential ϕ_d may be of the same order as the surge and sway terms of ϕ_r. However, we shall here assume that the complete potential, $-\phi_r$, much better than its leading term approximates the diffraction potential ϕ_d. This assumption is, in fact, supported by the results of figs. 9-11.

4) For axisymmetrical buoys the approximation (B.7) implies that the higher anisotropic terms - proporsional to $\cos(n\theta)$ and $\sin(n\theta)$ - is neglected for $n \geq 2$. See (3.6) and (A.30).

APPENDIX C. ANALYTICAL INVESTIGATION OF THE INTERACTION FACTOR FOR A TWO-BUOY SYSTEM.

The results shown in fig. 35 raise the following questions:

1) Why do the interaction factors Q^{LS} and Q^{E} - for LS absorbers and ideal point absorbers, respectively - display such a good agreement and

2) Why does the NS approximation lead to an interaction factor Q^{NS} seemingly less accurate than Q^{E}?

In order to give an answer to these questions we investigate the limit $\lim_{\alpha \to 0} Q^{LS}$ for two identical floating buoys of no losses and no constraints.

The Cartesian coordinates are chosen to be (0,0,0) and (0,d,0) for the centers of buoy no.1 and buoy no. 2, respectively. By means of the expression (2.17) for the maximum power it can be seen that

$$Q = \frac{\frac{1}{2}(|F_1/F^o|^2 + |F_2/F^o|^2)(R_{11}/R^o) - \mathrm{Re}\{F_1 F_2^*/|F^o|^2\}(R_{12}/R^o)}{(R_{11}/R^o)^2 - (R_{12}/R^o)^2} \qquad (C.1)$$

is a general and exact expression for the two-buoy interaction factors. It is convenient to introduce the non-dimensional parameters $\hat{\gamma}$, σ_1 , σ_2 , σ_{11} and σ_{12} by

$$\hat{\gamma} \equiv kd \sin\beta \qquad (C.2)$$

$$\frac{1}{2}(|F_1^{LS}|^2 + |F_2^{LS}|^2)/|F^o|^2 \equiv 1 + \sigma_1 \qquad (C.3)$$

$$\mathrm{Re}\{F_1^{LS} F_2^{LS*}/|F^o|\} \equiv \cos\hat{\gamma} + \sigma_2 \qquad (C.4)$$

$$R_{11}^{LS}/R^o \equiv 1 + \sigma_{11} \qquad (C.5)$$

$$R_{12}^{LS}/R^o \equiv J_o(kd) + \sigma_{12} \qquad (C.6)$$

By means of the two-buoy results (4.1)-(4.5)and the small-body approximations (3.17), (3.18) and (3.30) for κ^s, κ^o and $\arg\{\kappa^o\}$, respectively, it can be seen that

$$\sigma_1 = \pi Y_o \cos\hat{\gamma}\alpha^2 + O(\alpha^3) \tag{C.7}$$

$$\sigma_2 = \pi Y_o \alpha^2 + O(\alpha^3) \tag{C.8}$$

$$\sigma_{11} = \pi J_o Y_o \alpha^2 + O(\alpha^3) \tag{C.9}$$

$$\sigma_{12} = \pi Y_o \alpha^2 + O(\alpha^3) \tag{C.10}$$

The LS interaction term then may be written as

$$Q^{LS} = \frac{(1+\sigma_1)(1+\sigma_{11}) - (\cos\hat{\gamma}+\sigma_2)(J_o+\sigma_{12})}{(1+\sigma_{11})^2 - (J_o+\sigma_{12})^2} \tag{C.11}$$

or

$$Q^{LS} \approx \frac{1-\cos\hat{\gamma}J_o + \sigma_1+\sigma_{11}-J_o\sigma_2-\cos\hat{\gamma}\sigma_{12}}{1-J_o^2+2\sigma_{11}-2J_o\sigma_{12}} \tag{C.12}$$

when higher order terms of the numerator and the denominator have been omitted. Inserting (C.7)-(C.10) into (C.12) we find that the terms of order $O(\alpha^2)$ surprisingly vanish. Hence

$$Q^{LS} = \frac{1-\cos\hat{\gamma}J_o+O(\alpha^3)}{1-J_o^2+O(\alpha^3)} \tag{C.13}$$

Now, remember that the NS approximation includes the term σ_{12} but concurrently it neglects the terms σ_1, σ_2 and σ_{11}.(The term σ_{12} represents the"phase"shift of (R_{12}^{NS}/R^o) relative to $J_o(kd)$). Consequently,we have that

$$Q^{NS} = \frac{1-\cos\hat{\gamma}J_o-\pi\cos\hat{\gamma}Y_o\alpha^2+O(\alpha^3)}{1-J_o^2-2\pi\cos\hat{\gamma}Y_o\alpha^2+O(\alpha^3)} \tag{C.14}$$

It should be noted that when $\alpha \to o$ Q^{LS} as well as Q^{NS} reduce to the formula for Q^{E} previously found by Falnes[39] and by Evans[40].

$$Q^{E} = \frac{1-\cos\hat{\gamma}J_o}{1-J_o^2} \qquad (C.15)$$

However, (C.13) and (C.14) indicate that Q^{LS} reduces more rapidly to Q^{E} than what is the case for Q^{NS}. This fact probably explains the differences between Q^{LS}, Q^{NS} and Q^{E} as displayed in fig. 35.

APPENDIX D. NOMENCLATURE

The thesis contains a rather large number of symbols and, in many cases, a lot of variants of one basis symbol. In order to help the reader, we therefore enclose an alphabetic list of the most frequently used symbols. A symbol - or a symbol variant - is usually not included in the symbol list if i) it occurs rather locally in the text or ii) it differs from another symbol by one of the special superscript or subscripts; see below. For most of the symbols inclosed a reference is made to the equation or the figure where it is defined or first occurs.

Special superscripts or subscripts:

$\underset{\sim}{}$ - symbol denoting a matrix or a vector.

$\underset{\sim}{}^{T}$ - symbol denoting the transposed of a matrix or a vector.

* - complex conjugation.

$'$ - real and time-dependent quantity; eq. (A.10).

^{p} and ^{q} - mode indices. Default mode is heave (p,q = 3).

$_{i}$ and $_{j}$ - buoy number indices. Default number is i,j = 1 for one isolated buoy or many idendical buoys.

$^{(n)}$ - n'th harmonical component.

^{o} - isolated buoy.

^{NS} - non-scattering approximation.

^{LS} - low-scattering approximation.

$_{\infty}$ - far-field part of a wave or wave potential.

Symbol list:

A_n - far-field coefficient; eq. (A.30).

A_w - waterplane area; fig. 4.

a - buoy radius; fig.4.

$c_i(\underset{\sim}{x})$ - heave amplitude function; eq. (5.11).

D - depth factor; eq. (A.24).

d - buoy separation distance.

d_i - radial distance from buoy no. i to a point in the fluid; fig. 1.

d_{ij} - radial distance between the centers of two buoys; fig.3.

$e(kz)$ - depth function, eq. (A.21).

$\underset{\sim}{F}$ - generalised exciting force vector; eq. (2.1).

F_i^p - element of $\underset{\sim}{F}$; eq. (2.2).

$F(\underset{\sim}{x})$ - objective function; eq. (5.12).

f_1 - submergance factor; eq. (3.12).

g - acceleration of gravity.

g_1 - submergance factor; eq. (3.13).

H_n - Hankel function of order n and second kind ($\equiv J_n - iY_n$) ; eq. (A.26).

h - depth of water; fig. 1.

i - imaginary unity ($\equiv \sqrt{-1}$).

J_o - Bessel function of zero order.

k - wave number; eq. (A.20).

M - total number of oscillators.

N - number of buoys.

n_p - normal vector component; eq. (A.35).

n_{max} - number of real optimisation parameters.

P_c - useful converted power; eq. (2.9).

P_e - exciting power; eq. (2.10).

P_r - radiated power; eq. (2.11).

P_l - loss power; eq. (2.12).

P_c^o - amount of power available for one isolated buoy; eq. (6.1).

p - hydrodynamical pressure; eq. (A.17).

Q - interaction factor; eq. (6.1).

Q^E - interaction factor according to Evans; eq. (6.2).

R - horisontal distance from the origin to a point in the fluid; fig. 1.

$\underset{\sim}{R}$ - radiation resistance matrix; eq. (2.5).

R^o - radiation resistance for a heaving isolated buoy; eq. (A.46).

$\underset{\sim}{R}_c$ - conversion resistance matrix; eq. (2.7).

R_i - diagonal element of $\underset{\sim}{R}_c$; eq. (5.5).

$\underset{\sim}{R}_l$ - loss resistance matrix; eq. (2.7).

S_i - wetted buoy surface; fig. 1.

s_{max} - physical maximum for the heave amplitude; eq. (5.11).

T - wave period ($= 2\pi/\omega$).

t - variable of time.

$\underset{\sim}{u}$ - generalised velocity amplitude vector; eq. (2.1).

u_j^q - velocity amplitude for mode no. q of body no. J.j eq. (2.2).

V - immersed buoy volume; fig.4.

v_q - fluid velocity component in the q-direction; eq. (A.17).

(x_i, y_i, z_i) - cartesian coordinates for the center of buoy no. i ; fig. 1.

$\underset{\sim}{X}$ - radiation reactance matrix; eq. (2.5).

$\underset{\sim}{X}_m$ - mechanical reactance matrix.

X_i - diagonal element of $(\underset{\sim}{X} + \underset{\sim}{X}_m)$; eq. (5.5).

$\underset{\sim}{x}$ - vector of optimisation variables.

Y_o - Neuman function of zero order.

$\underset{\sim}{Z}$ - radiation impedance matrix; eq. (2.5).

$\underset{\sim}{Z}_m$ - mechanical impedance matrix; eq. (2.1).

Z_{ij}^{pq} - element of $\underset{\sim}{Z}$; eq. (2.2).

α - non-dimensional buoy radius; eq. (3.1).

β - angle of incidence; fig.3.

γ_i - azimutal angle for a fluid particle; fig. 3.

γ_{ij} - azimutal angle for buoy no. j relative to buoy no. i; fig. 3.

Δ_{ij} - non-dimensional scattering force; eq. (3.48).

Δ_{ikj} - non-dimensional scattering term of the radiation impedance Z_{ij} ; eq. (3.56).

δ_{ij} - Kronecher delta (= 1 for j=i, 0 otherwise).

ϵ^{pq} - non-dimensional radiation resistance; eq. (3.14).

ϵ - convergence parameter; eq. (5.15).

η - complex wave amplitude; eq. (A.18).

$\eta(i)$ - wave amplitude at buoy no. i.

η_o - incident wave amplitude; eq. (A.19).

η_i^o - radiated wave amplitude; eq. (3.33).

$\eta^{o}_{d,i}$ - scattered wave amplitude; eq. (3.47).

$\eta_{i,k}$ - scattered wave from buoy no. k caused by the radiated wave η^{o}_{i} ; eq. (3.54).

θ - azimutal angle; fig. 1.

κ^{p}_{i} - exctiting force coefficient; eq. (2.4).

κ^{o} - heave force coefficient for an isolated buoy; eq. (3.5).

κ^{s} - surge force coefficient for an isolated buoy; eq. (3.5).

λ - wavelength; eq. (A.20).

μ^{pq} - non-dimensional radiation reactance or added mass; eq. (3.14).

ν - wave frequency (= $1/T = \omega/2\pi$).

ξ - normalised buoy surface coordinate; eq. (3.23).

ρ - water density.

ϕ - total velocity potential; eq. (A.12).

ϕ_{o} - incident wave potential; eq.(A.19).

ϕ_{d} - diffracted or scattered wave potential; eq. (A.32).

$\phi^{o}_{d,i}$ - potential corresponding to $\eta^{o}_{d,i}$.

φ^{p}_{i} - normalised radiation potential; eq. (A.38).

ω - angular wave frequency; eq. (A.22).

REFERENCES

1. Mollison, D. et al. Wave power availability in the N.E. Atlantic. Nature, Vol. 263. 1976 pp. 223-226.

2. Torsethaugen, K. The Norwegian "Wave-climate mapping" program. Proc. 2nd Int. Symp. Wave Energy Utilization, Trondheim 1982. pp 81-97.

3. Greenhow, M.J.L. The hydrodynamic interactions of spherical wave-power devices in surface waves. "Power from Sea Waves", edited by B.Count. (Academic Press, 1980). pp 287-343.

4. Ohkusu, M. Hydrodynamic forces on multiple cylinders i waves. Proc. Int. Symp. Dynamics of Marine Vehicles and Structures in Waves. London 1974, paper 12, pp 107-12. London, Inst. Mech. Eng.

5. Count, B.M. and Jefferys, E.R. Wave power, the primary interface. Proc. 13th Symp. Naval Hydrodynamics. Tokyo 1980, paper 8, I, pp 1-10.

6. Matsui, T. and Tamaki, T. Hydrodynamical interaction between groups of vertical axisymmetric bodies floating in waves. Proc. Int. Symp. Hydrodyn. Ocean Eng., Trondheim 1981, pp 817-836.

7. Falnes, J. Radiation impedance matrix and optimum power absorption for interacting oscillators in surface waves. Appl. Ocean Res. 1980, Vol. 2, pp 75-80.

8. Mehlum, E and Stamnes,J. Power production based on focusing of ocean swells. Proc. First Symp. Wave Energy Utilisation, Goetenburg 1979. pp. 29-35.

9. Iversen, L.C. Numerical method for computing the power absorbed by a phase-controlled point absorber. Appl. Ocean Res., 1982, Vol. 4, No. 3. pp.173-180.

10. Evans, D.V. Some theoretical aspects of three-dimensional wave-energy absorbers. Proc. Symp. Ocean Wave Energy Utilization. Goetenburg 1979, pp 253-283. Eq.(4.3).

11. Cf. eq. (15) of ref. 7.

12. Budal,K., Falnes,J., Kyllingstad,Å. and Oltedal,G. Experiments with point absorbers. Proc. First Symp. Ocean Wave Energy Utilization. Goetenburg 1979, pp.253-283. Eq.(4.3).

13. Budal,K. et al. The Norwegian wave-power buoy project. Proc. 2nd Symp. Wave Energy Utilization. Trondheim 1982. pp 323-344.

14. Budal,K. and Falnes,J. A resonant point absorber of ocean wave power. Nature, 256 (1975). pp 478-479.

15. Newman,J.N. Marin Hydrodynamics, MIT Press, Cambridge 1977.

16. Falnes,J. and Iversen,L.C. Hydrodynamisk teori for bølgjekraftverk. Førelesingsnotat, Inst. for eksp. fysikk NTH. p 113.

17. Count,B.M. Private communication.

18. Cf. figs.6 and 7 of ref. 3.

19. Cf.,for instance, eq.(E20) of ref.16.

20. See,for instance, Panofsky,W.K.H and Phillips,M. Classical Electricity and Magnetism. Addison Wesley 1956, pp 37-38.

21. Cf. eq.(41) of ref. 7.

22. See, for enstance, Abramowitz and Stegun. Handbook of mathematical functions. Dover. Eq. (9.1.18)

23. Budal,K. Theory for Absorption of Wave Power by a System of Interacting Bodies. J.Ship Res. 1977,21, pp 248-253.

24. See, for instance, eq. (9.1.28) of ref. 22.

25. Cf. fig. 10 of ref. 6.

26. Cf. fig. 6 of ref. 6.

27. Cf. fig. 16 of ref. 3.

27b. Kyllingstad, Å. Computer program for calculating the wave-power absorption by small interacting buoys. Internal report. In Preparation.

28. Evans, D.V. Maximum wave-power absorption under motion constraints. Appl. Ocean Res., 1981, Vol.3, No.4, pp 200-203.

29. Falnes,J. and Budal,K. Wave power absorption by parallel rows of interacting oscillating bodies. Appl. Ocean Res. To be published.

30. Gill,P.E. and Murray,W. Numerical Methods for Constrained Optimization. Academic Press 1974.

31. Falnes,J. and Budal,K. Wave-Power conversion by point absorbers. Norw. Mar. Res. 6 4 (1978). pp 2-11.

32. Mehlum,E. Private communication.

33. Cf. fig. 4 of ref. 10.

34. Wehausen,J.V. and Laitone,E.V. Surface Waves. Handbuch der Physik, Springer (1960).

35. See, for instance, eq. (9.2.4) of ref. 22.

36. See, for instance, Newman,J.N. The interaction of stationary vessels with regular waves. Proc. 11th Symp. Naval Hydrodynamics, 1976, pp 491-501.

37. See, for instance, eq. (29) of ref. 7.

38. Cf. eqs. (45) and (46) of ref. 36.

39. Cf. eq. (50) of ref. 7.

40. Cf. eq. (4.13) of ref. 10.